AD

229400

1 OF 2

"NOTICE: When Government or other drawings, specifications or other data are used for any purpose other than in connection wit a definitely related Government procurement operation, the U.S. Government thereby incurs no responsibility, nor any obligation whatsoever; and the fact that the Government may have formulate furnished, or in any way supplied the said drawings, specifications or other data is not to be regarded by implication or otherwise a in any manner licensing the holder or any other person or corpor tion, or conveying any rights or permission to manufacture, use or sell any patented invention that may in any way be related theret

5

UNIVERSITY OF CALIFORNIA

INSTITUTE OF ENGINEERING RESEARCH

BERKELEY CALIFORNIA

WATER WAVES. IV.

by

E. V. Laitone

With partial support from

Contract Number N-onr-222(30)

SERIES NO. 82

ISSUE NO. 11

DATE November 1959

WATER WAVES. IV.

by

E. V. Laitone

with partial support

from

Contract Number N-onr-222(30)

University of California
Institute of Engineering Research
Berkeley 4, California

November, 1959

This report constitutes the fourth part of an article on Water Waves being prepared for the new edition of the Encyclopedia of Physics (Handbuch der Physik) published by Springer Verlag.

INDEX

E. Shallow water waves E-1

23. The fundamental equations for the first approximation . E-2

29. The linearized shallow-water theory E-4

29α. Linearized shallow-water theory applied to two-dimensional steady flow E-11

30. Nonlinear shallow-water theory E-17

30α. One-dimensional non-steady, first-order, shallow-water theory E-17

30β. Two-dimensional, steady, supercritical flow by the first-order shallow-water theory E-24

30γ. One-dimensional, steady, open channel hydraulics and the hydraulic jump. E-44

31. Higher order theories and the solitary and cnoidal waves E-55

31α. The first and second approximations to the cnoidal and solitary waves E-58

31β. The limiting height and velocity of propagation of cnoidal and solitary waves E-72

2. Shallow Water Waves

This chapter will deal with special solutions based on the shallow-water approximation, following the method of Friedrichs [1948] as presented in section 10β. The shallow-water approximation for the waves over a rigid bottom yields a set of nonlinear equations (cf. 10.32) even in the first approximation. If these equations are then linearized they result in a hyperbolic type equation which reduces to the simple wave equation for a flat horizontal bottom. Consequently the solutions resulting from the shallow-water approximation are completely different in character from those resulting from the infinitesimal-wave approximation of section 10α and chapter D, which resulted in linear equations and linear boundary conditions. That is, the shallow-water approximation leads to nonlinear hyperbolic type equations, whereas the infinitesimal-wave approximation leads to a set of linear equations satisfying the boundary conditions and having each successive approximation to the velocity potential satisfy the simplest elliptic equation, namely the Laplace equation.

After the first-order shallow-water approximation (10.32) has been applied to several problems, then the method of Friedrichs [1948] and Keller [1948] will be extended to obtain the second and third approximations of the shallow-water theory and thereby present, for the first time, the exact second approximation to the cnoidal wave of Korteweg and de Vries [1895], and the solitary wave of Boussinesq [1871], and Rayleigh [1876]. These higher order approximations lead directly to relations predicting the maximum heights of cnoidal waves and solitary waves.

28. The Fundamental Equations for the First Approximation.

The shallow-water expansion method introduced by Friedrichs [1948] is discussed in section 10. For this application the expansion parameter ε was selected so that the first approximation would be identical to the nonlinear equations of the classical shallow-water theory, which is based on the assumption of hydrostatic pressure variation throughout and the neglect of the variaton of the horizontal velocity components with depth, so the complicated boundary value problem is greatly simplified to the following nonlinear equations:

$$\begin{aligned} u_t + uu_x + wu_z &= -g\eta_x \\ w_t + uw_x + ww_z &= -g\eta_z \\ \eta_t + [u(\eta + h)]_x + [w(\eta + h)]_z &= 0 \end{aligned} \tag{28.1}$$

See Lamb [1932], page 254, or Stoker [1957], page 23.

Upon noting (see Figure 37) that the rigid bottom surface or the undisturbed water depth in (28.1) is designated by $y=-h(x,z)=b(x,z)$ for the corresponding designation in (10.32), we see that the (28.1) set of nonlinear equations are identical to (10.32) which correspond to the first approximation of Friedrichs [1948] shallow-water expansion method as discussed in section 10, thereby showing that the method has physical justification. It is seen that the higher order approximations following (10.23) and (10.33) will require that ε be sufficiently small, consequently, as will be shown, this expansion method is applicable only if the water depth and surface curvature are small in comparison to the equivalent of the wave length of the free surface profile disturbance.

Therefore, in some cases, this shallow water theory is applicable to extremely large water depths as long as the wave length is sufficiently long, the most common application being to tidal waves which are the oceanic tides produced by the gravitational action of the sun and the moon, e.g. see Lamb [1932].

The mathematical justification for this shallow-water expansion method, at least for special cases, lies in the existence proof of Friedrichs and Hyers [1954] for the solitary wave, and the existence proof of Littman [1957] for the more general cnoidal waves. Both of these proofs demonstrate that this expansion method will at least give asymptotic descriptions of the exact solutions for these particular problems.

The nonlinear first approximation given by (28.1) is considerably simplified if the rigid bottom surface h(x,z) is flat and horizontal, as may be seen by letting h = constant so that (28.1) may be written as

$$\begin{aligned} u_t + uu_x + wu_z &= -g(\eta + h)_x \\ w_t + uw_x + ww_z &= -g(\eta + h)_z \\ (\eta + h)_t + [u(\eta + h)]_x + [w(\eta + h)]_z &= 0 \end{aligned} \tag{28.2}$$

which is identical to the well known two-dimensional gas dynamics equation, e.g. see Lamb [1932], if we write

$$\rho(x,z,t) = [\eta(x,z,t) + h] \tag{28.3}$$

$$\frac{\gamma p}{\rho^2} = \frac{c^2}{\rho} = \frac{c^2}{\eta + h} = g = \text{constant}$$

Since the isentropic gas relationship is $p = (\text{constant} \cdot \rho^{\gamma})$, therefore the first order nonlinear shallow-water approximation for a flat horizontal bottom is identical to the isentropic two-dimensional gas flow having a specific heat ratio of $\gamma = 2$. This is the basis of the so called hydraulic analogy which has been

used for many experimental investigations, e.g., see Stoker [1957].

It must be noted, however, that this hydraulic analogy is only valid for a flat horizontal bottom, as may be seen by comparing (28.1) and (28.2), and even more important it is valid only as a first approximation even for the nonlinear case. It will be shown in section 31 that the second approximation to shallow-water theory yields finite amplitude waves (the solitary wave or cnoidal waves) that can be propagated without a change in shape or form, a fact which completely invalidates the hydraulic analogy to compressible gas flow since (28.2), or the gas dynamics equation , predicts that any finite disturbance quickly forms a finite discontinuity, e.g. see Lamb [1932] pages 278, 481.

In section 29, immediately following, it will be shown that even for the linearized first approximation the hydraulic analogy to compressible gas flow is limited to a flat horizontal bottom.

29. The Linearized Shallow-water Theory.

The first approximation to shallow-water theory can now be linearized by two different methods that are suitable for various problems. The first method is more appropriate for investigating steady water flow in canals or rivers and consists of the following approximations for carrying out the linearization

$$u(x,z) = U + \phi_x \approx U,\ w(x,z) = \phi_z \ll U \tag{29.1}$$

$$\eta(x,z) \ll h(x,z) \tag{29.2}$$

so that (28.1) is linearized to

$$\left(1 - \frac{U^2}{c^2}\right)\phi_{xx} + \phi_{zz} - Uh_x - \phi_z h_z = 0 \tag{29.3}$$

$$c^2 = gh(x,z) \tag{29.4}$$

In agreement with the previous discussion, (29.3) corresponds to the

linearized gas dynamics equation only if the bottom is flat and horizontal so h is constant.

The second method of linearization corresponds to the classical t. al wave theory, or long wave theory, e.g. see Lamb [1932], page 254, and can be obtained by writing

$$u(x,z,t) = \phi_x \ll 1, \quad w(x,z,t) = \phi_z \ll 1 \tag{29.5}$$

$$\eta(x,z,t) \ll h(x,z) \tag{29.6}$$

so that (28.1) is linearized to

$$(\phi_{xx} + \phi_{zz}) + \left(\frac{h_x}{h}\phi_x + \frac{h_z}{h}\phi_z\right) = \frac{1}{gh}\phi_{tt} \tag{29.7}$$

Again, as before, (29.7) corresponds to the linearized gas dynamic case, or the simple acoustic wave propagation equation, only if the bottom is flat and horizontal. In this case the general solution of (29.7) for one-dimensional flow is the well known d'Alembert solution of the simple wave equation.

$$\phi(x,t) = F(x-ct) + f(x+ct)$$
$$c = \sqrt{gh} = \text{constant} \tag{29.8}$$

which is used to study long wave length oscillations in canals when the water is either at rest or moving with a velocity of $U \ll c$. The limitation to linearized perturbations and ant h for one dimensional flow allows (28.1) to be linearized to

$$\phi_{xt} = u_t = -g\eta_x$$
$$\eta_{xx} = \frac{1}{gh}\eta_{tt} = \frac{1}{c^2}\eta_{tt} \tag{29.9}$$

and various applications of this, including the canal theory of tides, are given in Lamb [1932] pages 254-273.

For the case of a canal having a non-rectangular but constant cross-section, we may generalize (29.9) by letting h be the mean

depth defined as the undistrubed cross-sectional area (S) divided by the width (b) of the canal at the undisturbed free water surface, see Lamb [1932] page 256. When the canal has a variable depth h(x) and the disturbance may be considered one-dimensional, then (29.7) may be written in terms of the varying cross-sectional area S(x) for constant width b as follows

$$\frac{1}{gh}\phi_{tt} - \frac{1}{h}(h\phi_x)_x - \frac{1}{S}(S\phi_x)_x \qquad (29.10)$$

$S(x) = bh(x)$, b = constant

Then from (29.9) we obtain

$$\frac{1}{S}(S\eta_x)_x - \frac{1}{gh}\eta_{tt} \qquad (29.11)$$

which is the same as the expression derived by Green (1838) for a canal that is varying in both width b and depth h so that

$S(x) = h(x)b(x)$

However the exact linearized first order approximation is (29.7), and the form of this equation indicates that large values of b'(x) would invalidate the one-dimensional assumption, especially if h_z is relatively large. This is also indicated by Lamb [1932] page 274. However (29.7) provides the rigorous proof that (29.10) is applicable to one-dimensional, long wave length, small amplitude disturbances in a rectangular cross-section canal having a constant width and a varying depth.

Then if we analyze the long wave lengths having a simple harmonic oscillation with a frequency of $\omega/2\pi$, (29.11) reduces to

$$\frac{1}{S}(S\eta_x)_x + \frac{\omega^2}{gh}\eta(x,t) = 0 \qquad (29.12)$$

If we assume, following Lamb [1932] page 275, that this expression gives a satisfactory approximation to a varying width canal, when b varies linearly with x while the depth h remains constant, we obtan $\eta_{xx} + \frac{1}{x}\eta_x + \left(\frac{\omega_n}{c}\right)^2 \eta = 0$; $c = \sqrt{gh}$ = constant

whose general solution is given by the Bessel functions of zero order in the form

$$\eta(x,t) = \sum \left[J_o\left(\frac{\omega_n x}{c}\right) + D_n Y_o\left(\frac{\omega_n x}{c}\right)\right] \left[A_n \cos\omega_n t + B_n \sin\omega_n t\right] \qquad (29.13)$$

where in most applications $D_n = 0$ since $-Y_o(0) \to \infty$.

On the other hand if the canal width remains constant, while the depth varies linearly with x so that $h(x) = h_o \frac{x}{L} \ll \lambda$, b = constant, then there is no doubt that as long as the disturbance is small and one-dimensional equation (29.10) is applicable and may be written, with $C_o = \sqrt{gh_o}$ = constant, as

$$(x\,\phi_x)_x + \left(\frac{\omega_n \sqrt{L}}{C_o}\right)^2 \phi = 0$$

which has a solution suitable for most purposes as

$$\phi(x,t) = \sum \left[J_o\left(2\frac{\omega_n L}{C_o}\sqrt{\frac{x}{L}}\right) + D_n Y_o\right] \left[A_n \cos\omega_n t + B_n \sin\omega_n t\right] \qquad (29.14)$$

For another rectangular cross-section case let $h(x) = h_o\left(1 - \frac{x^2}{L^2}\right)$, b = constant so that (29.10), with $C_o = \sqrt{gh_o}$ = constant, becomes

$$\left(1 - \frac{x^2}{L^2}\right)\phi_{\frac{x}{L}\frac{x}{L}} - 2\frac{x}{L}\phi_{\frac{x}{L}} + n(n+1)\phi = 0$$

$$n(n+1) = \left(\frac{\omega_n L}{C_o}\right)^2 = \frac{(\omega_n L)^2}{gh_o}$$

Then if ϕ is finite for $|x| \leq L$, a solution is given by the Legendre polynomial $P_n(x/L)$, of degree n defining the natural oscillation frequencies by $\frac{\omega_n^2 L^2}{gh_o} = n(n+1) = 2, 6, 12, 20, \ldots$

$$\phi(x,t) = -\sum P_n\left(\frac{x}{L}\right)\left[A_n \cos\omega_n t + B_n \sin\omega_n t\right] \qquad (29.15)$$

These last problems could be considered as the long period oscillations called seiches which occur in certain lakes or canals throughout the world. Many applications are presented by Chrystal [1905, 1906] and the periods observed in several lochs and lakes seem to correspond to those calculated by the linear shallow water theory. The linear shallow water equation (29.7) should be very suitable for the study of seiches because of their long period and relatively small amplitude. Usually the complete equation (29.7) must be solved numerically by the method of finite differences because the contour of the body of water is quite irregular and the depth variation is important.

There are several simple two-dimensional cases that easily yield explicit solutions. For example, the long period oscillations in a rectangular tank having a constant shallow water depth could be obtained by reducing (29.7) to

$$\phi_{xx} + \phi_{zz} + \left(\frac{\omega_{m,n}}{c}\right)^2 \phi = 0$$

where the prescribed boundary conditions are

$$\phi_x(x_o,z,t) = o = \phi_x(o,z,t),\ \phi_z(x,z_o,t) = 0 = \phi_z(x,o,t)$$

so the appropriate solution for ϕ or η would be of the form

$$\sum\sum \operatorname{Cos}\left(\frac{m\pi x}{x_o}\right) \operatorname{Cos}\left(\frac{n\pi z}{z_o}\right)\left[A_{m,n}\operatorname{Cos}(\omega_{m,n}t) + B_{m,n}\sin(\omega_{m,n}t)\right] \qquad (29.16)$$

$$\frac{\omega_{m,n}}{c} = \pi\sqrt{\left(\frac{m}{x_o}\right)^2 + \left(\frac{n}{z_o}\right)^2}$$

Similarly for a circular tank having a constant depth (29.7) may be transformed into polar coordinates (r,θ) to give

$$\phi_{rr} + \frac{1}{r}\phi_r + \frac{1}{r^2}\phi_{\theta\theta} + \left(\frac{\omega_{m,n}}{c}\right)^2\phi = 0$$

$$\phi(r,\theta,t) = \sum\sum J_n\left(\frac{\omega_{m,n}}{c}\, r\right)\left[A_{m,n}\mathrm{Cos}n\theta + B_{m,n}\mathrm{Sin}\ n\theta\right]\left[\mathrm{Cos}\omega_{m,n}t + D_{m,n}\mathrm{sir}\omega_{m,n}t\right] \qquad (29.17)$$

The Y_n solution being omitted because it becomes infinite at r = 0. The admissible values of $\omega_{m,n}$ (which determine the natural frequencies of oscillation) are defined by the boundary condition

$$\phi_r(a,\theta,t) = 0 = J_n'\left(\frac{\omega_{m,n}a}{c}\right) = \left[\frac{dJ_n(\xi)}{d\xi}\right]_{\xi = \left(\frac{\omega_{m,n}a}{c}\right)} \quad \text{or,}$$

$$J_{n-1}\left(\frac{\omega_{m,n}a}{c}\right) = J_{n+1}\left(\frac{\omega_{m,n}}{c}\, a\right) \quad \text{for } n > 0, \text{ and}$$

$$J_1\left(\frac{\omega_m a}{c}\right) = 0 \text{ or } \left(\frac{\omega_m a}{c}\right) = 3.832,\ 7.016,\ 10.17,\ \ldots .$$

for n = 0 which corresponds to the symmetrical oscillations.

The Y_n solution, which behaves as $(r^n \ln r)$ as r approaches zero, is required for any ring type body of shallow water. For example an island in the center of a circular lake, or lagoon formed by an atoll would require that the term J_n in (29.17) be replaced by the complete general solution of Bessel's equation of order n, namely, $\left[J_n\left(\frac{\omega_{m,n}}{c}\, r\right) + E_n Y_n\left(\frac{\omega_{m,n}}{c}\, r\right)\right]$ (29.18)

so as to be able to satisfy the ring type boundary conditions

$$\phi_r(a,\theta,t) = 0 = \phi_r(b,\theta,t) \quad \text{or,}$$

$$J_n'\left(\frac{\omega_{m,n}}{c}\, a\right) + E_n Y_n'\left(\frac{\omega_{m,n}}{c}\, a\right) = 0$$

$$J_n'\left(\frac{\omega_{m,n}}{c}\, b\right) + E_n Y_n'\left(\frac{\omega_{m,n}}{c}\, b\right) = 0$$

Consequently the ring type boundary conditions are satisfied only by the particular values of $\omega_{m,n}$ defined by

$$-E_n = \frac{J_n'\left(\frac{a}{c}\omega_{m,n}\right)}{Y_n'\left(\frac{a}{c}\omega_{m,n}\right)} = \frac{J_n'\left(\frac{b}{c}\omega_{m,n}\right)}{Y_n'\left(\frac{a}{c}\omega_{m,n}\right)} \qquad (29.19)$$

These values of $\omega_{m,n}$ correspond to the natural frequencies of the long period oscillation of the ring shaped shallow body of water.

As a final example of two-dimensional seiches we analyze the long period simple harmonic oscillation in a shallow circular basin having a depth variation dependent only upon r so (29.7) transforms into polar coordinates as

$$\phi_{rr} + \frac{1}{r}\phi_r + \frac{1}{r^2}\phi_{\theta\theta} + \frac{hr}{h}\phi_r + \frac{\omega_n^2}{gh}\phi = 0 \qquad (29.20)$$

Lamb [1932] page 291, has shown that the solution for a parabolic depth variation $h(r) = h_o\left(1 - \frac{r^2}{a^2}\right)$ is given by

$$\phi\ (r,\theta,t) = A_m\left(\frac{r}{a}\right)^m \left\{\begin{matrix}\sin\\ \cos\end{matrix}\right\}(m\theta)\left\{\begin{matrix}\sin\\ \cos\end{matrix}\right\}(\omega_n t)\ F\left(\alpha, \beta, \gamma \frac{r^2}{a^2}\right) \qquad (29.21)$$

where F represents the hypergeometric series

$$F = \left[1 + \frac{\alpha\beta}{1.\gamma}\left(\frac{r}{a}\right)^2 + \alpha\frac{(\alpha+1)\beta(\beta+1)}{1\cdot 2\cdot\gamma(\gamma+1)}\left(\frac{r}{a}\right)^4 + \ldots\ldots\right]$$

with $\frac{\omega_n^2}{gh_o}a^2 = n(n-2)-m^2$

$\alpha = 1/2\ (m+n), \beta = 1/2\ (2+m-n), \gamma = (m+1)$

For the symmetrical modes (m = 0) this solution reduces to

$$\phi\ (r,t) = \sum(A_N \cos\omega_n t + B_N \sin\omega_n t)\ F\left(N, 1-N, 1, \frac{r^2}{a^2}\right)$$

$$F = \left[1 - \frac{N(N-1)}{1^2}\left(\frac{r}{a}\right)^2 + \frac{(N+1)\ N(N-1)(N-2)}{1^2\cdot 2^2}\left(\frac{r}{a}\right)^4 - \cdots\right] \qquad (29.22)$$

$$\frac{\omega_n^2}{gh_o}a^2 = 4N(N-1) = 8,\ 24,\ 48,\ 80\ \ldots$$

It is interesting to compare these long period oscillations ($\lambda >> h$), wherein the fluid particle motion is approximately independent of the depth y, with the short period oscillations ($\lambda << h$) which have a direct dependence on y. For example (23.14) would reduce to (29.16) as $(y+h) \to 0$ since $\cosh y \to 1$ and $\tanh y \to y$ as $y \to 0$. Also

$$c = \sqrt{\frac{g\lambda}{2\pi}\tanh\left(\frac{2\pi h}{\lambda}\right)} = \sqrt{gh}\left[1 - 1/6\left(\frac{2\pi h}{\lambda}\right)^2 + \ldots\right] = \sqrt{gh}\left[1 + O\left(\frac{h}{\lambda}\right)^2\right]$$

Similarly (23.15) would reduce to (29.17) and (23.16) would be equivalent to the additional results given by (29.18) and (29.19). This exact agreement of the linearized results in the limiting case is encouraging justification for both the shallow-water approximation and the infinitesimal-wave approximation since they originate not only from different physical considerations, but also by entirely different mathematical iterations as discussed in section 10. The shallow-water approximation leads to hyperbolic type nonlinear equations, while the infinitesimal-wave approximation deals with linear elliptic equations. Stoker [1947] page 32 gives a detailed comparison of the two linearized approximations for the case of one-dimensional flow over a flat bottom at a 6^{o} slope.

29- α Linearized Shallow-water Theory Applied to Two-Dimensional Steady Flow.

The first method of linearizing the shallow-water theory, as given by (29.3), would be applicable to the determination of the variation in water depth for the steady flow in a shallow open channel or river. However, in practically all cases, (29.3) must be solved numerically so it does not entail a prohibitive amount of extra labor to solve the more exact original nonlinear first-order equation (28.1) directly using the methods discussed in the next section (30) on nonlinear first-order theory. As a matter of fact, for supercritical flow defined by $U > \sqrt{gh}$, the method of characteristics is very easy to use in the numerical solution of the flat bottom nearly horizontal open channel having a varying width, as shown in section 30. The subcritical case, having a flow velocity everywhere $< \sqrt{gh}$, can be satisfactorily

approximated by the one-dimensional hydraulic theory which assumes that the velocity at each cross-section S(x) is independent of y and z. This method of course would yield a constant depth over a given cross-section and would therefore not be satisfactory for predicting the rise in water level about an island, or a jetty, or a pile in a swiftly moving relatively wide stream. For this particular application the linearized form of (29.3) is very useful, especially for subcritical flow.

We now consider the application of (29.3) to the problem of determining the water depth variation about a two-dimensional cylinder that is perpendicular to the bottom and has a narrow cross-section parallel to the flow as shown in Figure 38. If the bottom is approximately flat and horizontal everywhere near the vertical cylinder, then we may consider h as constant and write (29.3) as

$$\beta^2 \phi_{xx} + \phi_{zz} = 0 \text{ or } \frac{\partial^2 \phi}{\partial x^2} + \frac{\partial^2 \phi}{\partial (\beta z)^2} = 0 \tag{29.23}$$

$$\beta^2 = (1-F^2) = \left(1 - \frac{U^2}{gh}\right) = \text{constant} > 0$$

The fundamental solution of (29.23), in view of (29.1), for two-dimensional profiles that may be considered symmetrical about the z-axis as shown in Figure 38, is

$$\phi(x,z) = +\frac{1}{2\pi} \int_0^L f(\xi) \ln \sqrt{(x-\xi)^2 + (\beta z)^2}\, d\xi$$

$$u = U + \phi_x = U + \frac{1}{2\pi} \int_0^L \frac{(x-\xi) f(\xi)\, d\xi}{(x-\xi)^2 + (\beta z)^2} \tag{29.24}$$

$$w = \phi_z = \frac{\beta^2 z}{2\pi} \int_0^L \frac{f(\xi)\, d\xi}{(x-\xi)^2 + (\beta z)^2}$$

The boundary condition for the two-dimensional shape, as shown in Figure 38, is

$$\frac{dz_o}{dx} = \frac{w}{u} = \frac{\phi_z(x,z_o)}{U+\phi_x(x,z_o)} = \frac{\phi_z}{U}\left[1 + O\left(\frac{\phi_x}{U}\right)\right] \qquad (29.25)$$

where the same linearization procedure has been applied to the boundary condition as was used in deriving (29.3). Therefore (29.24) may also be similarly linearized by writing

$$U\frac{dz_o}{dx} = \phi_z(x,z_o) = \frac{\beta}{2\pi}\int_0^L \frac{f(\xi)\,\left(\frac{d\xi}{\beta z_o}\right)}{1+\left(\frac{x-\xi}{\beta z_o}\right)^2}$$

so if we let $\frac{x-\xi}{\beta z_o} = p$, then for $z_o \geq 0$

$$U\frac{dz_o}{dx} = \frac{\beta}{2\pi}\int_{-\left(\frac{L-x}{\beta z_o}\right)}^{\left(x/\beta z_o\right)} \frac{f(x-\beta z_o p)\,dp}{1+p^2} = \beta\,\frac{f(x)}{2} + O(z_o^2)$$

Therefore $$f(\xi) = \left(\frac{2U}{\beta}\right) z_o'(\xi) + O(z_o^2) \qquad (29.26)$$

so that the linearized form of (29.24) is

$$\frac{u(x,z)}{U} = \left[1 + \frac{1}{\pi\beta}\int_0^L \frac{(x-\xi)\,z_o'(\xi)\,d\xi}{(x-\xi)^2+(\beta z)^2}\right] = 1 + \frac{\phi_x}{U} \qquad (29.27)$$

$$\frac{w(x,z)}{U} = \frac{z\beta}{\pi}\int_0^L \frac{z_o'(\xi)\,d\xi}{(x-\xi)^2+(\beta z)^2} = \frac{\phi_z}{U}$$

On the actual surface of the two-dimensional profile (29.27) may be further linearized to

$$\frac{u(x,z_o)}{U} = 1 + \frac{1}{\pi\beta}\left[\lim_{\epsilon\to 0}\int_0^{x-\epsilon} + \int_{x+\epsilon}^{L}\frac{z_o'(\xi)\,d\xi}{(x-\xi)}\right] \qquad (29.28)$$

$$\frac{w(x,z_o)}{U} = z_o'(x)$$

On the other hand, for large values of z and $x \approx 0$ we may write

$$\frac{w(0,\infty)}{U} \to 1 + \frac{1}{\pi\beta^3 z^2}\int_0^L -\xi z_o'(\xi)\,d\xi \approx 1 + \frac{L}{2}\left[\frac{z_o(L)-z_o(0)}{\pi\beta^3 z^2}\right] \qquad (29.29)$$

$$\frac{w(0,\infty)}{U} \to \frac{1}{\pi\beta z}\int_0^L z_o'(\xi)\,d\xi = \left[\frac{z_o(L)-z_o(0)}{\pi\beta z}\right]$$

The change $\eta(x,z)$ in the original constant water depth h can then be determined by the linearized relations corresponding to (29.1) and (29.2) as

$$\frac{\eta(x,z)}{h} + O\left(\frac{\eta}{h}\right)^2 = \frac{U^2}{2gh}\left[-2\frac{\phi_x(x,z)}{U} - \left(\frac{\phi_z}{U}\right)^2 + O\left(\frac{\phi_x}{U}\right)^2\right] \quad (29.30)$$

where for any (x,z) we obtain ϕ_x and ϕ_z from (29.27). The term ϕ_z^2 must be included in (29.30), although ϕ_x^2 must be omitted in order to be consistent with linearized theory, for application to large values of z since (29.29) shows that ($\phi_z \sim 1/z$) whereas ($\phi_x \sim 1/z^2$) for large values of z. However for small values of z the term ϕ_z^2 must also be neglected. For example, on the surface of the two-dimensional profile ($z = z_o$), (29.30) reduces to

$$\frac{\eta(x,z_o)}{h} = -\frac{U^2}{gh}\frac{1}{\pi\beta}\left[\lim_{\epsilon\to 0}\left(\int_0^{x-\epsilon} + \int_{x+\epsilon}^{L}\right)\frac{z_o'(\xi)\,d\xi}{(x-\xi)} + O(z_o'^2)\right] \quad (29.31)$$

since ϕ_x and ϕ_z are both of $O(z_o')$.

These relations are of course completely restricted to flows that are everywhere subcritical since (29.23) shows that the Froude number ($F = U/\sqrt{gh}$) must be everywhere less than unity to keep $\beta > 0$. The effect of increasing Froude number is to increase ϕ_x, and therefore decrease η, since β decreases. It is seen that this effect increases as z increases, the greatest effect being on $\phi_x \sim 1/\beta^3$ in the limiting case of very large values of z as shown in (29.29). This relation, or preferably (29.27), could be used to predict the additional change in $\eta(x,y)$ due to a finite stream width by using the increment of ϕ_x from one mirror image to represent the first approximation to the channel boundary wall as indicated in Figure 38. For slender cylinders in a narrow channel the "one-dimensional" approximation of section 30-7 is generally used, this allows an approximation for frictional head loss which becomes relatively more important as the channel width decreases.

For supercritical flow ($F = U/\sqrt{gh} > 1$), (29.23) must be written as

$$B^2\phi_{xx} - \phi_{zz} = 0 \quad \text{or} \quad \frac{\partial^2\phi}{\partial x^2} = \frac{\partial^2\phi}{\partial (Bz)^2} \tag{29.32}$$

$$B^2 = (F^2 - 1) = \left(\frac{U^2}{gh} - 1\right) = \text{constant} > 0$$

Now, however (29.32) cannot provide a satisfactory approximation of the change in water depth at some distance from the two-dimensional profile since its general solution is

$$\phi(x,z) = G(x-Bz) + g(x + Bz) \tag{29.33}$$

which predicts no change, even upon approaching infinity, along the lines of constant slope $dz/dx = \pm \frac{1}{B} = \pm \frac{1}{\sqrt{F^2-1}}$

Consequently the nonlinear method of characteristics, as will be described in section 30, must be used in predicting the depth variation at any finite distance from the profile. Although the method of characteristics will directly and easily give the velocity distribution or depth variation on the profile itself, we will now derive the linearized variation valid on the profile surface. The result will be of crucial importance in evaluating the validity of the nonlinear first-order shallow-water theory (28.1), since any great discrepancy between the linearized result and the nonlinear results from (28.1) would indicate that the perturbations involved are sufficiently large that the second-order shallow-water theory of section 31 must be introduced.

The linearized solution of (29.32) for any sharp-nose slender two-dimensional profile, as in Figure 38, is obtained from the general solution (29.33) and the linearized boundary condition (29.24) as follows: $z_o'(x) = \frac{\phi_z(x,z_o)}{U} = -\frac{BG'(x-Bz_o)}{U}$; $z=z_o > 0$

therefore $G'(x-Bz_o) = -\frac{U}{B} z_o'(x)$

so that on the profile surface ($z = z_o$)

$$u(x,z_o) = U + \phi_x = U + G'(x-Bz_o) = U[1 - \frac{z_o'(x)}{B}]$$

$$w(x,z_o) = Uz_o'(x) \qquad (29.34)$$

Then the variation in water depth on the profile surface is given by (29.30) as

$$\frac{\eta(x,z_o)}{h} = F^2 [\frac{z_o'(x)}{B} + O(z_o')^2] \qquad (29.35)$$

For flow that is everywhere supercritical so $B^2 = (F^2 - 1) > 0$

It should be noted that (29.23) and (29.32) are identical to the linearized potential equations for two-dimensional steady subsonic flow and supersonic flow respectively if we simply replace the Froude number ($F = U/\sqrt{gh}$) by the Mach number ($M = U/C$), see (28.3). This is in complete accord with the statement that the hydraulic analogy is valid for the flow over a flat horizontal bottom (which is equivalent to the two-dimensional isentropic flow of a fictitous perfect gas having a specific heat ratio of $\gamma = 2$). Consequently equations (29.24) through (29.29) are identical to the subsonic flow about slender two-dimensional profiles in free air or in a rectangular cross-section wind tunnel as derived by Laitone [1946]. These equations confirm the known result that the linearized equations are independent of the value of the specific heat ratio γ. Similarly equation (29.34) is identical to the well-known linearized two-dimensional supersonic flow solution if we let
$(F^2 - 1) = B^2 = (M^2 - 1) > 0$.

Although these linearized results are very satisfactory for slender sharp nose profiles, they only apply for Froude numbers that are not too near unity. That is they are not applicable to flows near critical ($U = \sqrt{gh} = c$, equivalent to sonic flow). For these cases we must return to the nonlinear equation (28.1) as discussed in section 30.

30 - Nonlinear Shallow-water Theory.

This section will primarily discuss methods for obtaining solutions of the nonlinear equation (28.1) which provides the first-order approximation of the shallow-water theory. The special cases to be considered are the one-dimensional unsteady flow and the two-dimensional steady flow in open channels. This will provide a basis for discussing the one-dimensional assumption of open channel flow. Finally the hydraulic jumps, and their relation to the first-order shallow-water theory, will be discussed.

30 α - One-dimensional Non-steady, First-order, Shallow-water Theory.

By assuming one-dimensional flow in the x direction only, the nonlinear equation (28.1) reduces to

$$u_t + uu_x + g\,(\eta + h)_x = gh_x \qquad (30.1)$$

$$(\eta + h)_t + [u(\eta + h)]_x = h_t = 0$$

again it should be noted that these are equivalent to the gas dynamics equations upon introducing (28.3), only if the bottom is flat and horizontal so $h_x = 0$.

Now if we let

$$c^2(x,t) = g\,[\,\eta(x,t) + h(x)\,] \qquad (30.2)$$

$$2cc_x = g(\eta + h)_x$$

$$2cc_t = g(\eta + h)_t$$

and give the initial conditions as $du/d\alpha$ and $dc/d\alpha$ along a space curve defined by $x(\alpha)$, $t(\alpha)$, then we may write (30.1) as

$$u(u_x) + (u_t) + 2c(c_x) + 0 = gh_x\,; \quad c(u_x) + 0 + 2u(c_x) + 2(c_t) = 0$$

$$x_\alpha\,(u_x) + t_\alpha\,(u_t) + 0 + 0 = \frac{du}{d\alpha} \qquad (30.3)$$

$$0 + 0 + x_\alpha\,(c_x) + t_\alpha\,(c_t) = \frac{dc}{d\alpha}$$

This set of four equations can be solved uniquely for u_x, u_t, c_x, c_t as long as the determinant of the coefficients in (30.3) does not vanish. Consequently this necessary condition is violated along the characteristic curves $x(\alpha)$, $t(\alpha)$ defined by

$$\begin{vmatrix} u & 1 & 2c & 0 \\ c & 0 & 2u & 2 \\ x_\alpha & t_\alpha & 0 & 0 \\ 0 & 0 & x_\alpha & t_\alpha \end{vmatrix} = 0 \qquad (30.4)$$

which may be easily expanded by the minors of the bottom row to obtain

$$[x_\alpha^2 - 2ux_\alpha c_\alpha + (u^2 - c^2)t_\alpha^2] =$$

$$= [x_\alpha - (u - c)t_\alpha][x_\alpha - (u + c)t_\alpha] = 0$$

Therefore the characteristic curves are defined by

$$x_\alpha / t_\alpha = \left(\frac{dx}{dt}\right)_{C t_\pm} = [u(x,t) \pm c(x,t)] \qquad (30.5)$$

Since h_x is given, and appears only on the right hand side of the first equation in (30.3) therefore the characteristic curves as defined in (30.5) are identical to those in the gas dynamics case, e.g. see Courant and Friedrichs [1948]. However, the Riemann invariants, or quantities that can be constant along a characteristic curve, now depend upon the bottom slope as may be seen by adding the two equations in (30.1) after introducing (30.2) so as to obtain

$$(u + 2c)_t + (u + c)(u + 2c)_x = gh_x =$$

$$= \left[\frac{\partial}{\partial t} + (u + c)\frac{\partial}{\partial x}\right][u(x,t) + 2c(x,t)] \qquad (30.6)$$

These give the same Riemann invariants as in the isentropic one-dimensional unsteady gas flow with a specific heat ratio of $\gamma = 2$ only if $h_x = 0$, e.g. see Courant and Friedrichs [1948] page 87. No simple Riemann invariant involving only u and c is possible if h_x varies with x, however if h_x is constant, so $gh_x = m$ = constant,

then (30.6) may be written

$$\left[\frac{\partial}{\partial t} + (u + c) \frac{\partial}{\partial x} \right] [u + 2c - mt] = 0 \qquad (30.7)$$

Similarly, by subtracting the two equations in (30.1), we obtain

$$\left[\frac{\partial}{\partial t} + (u - c) \frac{\partial}{\partial x} \right] [u - 2c - mt] = 0 \qquad (30.8)$$

Consequently the basic statements relating the characteristic curves and Riemann invariants of equation (30.1) with $gh_x = m$ = constant may be summarized as follows:

$$(u + 2c - mt) = R(x, t) = \text{constant along a curve } C_+ \text{ defined by } \left(\frac{dx}{dt}\right)_{C_+} = (u + c) \qquad (30.9)$$

$$(u - 2c - mt) = -S(x,t) = \text{constant along a curve } C_- \text{ defined by } \left(\frac{dx}{dt}\right)_{C_-} = (u - c)$$

Figure 39 shows typical sets of curves in the (x,t) plane. The above equations show that in any given region in the (x,t) plane there are three basic types of solutions, namely:

(1) The constant steady state in which u and c remain constant everywhere in the region so all characteristics form straight lines,

(2) The general flow in which neither R nor S is constant in a finite region,

(3) The special case of a simple wave over a flat horizontal bottom (m = 0) wherein a constant steady state region is separated from a varying region by a straight characteristic line along which either R or S, is constant.

The first type solution obviously has R and S constant throughout the region only if the bottom is flat and horizontal (m = 0). The second type of solution is complicated and can best be obtained by the method of finite differences, e. g. see Stoker [1957] pages 293-300. The third type of solution will now be discussed since it has considerable physical significance for many problems concerning the propagation of

a disturbance into water that is originally at constant depth and constant velocity, and extends an unlimited distance for $x > 0$.

When a disturbance moves into still water at constant depth over a flat horizontal bottom ($m = 0$), then it is obvious that $(dx/dt)_o = c(\infty)$ is the characteristic, which is now a straight line, that must continually separate the steady state region from the disturbance region in the (x,t) plane as indicated in Figure 39. This characteristic curve must be a straight line since there is a constant steady state always ahead of it so that $(dx/dt)_o$ = constant and therefore $x_o = c(\infty)t$. Also either R or S must be constant along the characteristic, and since R_o corresponds to C_+^o or $(dx/dt)_o = c(\infty) > 0$, as in Figure 39, therefore $R_o = 2c(\infty)$ = constant. This type of simple wave having $\left(\frac{dx}{dt}\right)_o = c(\infty) > 0$ and $R_o = 2c(\infty)$ = constant is called a forward-facing wave since the particle paths enter from the side with greater values of x, as in Figure 39. The value of R varies on each C_+ characteristic inside the region of the disturbance since u and c both vary due to the disturbance and none of the C_+ characteristic lines can ever intersect C_+^o. However, every C_- characteristic terminates at C_+^o, as shown in Figure 39, and since S remains constant on any given C_- characteristic curve, therefore S is everywhere constant since every C_- characteristic must have the same value $S(x,t) = R_o = 2c(\infty)$ = constant on C_+^o.

The same considerations are true even if the steady state constant depth water into which the disturbance is being propagated is flowing with a constant velocity $u(\infty) < c(\infty)$. The only change is that now the following are constant,

$\left(\frac{dx}{dt}\right)_o = [u(\infty) + c(\infty)] > 0$, $R_o = [2c(\infty) + u(\infty)]$ on Q_+^o only, while on all C_-, $[2c(x,t) - u(x,t)] = S(x,t) = [2c(\infty) - u(\infty)] =$ constant. Similarly all R in the disturbance region vary as

$R(x,t) = [2c(x,t) + u(x,t)]$

as indicated in Figure 39 for the simple forward-facing (C_+^o) wave. As shown in Figure 40.a simple backward-facing(C_-^o)occurs if R=constant & S=2c-u.

These waves are called simple waves because all the characteristics of the family which has the Riemann invariant take on a different constant for each line, must form straight lines. For example, referring to Figure 39, the forward-facing waves ($dx/dt > 0$) have S(x,y) constant everywhere and R(x,y) varying so the C_+ characteristics form straight lines. On the other hand in Figure 40, the backward-facing wave ($dx/dt < 0$) has R(x,y) constant everywhere and S(x,y) varying so now only the C_- characteristics form straight lines. The characteristics of one family only must form straight lines in a simple wave because only one of the Riemann invariants (S or R) is constant in the entire region of the disturbance. For example, in the case of the forward-facing simple wave in Figure 39, we have S constant in the region of the disturbance. Therefore from (30.9) and Figure 39 we may write,

$-S_1 = -S_2 = -S_3 = -S_4 = (u_1 - 2c_1) = (u_2 - 2c_2) = (u_3 - 2c_3) = (u_4 - 2c_4) =$ constant.

$R_1 = R_3 = (u_1 + 2c_1) = (u_3 + 2c_3) \neq R_2 = R_4 = (u_2 + 2c_2) = (u_4 + 2c_4)$

Consequently, $u_1 = u_3$, $c_1 = c_3$, $u_2 = u_4$, $c_2 = c_4$, and

$u_1 \neq u_2$, $c_1 \neq c_2$, $u_3 \neq u_4$, $c_3 \neq c_4$ so that

$\left(\frac{dx}{dt}\right)_{C_-} = (u_1 - c_1) \neq (u_2 - c_2) \neq$ constant, so C_- is curved

$\left(\frac{dx}{dt}\right)_{C_+^o} = (u_1 + c_1) = (u_3 + c_3) =$ constant, so C_+^o is straight

$\left(\frac{dx}{dt}\right)_{C_+} = (u_2 + c_2) = (u_4 + c_4) =$ constant so C_+ is straight.

It is important to note that these simple waves can exist only over a flat horizontal bottom so m = 0.

We have now shown how the method of characteristics for one-dimensional unsteady flow has resulted in the concept of the simple wave which quickly gives a numerical evaluation of the propagation of a one-dimensional disturbance into water at a constant depth that is moving at constant speed. The solution of this problem in the (x,t) plane can be obtained by direct application of (30.9). For example, the usual case of a forward-facing wave having S everywhere constant, and straight C_+ characteristic lines, as shown in Figure 39, has the slope of the C_+ straight lines determined directly by the time history of the disturbance at x = 0, and equations (30.2) and (30.9) which show that

$$\left(\frac{dx}{dt}\right)_{C_+} = u(0,t) + c(0,t) = \text{constant} = u(0,t) + \sqrt{g[h + \eta(0,t)]} \quad (30.10)$$

and along any given C_+ straight line having this constant slope

$$R(x,t)_{C_+} = u(0,t) + 2c(0,t) = \text{constant} = u(0,t) + 2\sqrt{g[h+\eta(0,t)]} \quad (30.11)$$

Consequently the values of u and c are determined in the entire region shown in Figure 39 by the given values on the t-axis. The curved C_- characteristics need not be calculated, since the desired numerical solution is independent of them. Their existence however can lead to a simplification in the numerical calculation of (30.10) since, in the case shown in Figure 39, each curved C_- characteristic extends from the C_+^o characteristic to the t-axis, and on each and every C_- characteristic, $-S = [u(\infty) - 2c(\infty)] = \text{constant}$. Therefore at every point on the t-axis that can be reached by a C_- characteristic we must have

$$S = [2c(0,t)-u(0,t)] = [2c(\infty)-u(\infty)] = [2\sqrt{gh} - u(\infty)] = \text{constant} \quad (30.12)$$

Of course the c_- characteristics can continue from C_+^o to the t-axis only if $\left(\frac{dx}{dt}\right)_{C_-} = (u - c) < 0$, or $u < c$, so that in this case (30.10) may be simplified to

$$\left(\frac{dx}{dt}\right)_{C_+} = u(0,t) + c(0,t) = \text{constant} = \tag{30.13}$$

$$= \left\{(3/2)u(0,t) - (1/2)[u(\infty) - 2c(\infty)]\right\} = \left\{(3/2)u(0,t) - (1/2)u(\infty) + \sqrt{gh}\right\} =$$

$$= \left\{3c(0,t) + [u(\infty) - 2c(\infty)]\right\} = \left\{3\sqrt{g[h + \eta(0,t)]} + u(\infty) - 2\sqrt{gh}\right\}$$

Consequently the problem is solved in the region so defined if either $u(0,t)$ or $c(0,t)$ is alone given. The surface elevation would be given by (30.2) as

$$h + \eta(x,t) = \frac{c^2(x,t)}{g}, \quad h = \frac{c^2(\infty)}{g} = \text{constant} \tag{30.14}$$

in every case of disturbance propogations into a constant water depth over a flat horizontal bottom so $m = 0$.

Many other physical problems can be simulated by giving the data along a prescribed curve (x,t) for $x = 0$, e.g., see Stoker [1957] where the disturbance created by the breaking of a dam, and the effect of moving a vertical end plate in a rectangular cross-section tank of still water, $u(\infty) = 0$, are considered. Since the bottom is flat and horizontal and $m = 0$, all of the equations following (30.9) are equivalent to the gas dynamics equations with a specific heat ratio of $\gamma = 2$, consequently the problems in finite channel lengths which produce wave reflections at either end, as solved in Courant and Friedrichs [1948], are also applicable. In this hydraulic analogy to compressible flow it is important to note that (30.13) is only applicable to subcritical flow, which is equivalent to subsonic gas flow, since we must have $\left(\frac{dx}{dt}\right)_{C_-} = (u-c) < 0$, or $u(\infty) < c(\infty) = \sqrt{gh}$.

When the flow is supercritical, so that $u(\infty) > c(\infty) = \sqrt{gh}$, corresponding to supersonic gas flow, then the slope of both the C_+ and C_- characteristics are negative. Consequently the two families can meet in a cusp, and the C_- characteristics cannot intersect both the t-axis and the undisturbed steady supercritical state that lies at, and to the right of, C_+^o. Therefore, in order to apply (30.13) for supercritical flow the region of the constant value of S, as given by (30.12), must be very carefully defined.

Another limitation on all the preceding equations is indicated for the compression wave depicted in Figures 39 and 40. This limitation is defined by the envelope of the straight characteristic lines that must always form for a compression wave in this first order theory, as will be proven later. This envelope of the straight characteristic lines corresponds to a discontinuity that can be interpreted as a discontinuity in η, or the breaking of the wave crest. This leads to the hydraulic jump or surge that will be discussed later. The gas dynamic case has the envelope of the straight characteristic lines interpreted as a steady-state shock wave, e.g. see Courant and Friedrichs [1948] pages 110-181.

30-β - Two-dimensional, Steady, Supercritical Flow by the First-order Shallow-water Theory.

We will now investigate the characteristic curves of the nonlinear equations of the first-order shallow-water theory for the case of steady two-dimensional flow. We will find that real characteristic curves, that are a great aid to numerical calculations, exist only in the regions wherein the flow is everywhere supercritical.

If we consider the steady two-dimensional flow over a flat horizontal bottom, then we may write (28.2) as

$$\begin{aligned} uu_x + wu_z &= -g(\eta + h_o)_x = -(c^2)_x \\ uw_x + ww_z &= -g(\eta + h_o)_z = -(c^2)_z \\ [u(\eta + h_o)]_x + [w(\eta + h_o)]_z &= 0 = (uc^2)_x + (wc^2)_z = 0 \\ u = \phi_x,\ w = \phi_z,\ u_z &= w_x = \phi_{xz} \end{aligned} \tag{30.15}$$

By multiplying the first equation by $u = \phi_x$ and the second by $w = \phi_z$, and adding, we obtain

$$[\phi_x^2\phi_{xx} + 2\phi_x\phi_z\phi_{xz} + \phi_z^2\phi_{zz}] = -[\phi_x^2(c^2)_x + \phi_z^2(c^2)_z] =$$

$$= [(\phi_{xx} + \phi_{zz})\, c^2] \tag{30.16}$$

Therefore

$$\left(\frac{\phi_x^2}{c^2} - 1\right)\phi_{xx} + 2\,\frac{\phi_x\phi_z}{c^2}\,\phi_{xz} + \left(\frac{\phi_z^2}{c^2} - 1\right)\phi_{zz} = 0 \tag{30.17}$$

or,

$$\left(1-\frac{u^2}{c^2}\right)\phi_{xx} - 2\,\frac{uw}{c^2}\,\phi_{xz} + \left(1 - \frac{w^2}{c^2}\right)\phi_{zz} = 0 \tag{30.18}$$

where $c^2(x,z) = g[h_o + \eta(x,z)]$ and h_o now is the still water depth found whenever $(u^2 + w^2) = 0 = \eta$. Note that (30.18) immediately linearizes to (29.3), so the numerical differences between the solutions of (29.3) and (30.18) will provide an estimate of whether or not the second-order shallow-water theory, as discussed in section 31, must be introduced.

The characteristic curves of (30.18) may be found in a manner similar to that used for (30.3) by finding the space curve $[x(\alpha), z(\alpha)]$ along which prescribed values of ϕ_x and ϕ_z cannot determine ϕ_{xx}, ϕ_{xz}, and ϕ_{zz}. Therefore we write

$$(1-\frac{u^2}{c^2})\phi_{xx} + (-2\frac{uw}{c^2})\phi_{xz} + (1-\frac{w^2}{c^2})\phi_{zz} = 0$$

$$(x_\alpha)\phi_{xx} + (z_\alpha)\phi_{xz} + 0 = \frac{d(\phi_x)}{d\alpha} \qquad (30.19)$$

$$0 + (x_\alpha)\phi_{xz} + (z_\alpha)\phi_{zz} = \frac{d(\phi_z)}{d\alpha}$$

which may not have a solution if the determinant of the coefficient is zero, that is if

$$\begin{vmatrix} (1-\frac{u^2}{c^2}) & (-\frac{2uw}{c^2}) & (1-\frac{w^2}{c^2}) \\ (x_\alpha) & (z_\alpha) & 0 \\ 0 & (x_\alpha) & (z_\alpha) \end{vmatrix} = 0 \qquad (30.20)$$

or,

$$(1-\frac{u^2}{c^2})(z_\alpha)^2 + (2\frac{uw}{c^2})z_\alpha x_\alpha + (1-\frac{w^2}{c^2})(x_\alpha)^2 = 0$$

$$\frac{z_\alpha}{x_\alpha} = (\frac{dz}{dx})_{c_+,-} = \left[\frac{(\frac{uw}{c^2}) \pm \sqrt{(\frac{u^2+w^2}{c^2}) - 1}}{(\frac{u^2}{c^2} - 1)}\right] \qquad (30.21)$$

which therefore gives the slope of the two families (c_+ and c_-) of characteristic curves. Now however, entirely unlike the previous one-dimensional unsteady flow solution, the characteristics curves exist only for supercritical flow so that $(u^2 + w^2) > c^2 = g(h_o+\eta)$. The fact that the characteristic curves are real for supercritical flow means that in this case the nonlinear equation (30.17) is hyperbolic. However for subcritical flow, since the characteristic curves are then imaginary (complex) functions, it is of the elliptic type, e.g. see Courant and Friedrichs [1948] pages 40-55, or Preiswerk [1938].

We can obtain a solution for the variation of the quantity

$$F(x,z) = \sqrt{\frac{u^2+w^2}{c^2}} \gtrless 1 \qquad (30.22)$$

(Which defines the Froude number of the supercritical flow) along a characteristic curve by transforming (30.18) into the hodograph (u,w) plane through the use of the Legendre contact transformation which is given by,e.g. see Courant and Friedrichs [1948] page 249 or Preiswerk [1938]; $\chi = (x\phi_x + z\phi_z - \phi) = (xu + zw - \phi)$

$d\chi = (xdu + udx + zdw + wdz - d\phi) = (xdu + zdw)$

therefore $x = \chi_u$, $z = \chi_w$. $dx = x_u du + x_w d_w = \chi_{uu} du + \chi_{uw} dw$

$dy = z_u du + z_w dw = \chi_{uw} du + \chi_{ww} dw$.

Solving for du and dw we obtain

$du = 1/N\,(\chi_{ww} dx - \chi_{uw} dz) = d\phi_x = (\phi_{xx} dx + \phi_{xz} dz)$

$dw = 1/N\,(-\chi_{uw} dx + \chi_{uu} dz) = d\phi_z = (\phi_{xz} dx + \phi_{zz} dz)$

where $N = \begin{vmatrix} \chi_{uu} & \chi_{uw} \\ \chi_{uw} & \chi_{ww} \end{vmatrix} \neq 0$

so that $\phi_{xx} = \frac{\chi_{ww}}{N}$; $\phi_{xz} = -\frac{\chi_{uw}}{N}$; $\phi_{zz} = \frac{\chi_{uu}}{N}$

and therefore the nonlinear equation (30.17) in the physical (x,z) plane is transformed into a linear equation in the hodograph (u,w) plane, as given by

$$\left(\frac{w^2}{c^2} - 1\right)\chi_{uu} - 2\,\frac{uw}{c^2}\,\chi_{uw} + \left(\frac{u^2}{c^2} - 1\right)\chi_{ww} = 0 \qquad (30.23)$$

The same procedure as used in (30.19) through (30.21) or a simple comparison of (30.17), (30.21), and (30.23), shows that the characteristic curves of (30.23) in the hodograph (u,w) plane are defined by

$$\frac{w_\alpha}{u_\alpha} = \left(\frac{dw}{du}\right)_{\Gamma_+} = \left[\frac{-\left(\frac{uw}{c^2}\right) \pm \sqrt{\left(\frac{u^2 + w^2}{c^2}\right) - 1}}{\left(\frac{w^2}{c^2} - 1\right)}\right] \qquad (30.24)$$

The characteristic curve Γ_- in the hodograph (u,w) plane is orthogonal to the characteristic curve C_+ in the physical (x,z) plane if we superimpose the two planes so that the velocity vectors coincide. This may be easily shown by rotating the axes for (30.21) and

(30.24) so that w = 0 (see Figure 41), and the equations for the slopes of the characteristic curves C_+ and Γ_- simplify to

$$\left(\frac{dz}{dx}\right)_{C+} = \frac{1}{\sqrt{\frac{u^2}{c^2} - 1}} = \frac{1}{\sqrt{F^2 - 1}} = -1/\left(\frac{dw}{du}\right)_{\Gamma_-} \qquad (30.25)$$

Similarly Γ_+ is orthogonal to C_- when the planes are superimposed so the velocity vectors are coincident (see Figure 41).

Equations (30.24) and (30.25) show that along any characteristic curve there exists a simple solution which is independent of the boundary conditions of a particular problem, since we can directly integrate (30.25)

$$\left(\frac{dw}{du}\right)_{\Gamma_-} = \left(\frac{ud\theta}{du}\right)_{\Gamma_-} = -\sqrt{\frac{u^2}{c^2} - 1} = -\sqrt{F^2 - 1}$$

for axes rotated so w = 0 (dw = udθ), see Figure 41. We thereby integrate* (30.25) as

$$\int_{\Gamma_-} d\theta = -\int_{\Gamma_-} \sqrt{\frac{u^2}{c^2} - 1}\ \frac{du}{u} = -\int_{\Gamma_-} \frac{\sqrt{F^2-1}}{1 + \frac{F^2}{2}}\ \frac{dF}{F}$$

$$|\Delta\theta| = \left[\sqrt{3}\ \tan^{-1}\sqrt{\frac{F^2-1}{3}} - \tan^{-1}\sqrt{F^2-1}\right] = f(F) \qquad (30.26)$$

Consequently (30.26) provides a general solution, independent of the boundary conditions in the physical plane, for any two-dimensional potential flow that possesses the property of having simple waves in the given region so that the velocity vector follows Γ_- in the hodograph plane. The numerical values from (30.26) are

---

* see (30.27) and (30.29) which show that with w = 0

$$\frac{du}{u} = -\frac{d(c^2)}{u^2} = +\frac{c_o^2}{u^2}\left(1 + \frac{F^2}{2}\right)^{-2} F dF = +\frac{dF}{F(1+F^2/2)}$$

indicated in Figure 41 and are tabulated in Table I (taken from Freiswerk [1938].

The useful relation between c and (u,w) that was used to integrate (30.26) and calculate Table I is obtained by ultiplying the first equation in (30.15) by dx and the second equation by dz, and then adding them so as to obtain

$$u(u_x d_x + u_z d_z) + w(w_x d_x + w_z d_z) = -[(c^2)_x dx + (c^2)_z dz]$$

$$udu + wdw = -d(c^2) = -gd\eta$$

$$1/2\,(u^2 + w^2) + c^2 = \text{constant} = 1/2(u^2 + w^2) + g(h_o + \eta) \qquad (30.27)$$

Therefore

$$\left(\frac{u^2 + w^2}{2}\right) + c^2 = \left(\frac{u^2+w^2}{2}\right) + g(h_o + \eta) =$$

$$= (gh_o) = \left(\frac{u^2+w^2}{2}\right)_{max} = \left(\frac{3}{2} c_*^2\right) = \frac{1}{2} q^2 + c^2 = \frac{1}{2} q_{max}^2 \qquad (30.28)$$

where (see Figure 42) h_o is the still water depth (or stagnation total head depth) that corresponds to $(u_o^2 + w_o^2) = 0 = \eta_o$, $(u^2 + w^2)_{max}$ is the limiting resultant velocity squared that is approached when the flowing water depth approaches zero ($\eta \to -h_o$), and c_* is the critical (F=1) speed when the resultant velocity $\sqrt{u^2 + w^2} = c_*$ is critical (F=1), so that

$$c_* = \sqrt{g(h_o + \eta_*)} = \sqrt{(2/3)(gho)} = \sqrt{(2/3)\left[\frac{c_*^2}{2} + g(h_o + \eta_*)\right]} =$$

$$= \sqrt{(1/3)(u^2 + w^2)_{max}} \;;\; \left(\frac{c_*}{c_o}\right)^2 = \frac{c_*^2}{gho} = 2/3 = -2\frac{\eta_*}{h_o}$$

$$\frac{\eta_*}{h_o} = -1/3, \quad \left(\frac{h_o + \eta_*}{h_o}\right) = 2/3, \quad \frac{(u^2 + w^2)_{max}}{c_*^2} = 3 \qquad (30.29)$$

$$\left(\frac{c_o}{c}\right)^2 = \frac{gh_o}{c^2} = \left(1 + \frac{u^2+w^2}{2c^2}\right) = \left(1 + \frac{F^2}{2}\right) = \left(\frac{c_o}{c_*}\right)^2 \left(\frac{c_*}{c}\right)^2 = (3/2)\left(\frac{c_*}{c}\right)^2 = \frac{h_o}{h}$$

$$F^2 = \left(\frac{u^2+w^2}{c^2}\right) = \left(\frac{c_*}{c}\right)^2 F_*^2 = \left[\frac{2F_*^2}{3 - F_*^2}\right]$$

$$F_*^2 = \left(\frac{u^2+w^2}{c_*^2}\right) = \left(\frac{c}{c_*}\right)^2 F^2 = \left[\frac{3F^2}{2+F^2}\right] \qquad (30.29)\ \text{cont'd}$$

It is very useful to note that equations (30.26) through (30.29) may all be obtained directly from the two-dimensional isentropic gas flow equations by simply letting the specific heat ratio $\gamma = 2$ and $F \equiv M$, $F_* \equiv M_*$; e.g. compare with Courant and Friedrichs [1948], as had been previously shown by Preiswerk [1938].

The Riemann invariants for the characteristic curves (C_+, C_-) will now be determined. First we can show that the velocity component normal to the characteristic curves is always the local velocity of the shallow-water wave propagation, $c(x,z)$, by writing (30.21) as

$$(udz - wdx)^2_{C_+} = c^2[(dx)^2 + (dz)^2]_{C_+} = c^2(d\lambda)^2_{C_+}$$

$$c^2 = \left(u\frac{dz}{d\lambda} - w\frac{dx}{d\lambda}\right)^2_{C_+} = (\phi_x x_n + \phi_z z_n)^2_{C_+} = (\phi_n)^2_{C_+} \qquad (30.30)$$

since the relation between the normal direction (n), and the tangential direction (λ) along the characteristic curve (C_+) is given by (see Figure 41) $\left(\frac{dx}{dn}\right)_{C_+} = \left(\frac{dz}{d\lambda}\right)_{C_+}, \left(\frac{dz}{dn}\right)_{C_+} = -\left(\frac{dx}{d\lambda}\right)_{C_+}$

Similarly, if μ is the tangential direction along C_-,

$$c^2 = \left(u\frac{dz}{d\mu} - w\frac{dx}{d\mu}\right)^2_{C_-} = (\phi_x x_n + \phi_z z_n)^2_{C_-} = (\phi_n)^2_{C_-}$$

Also, from Figure 41 and (30.21)

$$\tan\alpha = \left(\frac{dz}{dx}\right)_{\substack{\phi=0 \\ C_+,\,-}} = \pm\frac{1}{\sqrt{F^2-1}}, \quad \sin\alpha = \frac{\pm 1}{F} = \pm\frac{c}{q} \qquad (30.31)$$

where q is the resultant velocity magnitude so

$$q^2 = (u^2+w^2) = (\phi_\lambda^2 + c^2) = (\phi_\mu^2 + c^2); \quad \theta = \tan^{-1}\left(\frac{w}{u}\right)$$

$$u = q\cos\theta, \quad w = q\sin\theta, \quad \phi_n = c = q\sin\alpha \qquad (30.32)$$

$$\phi_\lambda = q\cos\alpha = \phi_\mu$$

Substituting (30.31) and (30.32) into (30.21) and (30.24) we obtain

$$\left(\frac{dz}{dx}\right)_{C_+,-} = \left[\frac{\frac{\cos\theta\sin\theta}{\sin^2\alpha} \pm \frac{1}{\tan\alpha}}{\frac{\cos^2\theta}{\sin^2\alpha} - 1}\right] = \tan(\theta \pm \alpha) \qquad (30.33)$$

$$\left(\frac{dw}{du}\right)_{\Gamma_-,+} = \left[\frac{-\frac{\cos\theta\sin\theta}{\sin^2\alpha} \pm \frac{1}{\tan\alpha}}{\frac{\sin^2\theta}{\sin^2\alpha} - 1}\right] = -\cot(\theta \pm \alpha) \qquad (30.34)$$

Therefore, as proven before in (30.25),

$$\left(\frac{dz}{dx}\right)_{C_+}\left(\frac{dw}{du}\right)_{\Gamma_-} = -1 = \left(\frac{dz}{dx}\right)_{C_-}\left(\frac{dw}{du}\right)_{\Gamma_+} \qquad (30.35)$$

that is, as shown in Figure 41, the C_+ characteristic curves in the physical (x,z) plane are at every corresponding point orthogonal to the Γ_- characteristic curves in the hodograph (u,w) plane. All these results are the same as in the gas dynamics case where the $C_+,-$ characteristic curves are referred to as the Mach lines since, as shown by (30.30), the normal velocity component is always the local speed of sound.

Now, as shown in Figure 41,

$$\left(\frac{dw}{du}\right)_{\Gamma_-} = \tan\omega_{\Gamma_-}\ ; \quad \omega_{\Gamma_-} = (\theta + \alpha - \tfrac{\pi}{2})$$

$$\left(\frac{dw}{du}\right)_{\Gamma_+} = \tan\omega_{\Gamma_+}\ ; \quad \omega_{\Gamma_+} = (\theta - \alpha + \tfrac{\pi}{2})$$

therefore (30.33) may be written as

$$\left(\frac{dz}{dx}\right)_{C_+} = \tan(\theta + \alpha) = \tan\left(\omega_{\Gamma_-} + \tfrac{\pi}{2}\right)$$

$$\left(\frac{dz}{dx}\right)_{C_-} = \tan(\theta - \alpha) = \tan\left(\omega_{\Gamma_+} - \tfrac{\pi}{2}\right)$$

Consequently the Riemann invariants are given by

$$R = (\theta + \alpha - \omega_{\Gamma_-} - \tfrac{\pi}{2}) \qquad S = (\theta - \alpha - \omega_{\Gamma_+} + \tfrac{\pi}{2})$$

This may be simplified by calculating

$$\omega_{\Gamma_-} = \tan^{-1}\left(\frac{dw}{du}\right)_{\Gamma_-} = -\sqrt{3}\,\cot^{-1}\left[\sqrt{\frac{3}{F^2-1}}\right] = -\sqrt{3}\,\tan^{-1}\left[\sqrt{\frac{F^2-1}{3}}\right]$$

from (30.24) and Figure 41 since

$$\frac{1}{\sqrt{F^2-1}} = \left|\tan\alpha\right| = \sqrt{\frac{1}{3}}\,\left|\cot(\omega/\sqrt{3})\right| ,$$

or see Courant and Friedrichs [1948] page 266.

Therefore $R = \left(\theta + \tan^{-1}\frac{1}{\sqrt{F^2-1}} - \frac{\pi}{2} + \sqrt{3}\,\tan^{-1}\sqrt{\frac{F^2-1}{3}}\right) =$

$$= \left(\theta + \sqrt{3}\,\tan^{-1}\sqrt{\frac{F^2-1}{3}} - \tan^{-1}\sqrt{F^2-1}\right) = [\theta + f(M)]$$

$S = (\theta - \tan^{-1}\frac{1}{\sqrt{F^2-1}} + \frac{\pi}{2} - \sqrt{3}\,\tan^{-1}\sqrt{\frac{F^2-1}{3}}) =$

$$= (\theta - \sqrt{3}\,\tan^{-1}\sqrt{\frac{F^2-1}{3}} + \tan^{-1}\sqrt{F^2-1}) = [\theta - f(M)]$$

where f(M) is given by (30.26) and Table I. Consequently the Riemann invariants are very simply expressed for the characteristic curves in the physical plane as

$[\theta - f(M)]$ = constant on C_+ $\qquad$ $[\theta + f(M)]$ = constant on C_- (30.36)

The function f(M), which was derived from the trace of the velocity vector following the characteristics in the hodograph plane in (30.26), is seen to have important physical significance, and directly provides the Riemann invariants for the steady two-dimensional potential flow. In gas dynamics f(F) = f(M) is referred to as the Prandtl-Meyer expansion function and, in the form in which it is given in Table I, it corresponds to the supersonic free expansion about a sharp corner as shown in Figure 44 for the centered simple wave with a specific heat ratio of $\gamma = 2$. Since this Prandtl-Meyer function is so important, let us re-derive it on another basis that will further illustrate its physical significance. From the

fact that f forms the Riemann invariant, or from the nature of F or F_* alone, it is evident that u and w cannot be independent of one another on any such simple characteristic. Consequently, if we write the original potential equation (30.18) in the physical plane as

$$\left(\frac{u^2}{c^2} - 1\right) u_x + 2\,\frac{uw}{c^2}\,u_y + \left(\frac{w^2}{c^2} - 1\right) w_y = 0$$

and introduce $w = w(u)$ so that

$$w_y = u_y w'(u),\quad u_x w'(u) = w_x = \phi_{xz} = u_y$$

we obtain $$\left(\frac{u^2}{c^2} - 1\right)\frac{u_y}{w'} + 2\,\frac{uw}{c^2}\,u_y + \left(\frac{w^2}{c^2} - 1\right) u_y w' = 0$$

$$\text{or}\quad \frac{dw}{du} = w'(u) = \frac{-\frac{uw}{c^2} \pm \sqrt{\frac{u^2 + w^2}{c^2} - 1}}{\left(\frac{w^2}{c^2} - 1\right)} \qquad (30.24')$$

This derivation gives exactly the same result as in (30.24) and verifies the fact that discontinuities can occur in the first derivatives normal to a characteristic curve. If we introduce (30.32) into (30.24) we obtain the equivalent of (30.26)

$$\frac{1}{q}\left(\frac{dq}{d\theta}\right) = \tan\alpha = \frac{1}{\sqrt{F^2 - 1}} \qquad (30.37)$$

which again has f(F) as the general integral because (30.28) shows that

$$\frac{d\theta}{\sqrt{F^2 - 1}} = \frac{dq}{q} = \frac{d(q/C_*)}{(q/C_+)} = \frac{dF_+}{F_*} = \frac{1}{1 + \frac{F_2}{2}}\,\frac{dF}{F} \qquad (30.38)$$

However, neither of these methods gives the direct proof that f(F) provides the Riemann invariant. This fact may be proved directly by the following derivation which utilizes the velocity component ϕ_λ along the C_+ characteristic, and $\phi_n = c$, from (30.30), normal to C_+ as shown in Figure 41, so that

$$\phi_\lambda = q\cos\alpha\,, \quad \phi_n = c = q\sin\alpha$$

$$d(\phi_\lambda) = (\cos\alpha\, dq - q\sin\alpha\, d\alpha) = c(d\theta - d\alpha) \tag{30.39}$$

$$\lambda_z = 1/\sin(\theta+\alpha),\ \mu_z = 1/\sin(\theta-\alpha)$$

since, from (30.37), $dq = \frac{\sin\alpha}{\cos\alpha}\, q\,d\theta$

Then from (30.28) and (30.32) we have

$$\left(\frac{q^2}{2} + c^2\right) = \left(\frac{\phi_\lambda^2 + \phi_n^2}{2} + c^2\right) = \left(\frac{\phi_\lambda^2}{2} + \frac{3}{2}c^2\right) = \frac{q^2_{max}}{2} = \frac{3}{2}c_*^2 \tag{30.40}$$

$$c^2 = 1/3(q^2_{max} - \phi_\lambda^2) = (c_*^2 - 1/3\,\phi_\lambda^2)$$

so that (30.39) may be written

$$(\theta - \alpha) + \text{constant} = \int \frac{d(\phi\lambda)}{c} = \int \frac{d(\phi\lambda)}{\sqrt{1/3(q^2_{max} - \phi_\lambda^2)}} = \sqrt{3}\int \frac{d(\phi_\lambda/q_{max})}{\sqrt{1-(\phi_\lambda/q_{max})^2}}$$

$$= \sqrt{3}\ \sin^{-1}\left(\frac{\phi_\lambda}{q_{max}}\right) = \sqrt{3}\sin^{-1}\left(\frac{\phi_\lambda}{\sqrt{3c^2+\phi_\lambda^2}}\right) = \sqrt{3}\tan^{-1}\left(\frac{\phi\lambda}{c\sqrt{3}}\right) \tag{30.41}$$

This may be finally written in terms of (F) alone by noting from (30.39) that

$$\frac{\phi_\lambda}{c} = \frac{\phi_\lambda}{\phi_n} = \frac{q\cos\alpha}{q\sin\alpha} = \frac{1}{\tan\alpha} = \sqrt{F^2 - 1},$$

consequently (30.41) reduces to

$$\left[\theta(F) - \sqrt{3}\tan^{-1}\left(\sqrt{\frac{F^2-1}{3}}\right) - \tan^{-1}\frac{1}{\sqrt{F^2-1}} + \text{constant}\right] =$$

$$\left[\theta(F) - \sqrt{3}\tan^{-1}\left(\sqrt{\frac{F^2-1}{3}}\right) + \tan^{-1}\sqrt{F^2-1}\right] = [\theta - f(F)] = \text{constan} \tag{30.42}$$

where f(F) is the same Prandtl-Meyer function as given in (30.26) and Table I. Therefore we have proven that the Riemann invariants are given by (30.36) and (30.26). In addition to the relation between f and F in (30.26) it is sometimes convenient to use one of the following

$$f(\alpha) = [\sqrt{3}\cot^{-1}(\sqrt{3}\tan\alpha) + \alpha - \frac{\pi}{2}] =$$

$$- f(F_*) = [\sqrt{3}\tan^{-1}\sqrt{\frac{F_*^2 - 1}{3 - F_*^2}} - \tan^{-1}\sqrt{\frac{F_*^2 - 1}{1 - F_{*/3}^2}}] = \left(\frac{\lambda+\mu}{2}\right) \qquad (30.26')$$

Therefore a numerical solution can now be obtained for the general problem having both families of characteristics represent curved non-simple waves by carrying on a simultaneous finite difference solution in the physical (x,z) plane with (30.33), and in the hodograph (u,w) plane by (30.26), (30.34), and (30.36). Almost any initial or boundary value data can be handled in this manner as long as the curve on which the data is given is not coincident with a characteristic curve. The solution cannot be obtained in the neighborhood of any portion of the boundary value curve that happens to be tangent to any characteristic curve, because, as proven by (30.20), the solution is indeterminate for boundary value data given on a characteristic. It is easily seen by this finite difference method that the data along a smooth non-characteristic curve can only determine the solution inside the quadrilateral formed by the characteristic curves passing through its end points (Figure 43) e.g., see Preiswerk [1938]. This well-known behavior of hyperbolic type partial differential equations is most directly demonstrated by writing them in their normal or cannonical form by transforming the coordinates to curvilinear axes which are the characteristic curves themselves. For example, Preiswerk [1938] transforms the equivalent of (30.23) onto the curvilinear characteristic coordinate (λ, μ) system to obtain

$$f(F_*) = 1/2\,(\lambda+\mu), \quad \theta = 1/2\,(\lambda-\mu)$$

$$\chi_{\lambda\mu} = -K(\lambda,\mu)\,(\chi_\lambda + \chi_\mu) \tag{30.43}$$

$$K(\lambda,\mu) = \frac{F_*^2\,(1 - F_*^2/2)}{\sqrt{3}(3-F_*^2)^{1/2}(F_*^2-1)^{3/2}}$$

This normal or cannonical form is so useful in carrying out the finite difference method of solution that the values of K have also been included in Table I. It could be used in the following type of approximation, as indicated in Figure 43 where (1, 3) are known values and (2, 4) are to be calculated,

$$\chi_\lambda = \frac{\chi_4 - \chi_1}{\lambda_4 - \lambda_1}, \qquad \chi_\mu = \frac{\chi_2 - \chi_1}{\mu_2 - \mu_1},$$

$$\left(-\frac{K_1 + K_3}{2}\right)\left(\chi_\lambda + \chi_\mu\right) = \chi_{\lambda\mu} = \frac{(\chi_3 + \chi_1) - (\chi_4 + \chi_2)}{(\lambda_4 - \lambda_1)(\mu_2 - \mu_1)} \tag{30.43'}$$

Consequently if the data were given on only one characteristic curve the method would fail since the values must be known on <u>both</u> characteristics, or on the non-characteristic curve s in Figure 43 so that one can also write

$$\chi_s = \chi_\lambda \lambda_s + \chi_\mu \mu_s = g(s)$$

$$\chi_n = \chi_\lambda \lambda_n + \chi_\mu \mu_n = G(s)$$

The numerical method of solution by finite differences following (30.43') is known as the "lattice point method" and replaces the original partial differential equation (30.43) by a set of linear algebraic equations. The other commonly used semi-graphical method of solving hyperbolic partial differential equations is called the network or "mesh method" and can be illustrated by writing (30.43)

in the form

$$\Delta(\lambda_\lambda) = -K(\lambda_\lambda + \lambda_\mu)\,\Delta\mu$$
$$\Delta(\lambda_\mu) = -K(\lambda_\lambda + \lambda_\mu)\,\Delta\lambda \qquad (30.43'')$$

The average value at the center of each mesh formed by the characteristic network is used for the trial and error numerical calculation of each Δ increment. The increments are drawn tangent to the characteristic curves as indicated in Figure 43. The simultaneous semi-graphical solution must be carried out in the physical plane as shown in Figure 43 by using (30.33) and writing (30.39) and (30.41) in finite difference form.

As a further aid to numerical and graphical solutions it is useful to plot $f(F_*)$ from (30.26') or Table I on the hodograph $(u/c_*, w/c_*)$ plane as shown in Figure 43. The single curve defined by Table I may be drawn and then rotated by equal increments of $\Delta\theta$, or the construction may be accomplished entirely by graphical means as indicated in Figure 43 by rotating the small circle upon the inner unit circle representing critical flow, while the outer maximum circle has a radius of $\sqrt{3}$ representing q_{max}/c_* from (30.29). This geometrical construction yields $f(F_*)$ since it is an epicycloid, as proven by Preiswerk [1938], or Courant and Friedrichs [1948] page 262. All simple waves must follow the characteristic epicycloid in the hodograph plane because simple waves are defined by (30.37) which has been proven to have $f(F_*)$ as its integral. It can be shown that all streamlines corresponding to non-simple waves must lie within the corresponding characteristic epicycloids as indicated in Figure 43, since the streamline must have

$$\left| \frac{1}{F_*} \left(\frac{dF_*}{d\theta} \right)_{\psi \text{ const.}} \right| \leq \tan \alpha \qquad (30.44)$$

unless a finite discontinuity corresponding to a hydraulic jump (or shock wave in a gas) is formed.

Another useful aid in the hodograph graphical construction is the velocity ellipse which is also drawn in Figure 43. Wherever the velocity vector q touches the curve of the ellipse, it will be found that the major axis of the ellipse is in the direction of the tangent to the corresponding characteristic (either C_+ or C_-) in the physical plane because, as a consequence of (30.29) and (30.32), if we assume that $\theta = \alpha$ then

$$\left(\frac{w}{c_*} \right)^2 = F_*^2 \sin^2 \alpha = (F_*^2 \frac{1}{F^2}) = \left(\frac{3 - F_*^2}{2} \right)$$

$$\left(\frac{u}{c_*} \right)^2 = F_*^2 (1 - \sin^2 \alpha) = 3/2 \, (F_*^2 - 1)$$

$$\left[\frac{2}{3} \left(\frac{u}{c_*} \right)^2 + 1 \right] = F_*^2 = \left[3 - 2 \left(\frac{w}{c_*} \right)^2 \right]$$

$$\text{or} \quad \left[\frac{(u/c_*)^2}{3} + (w/c_*)^2 \right] = 1 = \left[\frac{(\phi_\mu / c_*)^2}{3} + \left(\frac{c}{c_*} \right)^2 \right]_{C_-(\theta=0)} =$$

$$= \left[\frac{(\phi_\lambda / c_*)^2}{3} + \left(\frac{c}{c_*} \right)^2 \right]_{C_+(\theta=0)} . \qquad (30.45)$$

This gives the velocity ellipse shown in Figure 43 with a major axis of $\sqrt{3}$ and a minor axis of unity. The major axis is always at the Mach angle α with respect to the velocity vector q because we find from (30.28) and (30.32) that when $\alpha = 0$

$$\left(\frac{w}{c_*} \right)^2 = \left(\frac{\phi_n}{c_*} \right)^2 = \left(\frac{c}{c_*} \right)^2 = [1 - 1/3 \left(\frac{u}{c_*} \right)^2]$$

As in the previous case of unsteady one-dimensional flow over a flat bottom we can obtain very simple solutions for the case of simple waves. In this case there is an analogy between the (t,x) diagram and the (x,z) diagram, e.g., see Courant and Friedrichs [1948]. As before the simple wave corresponds to the $(\frac{dz}{dx})$ characteristics of one family becoming straight lines, as in the examples shown in Figure 44, so that $(q, \theta, \alpha, \eta)$ are all constant on the straight line dz/dx = constant in the physical plane. Therefore any given straight characteristic line has all of its properties determined by $f(F_*)$ from (30.26) and each of the straight lines in the physical plane maps onto a single point of the same single characteristic epicycloid in the hodograph plane. The characteristics of the other family remain curved in the physical plane and map in a unique continuous manner upon the corresponding characteristic epicycloid arcs in the hodograph plane. As before, in a simple wave, these curved characteristics are not required for a numerical solution.

Common examples of simple wave problems are shown in Figure 44, and they always occur whenever a region of constant uniform properties adjoins a region having any variation in its properties, the two regions always being joined by a straight line physical characteristic ($\frac{dz}{dx}$ = constant) as long as no finite discontinuities, corresponding to hydraulic jumps or shock waves, have been formed. These finite discontinuities correspond to an envelope of the straight characteristic lines that must form whenever the boundary surface curves towards the oncoming flow, resulting in a flow compression or decrease of velocity and increase in water depth as indicated in Figure 44. The solution is no longer single valued at, or downstream of the

envelope so this region must be replaced by a hydraulic jump having a finite discontinuity and non-isentropic flow.

If the local flow velocity and water depth are required only on the curved boundary itself, then neither family of characteristics have to be determined (except as a precaution to verify that no finite discontinuities have formed near the boundary due to flow compression). The solution on the curved boundary itself is given directly from Table I by simply measuring $f(F_*)$ as the value corresponding to (see Figure 44)

$$f[F_*(\theta)] = f[F_{*_\infty}] \pm \theta \qquad (30.46)$$

If this expression becomes zero it signifies that the supercritical flow has been compressed to critical speed and a detached hydraulic jump can occur as in Figure 44.

Whenever disturbance waves enter along both families, either due to another boundary or by reflection from a hydraulic jump, as in Figure 42, then the mixed region contains non-simple waves, and only a numerical solution, similar to the ones discussed in conjunction with (30.43), can yield the exact solution. However, an approximate solution for the particular cases shown in Figure 42 can be obtained by approximating the curved characteristics in the non-simple region by means of simple wave, straight characteristic lines. The geometrical construction assumes that the curved boundary wall of the nozzle can be replaced by a series of straight chord lines that each have the same magnitude of $\Delta\theta$ at every corner as depicted in Figure 45. At each expansion corner it is assumed that the centered simple wave (corresponding to a portion of the complete Prandtl-Meyer expansion, f) can be approximated by a single physical characteristic that is the average of the actual expansion fan of

characteristics. This is the(dz/dx) straight line that is normal to the midpoint of the $\Delta\theta$ epicycloid arc representing the expansion angle change at this corner, as shown in Figure 45. Similarly, the compression corner that turns into the flow is represented by the single compression simple wave that is normal to the midpoint of the $\Delta\theta$ epicycloid arc representing the compression angle change at this corner. It will be shown that the angle of this single average compression wave is actually the correct limiting value for a weak hydraulic jump. The geometrical construction is carried out in the manner indicated in Figure 45. Whenever a streamline crosses one of these finite amplitude construction characteristics the flow is assumed to bend through the $\Delta\theta$ associated with the finite corner bend which supposedly produced this single finite wave. The corresponding construction in the hodograph plane transfers to the epicycloid arc that is normal to the single finite wave in the physical plane as shown in Figure 45.

Also shown in Figure 45 are the geometric constructions required for the reflection of these simple finite waves in the physical plane from either solid boundaries, or constant water depth free boundaries. In the reflection from a solid boundary the original boundary slope is again attained by the velocity vector after passing through the reflected wave which has the same strength for flow deflection as the original oncoming finite simple wave. In the hodograph plane the streamline has gone from one family of epicycloids to the other, ending at the same value of θ. The completed solution for the flow inside a varying width channel having supercritical flow ($F > 1$) is presented in Figure 42. For additional details and aids on the graphical constructions see Preiswerk [1938]. As another example

in Figure 45, consider the reflection from a free jet, hydraulic jump, or any constant water depth free boundary, which must occur in such a manner that the same water depth is maintained after passing through the reflected wave which is not only on the opposite family of epicycloid arcs, but now must have the negative algebraic strength of the flow deflection of the original oncoming wave; consequently the value of $\Delta\theta$ is exactly doubled after passing through the reflected wave. That is to say, unlike the ordinary reflection from a solid boundary, the reflection from a constant depth free boundary results in the opposite type of wave, an expansion wave becomes a compression wave and vice versa.

In conclusion it must be noted that this two dimensional steady flow analysis is only valid for a flat horizontal bottom as was already shown by (29.3) for the linearized equations. If the bottom slope varies then the Riemann invariants do not exist, simple waves do not occur, and the numerical solution is much more complicated. However, there is an even more important criterion that must be satisfied before <u>any</u> of the solutions given so far can be applicable. This is the necessary requirement that all the perturbation quantities involved ($u - U$, w, η) must be sufficiently small so that it is not necessary to introduce the second order terms from section 31. A satisfactory evaluation of this criterion, at least for F not too near unity, can be obtained by comparing the solutions of the non-linear equation (30.17) with the linearized equation (29.23) or (29.32). As is well-known in gas dynamics, and is apparent by inspection, (29.23) and (29.32) are not satisfactory for F approaching unity since additional terms must then be retained. For example, on the boundary profile itself, (29.3) for a flat horizontal bottom

must include the additional term $3F^2(\phi_x/U)\phi_{xx}$, which corresponds to the "transonic approximation" of the gas dynamic equation (with a specific heat ratio of $\gamma = 2$), in the limit as F approaches unity. However, for the solution of the steady flow everywhere about a two-dimensional profile it may be necessary to use

$$[(1 - F^2)\,\phi_{xx} + \phi_{zz}] = F^2[3\,\frac{\phi_x}{U}\,\phi_{xx} + 2\,\frac{\phi_z}{U}\,\phi_{xz}] \qquad (30.47)$$

since (29.29) indicates that far from the profile $(w/U) = (\phi_z/U) \sim 1/z$ whereas $\left(\frac{u-U}{U}\right) = (\phi_x/U) \sim 1/z^2$.

In any case any radical increase in the order of magnitude of any perturbation term immediately indicates that the second order terms discussed in section 31 must be introduced, since the non-linear equation (28.1) and all the preceding results are based only on the first order terms of the shallow-water theory.

30-γ. One-Dimensional, Steady, Open Channel Hydraulics and the Hydraulic Jump.

The relations given in equations (30.27), (30.28) and (39.29), and shown in Figure 42, can be used in what is commonly known as the steady "one-dimensional" hydraulics of open channel flow. Here we assume that even though the channel width b(x) is varying, still the values of q(x) and η(x) do not depend upon z and therefore do not vary on any given cross-section. In conjunction with the steady "one-dimensional" concept it is necessary that $w \approx 0 \approx \theta$. Consequently the basic equations to be used for a flat horizontal bottom are given by q(x) = u(x) in (30.27), (30.28) and (30.29), and, in addition, by the "one-dimensional" continuity equation

$$b(x)d(x)u(x) = A(x)u(x) = Q = \left(\frac{\text{Meters}^3}{\text{sec.}}\right) = \text{constant} \qquad (30.48)$$

where, from Figure 42, $d(x) = [h_o + \eta(x)] = [A(x)/b(x)]$.

The validity of the "one-dimensional" assumption can be considerably in error if b'(x) is large since it is obvious that in this case w or θ cannot be small. However, the "one-dimensional" approximation gives surprisingly good numerical values, even in supercritical flow <u>if</u> the channel is well designed as in Figure 42 so as to maintain the flow as uniform as possible. However in supercritical flow the velocity over any cross-section remains uniform only near the design Froude number (F). Preiswerk [1938] gives the calculated and measured water depths in a Laval-type nozzle (the same one as duplicated in Figure 42) at various supercritical Froude numbers (F > 1). His results indicate that "one-dimensional" hydraulics give a satisfactory approximation, probably having an

error less than 10 per cent, even for critical or supercritical flow. This method should be especially useful for subcritical flow since the more exact numerical solution is now very difficult to obtain because the simple method of characteristics is no longer applicable.

The most useful, and obviously the most accurate, application of "one-dimensional" hydraulics is to the constant width rectangular cross-section open channel flow. In this application the friction effect of the vertical channel walls generally has a greater effect on the variation of q(x,y,z) than would any of the more exact terms of the complete first order shallow water equations(28.1), which have been derived on the assumption of negligible viscosity effects. Consequently the "one-dimensional" assumption that q = u(x) provides a satisfactory approximation for the constant width (b), rectangular cross-section, vertical wall channel having A(x) = bd(x). Even more important, this open channel flow analysis may be further generalized, with but little additional difficulty, to apply to a bottom slope varying also with x. The "one-dimensional" continuity equation (30.48) then becomes

$$u(x)d(x) = \frac{Q}{b} = \text{constant} \tag{30.49}$$

where d(x) is measured vertically from the varying bottom as shown in Figure 46. The generalization of the Bernoulli equation (30.27) to include extraneous head losses (h_L) other than those due to friction, and local variations in the bottom contour y(x) as shown in Figure 46, may be written as

$$\left(\begin{matrix}\text{SPECIFIC}\\ \text{ENERGY}\end{matrix}\right) = \frac{\text{kg. meters}}{\text{kg}} = (\text{meters}) = \left[d(x) + \frac{u^2(x)}{2g} + y(x) + h_L(x)\right] =$$

$$= \left[d(x) + \frac{(Q/b)^2}{2gd^2(x)} + y(x) + h_L(x)\right] = \text{constant} \tag{30.50}$$

This assumes that in steady flow the work of gravity, through the known average slope of the flow, is wholly spent on overcoming the

frictional resistance.

Another relation, that is necessary for calculating the sudden additional head loss h_L in hydraulic jumps or other discontinuous flow phenomenon, is given by the impulse-momentum relation, see Kelvin [1886], Rayleigh [1914], or Bakhmeteff [1932],

$$\left(\begin{matrix}\text{SPECIFIC}\\ \text{MOMENTUM}\end{matrix}\right) = \left(\frac{\text{meters}^3}{\text{sec}^2}\right) = [1/2\ gd^2(x) + d(x)u^2(x)] =$$

$$= [1/2\ gd^2(x) + \frac{(q/b)^2}{d(x)}] \qquad (30.51)$$

which is constant across the hydraulic jump over a flat horizontal bottom as shown in Figure 46.

Equation (30.50) with zero additional head loss ($h_L = 0$), gives the "one-dimensional" solution for the open channel flow that has no finite discontinuities in the flow itself, and either has the hydraulic frictional resistance exactly balanced by the given average slope for steady flow (so if $y = 0$ the surface slope is parallel to the bottom), or the hydraulic frictional resistance can be approximated by the Chézy formula for the case of varying open channel flow, see Bakhmeteff [1932] or Stoker [1957]. A useful concept for nearly all solutions is the definition of the critical depth d_*, which corresponds to our previous definition of critical flow velocity in (30.28), that is, with $w \approx 0 \approx \theta$ we assume that

$$u_* = c_* = \sqrt{\frac{2}{3}\, gh_o} = \frac{u_{max}}{\sqrt{3}} \qquad F_* = 1 = F$$

$$d_* = 2/3\ h_o = \frac{c_*^2}{g} = \left[\frac{(q/b)^2}{g}\right]^{1/3} \qquad (30.52)$$

The last relation for d_* can be obtained either directly from (30.27), or by substituting the expression $u_* = \sqrt{(2/3)gh_o}$ into (30.50) with y and h_L both zero. Also from (30.29) we have

$$\frac{d}{h_o} = \frac{2}{2 + F^2} \quad , \quad F_*^2 = F^2\left(\frac{C}{C_*}\right)^2 = \frac{3F^2}{2 + F^2} \quad ,$$

$$F^2 = \frac{u^2}{gd} = \frac{(Q/b)^2}{gd^3} = \left(\frac{d_*}{d}\right)^3 \qquad (30.53)$$

As an example, if we apply equations (30.50) and (30.52) to determine the flow relations between stations (1) and (2) in Figure 46a we obtain, since h_L is generally negligible for a smooth variation in y_2,

$$\left[\left(\frac{d_2}{d_*}\right) + 1/2\ \left(\frac{d_*}{d_2}\right)^2\right] = \left[\left(\frac{d_1}{d_*}\right) + 1/2\ \left(\frac{d_*}{d_1}\right)^2\right] - \left(\frac{y_2}{d_*}\right)$$

as a satisfactory approximation from "one-dimensional" hydraulics at least as long as (y_2/d_*) is sufficiently small. It is interesting to note that here is another resemblance to gas dynamics behaviour since

$$\left(\frac{y_2 + d_2}{d_*}\right) < \left(\frac{d_1}{d_*}\right) > 1, \text{ for } F_1 < 1$$

$$\left(\frac{y_2 + d_2}{d_*}\right) > \left(\frac{d_1}{d_*}\right) < 1, \text{ for } F_1 > 1$$

As another example, if we consider the hydraulic jump shown in Figure 46b, now we find that a solution can only be obtained by using the impulse-momentum relation (30.51), thereby proving that the discontinuous change occurring in a hydraulic jump must result in a head loss. If the bottom slope is negligible, as indicated in Figure 46b, then the impulse-momentum relation (30.51) may be written with $(Q/b) = (u_1\ d_1) = (u_2\ d_2)$ as first given by Rayleigh[1914]

$$\left[\tfrac{1}{2}gd_1^2 + d_1u_1^2\right] = \left[\tfrac{1}{2}\ gd_2^2 + \frac{(Q/b)^2}{d_2}\right] = \left[\tfrac{1}{2}\ gd_2^2 + \frac{(u_1d_1)^2}{d_2}\right]$$

$$F_1^2 = \frac{(Q/b)^2}{gd_1^3} = \left(\frac{u_1^2}{gd_1}\right) = \tfrac{1}{2}\left[\frac{\left(\frac{d_2}{d_1}\right)^2 - 1}{1 - \left(\frac{d_1}{d_2}\right)}\right] = \tfrac{1}{2}\ \left(\frac{d_2}{d_1}\right)\left(1 + \frac{d_2}{d_1}\right) \qquad (30.54)$$

or, if we let the actual rise in water level be $a = (d_2 - d_1)$

$$F_1 = \frac{u_1}{\sqrt{gd_1}} = \left[1 + 3/2\left(\frac{a}{d_1}\right) + 1/2\left(\frac{a}{d_1}\right)^2\right]^{1/2} \tag{30.55}$$

where

$$\left(1 + \frac{a}{d_1}\right) = \frac{d_2}{d_1} = 1/2\left[\sqrt{1 + 8\frac{(Q/b)^2}{gd_1^3}} - 1\right] = 1/2\left[\sqrt{1 + 8F_1^2} - 1\right] \tag{30.56}$$

Similarly (30.54) can also be solved for

$$F_2^2 = \frac{(Q/b)^2}{gd_2^3} = \left(\frac{u_2^2}{gd_2}\right) = 1/2\left(\frac{d_1}{d_2}\right)\left(1 + \frac{d_1}{d_2}\right) = F_1^2\left(\frac{d_1}{d_2}\right)^3 \tag{30.57}$$

Equations (30.54) and (30.57) may be multiplied together to yield

$$u_1 u_2 = g\left(\frac{d_1+d_2}{2}\right) = c_{1_*}^2\left[\frac{3}{2 + F_1^2}\right]\left[\frac{1 + \sqrt{1 + 8F_1^2}}{4}\right] < c_{1_*}^2 > c_{2_*}^2 \tag{30.58}$$

The last inequality in (30.58) is obtained from (30.50) and (30.52) by noting that in any finite hydraulic jump the head loss must also be finite, so $h_L = (h_{o_1} - h_{o_2}) > 0$ and (30.50) must be written as

$$d_1^2 + \frac{u_1^2}{2g} = d_2^2 + \frac{u_1^2}{2g}\left(\frac{d_1}{d_2}\right)^2 + (h_{o_1} - h_{o_2})$$

$$h_L = (h_{o_1} - h_2) = \frac{1}{2}F_1^2\left[\frac{\left(1 - \frac{d_1}{d_2}\right)^3}{\left(1 + \frac{d_2}{d_1}\right)}\right] d_2 =$$

$$= \frac{1}{4}F_1^2\left[\sqrt{1 + 8F_1^2} - 1\right]\left[\frac{\left(1 - \frac{d_1}{d_2}\right)^3}{\left(1 + \frac{d_2}{d_1}\right)}\right] d_1 \tag{30.59}$$

so (30.52) and (30.59) give the total head ratio, and therefore the critical speed ratio, as

$$\frac{h_{o_2}}{h_{o_1}} = \left(\frac{c_{2_*}}{c_{1_*}}\right)^2 = \left(1 - \frac{h_L}{h_{o_1}}\right) = \frac{d_{2_*}}{d_{1_*}} = \tag{30.60}$$

$$- \left\{ \frac{\left(\sqrt{1 + 8F_1^2} - 1 \right)^3 + 4F_1^2}{\left(\sqrt{1 + 8F_1^2} - 1 \right)^2 (2 + F_1^2)} \right\} < 1 \qquad (30.60) \text{ continued}$$

Consequently there is no direct analogy between finite hydraulic jumps and gas dynamic shock waves, as pointed out by Preiswerk [1938], since in gas dynamics the well-known Prandtl relation for normal shock waves gives $u_1 u_2 = c_*^2$, and c_* is constant through the shock wave, e.g. see Courant and Friedrichs [1948] page 146. The equations are similar only for the limiting case as the hydraulic jump vanishes so $F_1 = F_2 = 1$, $d_2 = d_1$, and $h_{o_2} = h_{o_1}$. However this limiting process corresponds to the isentropic, potential flow case where there is an analogy for small perturbations over a flat horizontal bottom, as previously discussed. Also, as indicated by (30.59) the head loss and variation in c_* could be neglected until the third order terms become important, so for F_1 near unity the first and second order terms of the hydraulic jump relations correspond to the gas dynamic shock wave relations having a specific heat ratio of $\gamma = 2$. However, this is identical to the known fact that weak shock waves may be considered isentropic to the third order of approximation, consequently the hydraulic analogy to compressible gas dynamics exists only for small perturbations in potential flow.

There is no direct analogy between the finite hydraulic jump and the gas dynamic shock wave because the hydraulic jump has a head loss that must be included in the specific energy equation (30.50). This head loss results in a loss of Kinetic energy that is no longer available as flow energy since it is converted into an

insignificant temperature rise in the water itself. In the gas dynamics energy equation the entropy increase through a shock wave of course corresponds to a loss of Kinetic energy but this is converted, through the increase of the temperature of the gas, into an adiabatic enthalpy increase that maintains constant flow energy through the shock wave, e.g., see Courant and Friedrichs [1948] page 125. The most unusual effect of this loss in flow energy (or h_L) in the hydraulic jmp is revealed in (30.58) which shows that the flow velocity downstream of a hydraulic jump is always less than the corresponding gas dynamics case, which maintains c_* constant so $u_1 u_2 = c_*^2$. For example, in the gas dynamic case when $F_1 \to \infty$, then $u_1/c_* \to \sqrt{3}$ (for $\gamma = 2$), and therefore $u_2/c_* \to 1/\sqrt{3}$. However in a hydraulic jump (30.58) shows that $u_2/c_* \to 0$ when $F_1 \to \infty$ (or $u_1/c_* \to \sqrt{3}$).

The experimental investigations by Bakhmeteff [1932] have shown that the hydraulic jumps in a horizontal rectangular channel are in excellent agreement with the predictions of the "one-dimensional" hydraulic equations (30.54) through (30.60). Bakhmeteff found that depth increases as high as $10(d_1)$ were in excellent agreement with (30.56). However, he found that for oncoming Froude numbers less than $\sqrt{3}$, (i.e., $F_1 < \sqrt{3}$) the profile of the normal hydraulic jump developed undulations, and the relative length of transition became indeterminate because the undulating surface made the region of parallel flow increasingly remote from the start of the wave front as indicated in Figure 46c. It is interesting to note that $F_1 = \sqrt{3}$ corresponds to the maximum absolute elevation that a hydraulic jump can reach with a given h_o (although there is no limit to d_2/d_1), since (30.53) and (30.56) may be combined to give

$$\frac{d_2}{h_{o_1}} = \frac{1}{2 + F_1^2} \left(\sqrt{1 + 8F_1^2} - 1\right) \leq \frac{4}{5}$$

which attains its maximum elevation of $(\frac{4}{5}h_{o_1})$ above the channel bottom only for $F_1 = \sqrt{3}$, at this condition we have

$$\frac{d_2}{d_1} = 2, \quad F_2^2 = 3/8, \quad \frac{h_L}{d_1} = \frac{1}{8}, \quad \frac{h_{o_2}}{h_{o_1}} = \frac{19}{20}$$

$$u_1 u_2 = \frac{9}{10} c_{1_*}^2$$

This shows that for all the undulating hydraulic jumps ($F_1 < \sqrt{3}$) the change in total head is less than 5 per cent, consequently these jumps can be approximated by the isentropic, potential flow relations. This is of great aid in calculating the slant or oblique hydraulic jumps, as shown in Figure 46d, since the characteristic epicycloid values of $f(F_*)$, as given in Table I, may be used in the manner indicated in (30.46) to approximate the change in F_*, F, or η upon turning through an angle θ by means of an oblique hydraulic jump whenever $(d_2/d_1) \to 1$. The comparison between the value given by $f(F_1)$ in Table I for compression to $F_2 = 1$, is compared with the exact values for the corresponding oblique hydraulic jumps in Figure 47. It is seen that although the gas dynamic shock wave is not a satisfactory approximation for $F_1 > \sqrt{3}$, still the isentropic potential relation $f(F_1)$ provides an excellent approximation for much greater values of F_1 since the criterion for oblique hydraulic jumps is that the flow component normal to the discontinuity $(F_1 \sin \alpha) < \sqrt{3}$.

The exact relations for the oblique hydraulic jump are given by Preiswerk [1938] and can be obtained by simply adding the same

velocity component ($w = w_1 = w_2$) tangent to both faces of the hydraulic jump as shown in Figure 46d. This results in the following equations (which reduce to the preceding ones for a normal hydraulic jump by simply letting $\theta \to 0$ and $\alpha \to \pi/2$):

$$F_1^2 = \frac{1}{2\sin^2\alpha}\,\frac{\tan\alpha}{\tan(\alpha-\theta)}\left[1+\frac{\tan\alpha}{\tan(\alpha-\theta)}\right] = \left[\frac{u_1/\sqrt{gd_1}}{\sin\alpha}\right]^2$$

$$F_2^2 = F_1^2\left(\frac{d_1}{d_2}\right)^3\left[\frac{\sin\alpha}{\sin(\alpha-\theta)}\right]^2 = \left[\frac{u_2/\sqrt{gd_2}}{\sin(\alpha-\theta)}\right]^2$$

$$\frac{d_2}{d_1} = \frac{\tan\alpha}{\tan(\alpha-\theta)} = \frac{1}{2}\left[\sqrt{1+8F_1^2\sin^2\alpha}-1\right] = \frac{u_1}{u_2}$$

$$\tan\theta = \frac{\tan\alpha\left[\sqrt{1+8F_1^2\sin^2\alpha}-3\right]}{(2\tan^2\alpha-1)+\sqrt{1+8F_1^2\sin^2\alpha}}$$

$$\sin\alpha = \frac{1}{F_1}\sqrt{\frac{1}{2}\left(\frac{d_2}{d_1}\right)\left(1+\frac{d_2}{d_1}\right)} = \left[\frac{u_1/\sqrt{gd_1}}{F_1}\right]$$

$$\sin(\alpha-\theta) = \frac{1}{F_2}\sqrt{\frac{1}{2}\left(\frac{d_1}{d_2}\right)\left(1+\frac{d_1}{d_2}\right)} = \left[\frac{u_2/\sqrt{gd_2}}{F_2}\right] \qquad (30.61)$$

The last two equations in (30.61) clearly show how the oblique hydraulic jump approaches the same value as given by the isentropic, potential relation $f(F_1)$ at <u>any</u> value of F_1 as long as $(d_2/d_1) \to 1$, since they reduce to the isentropic, potential characteristic curve given by (30.31) whenever $\theta \to 0$ and $(\frac{d_2}{d_1}) \to 1$. As a matter of fact, as previously mentioned, (30.61) shows that the oblique hydraulic jump angle (α) can be approximated as in Figure 45 by

$$\alpha = \left(\frac{\sin^{-1}\frac{1}{F_1}+\sin^{-1}\frac{1}{F_2}+\theta}{2}\right)+0\left(\frac{d_2}{d_1}-1\right)^2+0(\theta^3) \qquad (30.62)$$

that is, by taking α as defined by the average line between the two characteristics in the physical plane, or the line normal to

the midpoint of the corresponding characteristic epicycloid arc in the hodograph plane (see Figure 45). The close approximation of the characteristic epicycloid as given by f from (30.26) and Table I, to the oblique hydraulic jump relations (30.61) is strikingly illustrated when they are both plotted in the hodograph plane as in Figure 46d (see also Preiswerk [1938]). The trace of the velocity vector for the oblique shock wave of gas dynamics, generally called the "shock polar", is also shown in Figure 46d for a specific heat ratio of $\gamma = 2$.

As long as f from (30.26) is in close agreement with the oblique hydraulic jump relations (30.61), then the problems involving the interaction and reflection of hydraulic jumps can be closely approximated by the same procedure as detailed previously for the characteristic epicycloids involving compression waves in Figures 44 and 45. Whenever the required flow deflection (θ) is greater than that provided by the epicycloid passing through F_1, as shown in Figure 46d, then subcritical flow follows the curved or normal hydraulic jump as indicated by N = 1 in Figure 47. Similarly N = 2 defines the maximum flow reflection angle (θ) that can occur without ending in subcritical flow with a curved or normal hydraulic jump. In both cases two curves are shown for the oblique hydraulic jump, one for the turning angle θ that will make the flow critical ($F_2 = 1$), and the other one is the maximum possible turning angle (θ_{max}) for any oblique hydraulic jump at the given value of F_1. The latter always produces subcritical flow ($F_2 < 1$) as indicated in Figure 46d.

All of the preceding results primarily hold for hydraulic jumps in rectangular cross-section channels with a nearly horizontal

bottom. Bakhmeteff [1932] experimentally shows the various effects of steepening bottom slopes. He also generalizes (30.51) so it will apply to any constant cross-section shape. However, it must be noted that our equation (29.3) shows conclusively that (30.51) which completely neglects the w velocity component, cannot be applicable to channel walls that are not nearly vertical. Sloping sides on a channel would increase the vertical velocity gradients, make a normal hydraulic jump impossible, and induce unsteady vortex motions.

It must also be noted that all of the preceding results are valid only for relatively small bottom slopes, as indicated by the direct comparison of (30.50) and (30.51) with (28.1) and (29.3). When the flow is rapidly varying because of large changes in the bottom slope, then the change in surface profile curvature is so pronounced that the pressure variation can no longer be considered as hydrostatic. For example, over the spillway of a dam the centrifugal force due to the streamline curvature can actually exceed the hydrostatic pressure, thereby leading to a pressure less than atmospheric with flow separation or violent oscillations. At present spillway design is based on semi-empirical methods or model tests since no satisfactory mathematical analysis is available.

31 - Higher-order Theories and the Solitary and Cnoidal Waves.

It will now be shown that many of the preceding methods and results based on the shallow-water approximation are valid only if the local variations in water depth are not too large, and the average or undisturbed water depth is sufficiently small. The first requirement implies that the solutions of the first order nonlinear shallow-water equations (28.1) do not greatly differ (at least for Froude numbers not near unity) from the linearized solutions given by (29.3) or (29.7). The second requirement essentially demands that the depth h be much less than the effective wave length λ in any application, that is $(h/\lambda) = 0(1/10)$, in order to reduce the effects associated with the infinitesimal-wave approximation.

As already discussed the infinitesimal-wave approximation gives a direct variation of the fluid particle motion with the distance below the free surface, and also has the propagation velocity depend directly upon the wave length, as shown in section 15. There it was proved that the velocity defined by

$$c = \sqrt{\frac{g\lambda}{2\pi}\tanh\left(\frac{2\pi h}{\lambda}\right)} = \sqrt{gh}\left[1 - (1/6)\left(\frac{2\pi h}{\lambda}\right)^2 + \cdots\right] \qquad (31.1)$$

can only be considered a phase velocity while the actual rate of propagation of energy is associated with the group velocity defined by

$$\left(c - \lambda\frac{dc}{d\lambda}\right) = (1/2)\,c\left(1 + \frac{4\pi h/\lambda}{\sinh 4\pi h/\lambda}\right) = c\left[1 - 1/3\left(\frac{2\pi h}{\lambda}\right)^2 + \cdots\right] \qquad (31.2)$$

(see also Lamb [1932] page 381). Any such variation will directly interfere with the applicability of the shallow-water results. However, as long as $h/\lambda < 1/10$ it is seen that the phase velocity

and the group velocity are both satisfactory approximations to the shallow-water first order result that $c = \sqrt{gh}$ and is independent of the effective wave length.

This means that if small scale model tests are used to simulate results appropriate to the shallow-water theory, then the undisturbed water depth should be less than 1/10 the principal model dimensions. Consequently if models less than 10 cm. in effective dimensions are used, then the test water depth should be less than 1 cm., so the capillary ripples produced by surface tension must be considered. As shown in sections 15 and 24 the effect of the surface tension (T) is to increase the phase velocity for the short wave length capillary ripples so that (31.1) is replaced by

$$c = \sqrt{\left(\frac{g\lambda}{2\pi} + \frac{2\pi T}{\lambda \rho}\right)\tanh\frac{2\pi h}{\lambda}} \qquad (31.1')$$

For ordinary water (at 20°C, T = 72.8 dynes/cm., ρ = 0.998 gm/cm^3) this gives the interesting result that both the phase velocity and the group velocity are closely approximated by $\sqrt{gh}$ for all $\lambda > 2$ cm. if $h \simeq 1/2$ cm. However in any small model tests the surface wave patterns formed by the capillary ripples must be ignored since they are short wave length surface waves that are never in accord with the long wave length shallow water theory.

Except for the section on hydraulic jumps the preceding shallow-water results have all been based entirely on (28.1), the first approximation to shallow-water theory, and this will now be shown to be limited to relatively small wave amplitudes even though the complete nonlinear equation (28.1) be used, and even though the bottom surface be flat and horizontal. The second approximation to

shallow-water theory will be shown to immediately yield particular solutions corresponding to continuous permanent wave profiles of finite amplitude that can be propagated without a change in form or shape if viscosity effects are neglected. These permanent, finite amplitude wave forms are the cnoidal waves discovered by Korteweg and de Vries [1895] which reduce, in the limiting case of essentially infinite wave length, to the solitary wave of Russell [1837, 1844] which was first analyzed theoretically by Boussinesq [1871, 1872] and Rayleigh [1876].

The second approximation to shallow-water theory will show that the limitation of the nonlinear first approximation to relatively small amplitudes is primarily due to the fact that the variation in the vertical velocity cannot be neglected as the wave amplitude is increased. This of course invalidates even the rectangular channel hydraulic analogy to compressible gas flow, since, as previously discussed, the principal assumption of the hydraulic analogy is that the vertical acceleration be negligible.

The third approximation to shallow-water theory will then be presented to obtain new relations which will predict the limiting heights of the continuous finite amplitude steady state wave forms and give, for the first time, the complete second approximation to the cnoidal and solitary waves. It will be found that the pressure is no longer hydrostatic, thereby violating the remaining principal assumption of the hydraulic analogy and the ordinary classical shallow-water theory.

31 α - The First and Second Approximations to the Cnoidal and Solitary Waves.

We will now extend the perturbation method of Friedrichs [1948], which was used to derive the nonlinear first order approximation (28.1) to shallow-water theory, to obtain the second and higher orders of approximations for the special case of the steady state propagation of a wave independent of z and t over a flat horizontal bottom having $y = -h_\infty$ = constant as in Figure 37.

First we will show that the only steady state finite amplitude solution of the first order equation (28.2) is $y^{(o)} = \eta_o$ = constant and $u^{(o)} = u_o$ = constant. This is most easily proved by substituting the solution of the zeroth order terms in (10.24) for steady water flow over a flat horizontal bottom, namely

$$u^{(o)} = u^{(o)}(x), \quad v^{(o)} = 0, \quad p^{(o)} = 0, \quad \eta^{(o)} = \eta^{(o)}(x) \tag{31.3}$$

into the first order terms in (10.27) to obtain

$$u^{(o)} = u_o = \text{constant}, \quad v^{(1)} = 0, \quad p_y^{(o)} = -\rho g, \quad \eta^{(o)} = \eta_o = \text{constant} \tag{31.4}$$

since $\eta_x^{(o)} = 0 = p_x^{(o)}$

Consequently the only finite amplitude first order steady state solution must have $\eta_x^{(o)} = 0$, which would only permit the hydraulic jump as a solution since $\eta_x^{(o)} = 0$ and $u^{(o)}$ = constant on each side of the finite discontinuity defining the hydraulic jump. This is in agreement with the well-known fact that the gas dynamics equation or (28.2), predicts that any finite amplitude disturbance must form a finite discontinuity which is a shock wave, or hydraulic jump, e.g., see Lamb [1932] pages 278, 481. However, the second order approximation of shallow-water theory (10.33) does yield a permanent finite amplitude, steady state wave profile that does not form a discontinuity.

These are called the cnoidal waves, as discovered by Korteweg and de Vries [1895], and the solitary waves of Russell [1837, 1844], Boussinesq [1871, 1872], and Rayleigh [1876]. In order to obtain the higher order approximations and limiting heights of these waves it is more convenient to use exactly the same non-dimensional variables as introduced by Friedrichs [1948], and also used by Keller [1948], namely,

$$\left.\begin{aligned}
&\varepsilon = \omega^2 h^2, \quad \alpha = \omega x, \quad \beta = y/h, \quad H = h_\infty/h \\
&u(\alpha,\beta) = u(x,y)/\sqrt{gh}, \quad v(\alpha,\beta) = \frac{v(x,y)}{\sqrt{gh}} \ (\omega h) \\
&Y(\alpha) = \eta(x)/h, \quad \Pi(\alpha,\beta) = p(x,y)/\rho gh \\
&Y(\alpha) = Y^{(0)} + \varepsilon Y^{(1)} + \varepsilon^2 Y^{(2)} + \ldots \\
&\eta(x) = h Y^{(0)} + \omega^2 h^3 Y^{(1)} + \omega^4 h^5 Y^{(2)} + \ldots
\end{aligned}\right\} \qquad (31.5)$$

the only difference in notation being that x and y are now defined as in Figure 37, consequently the flat horizontal bottom is given by $y = -h_\infty$ or $\beta = -h_\infty/h = -H$, and the expansion parameter $\varepsilon = \omega^2 h^2$ is used as defined in (10.23), with (31.5) replacing (10.21).

Introducing the transformation defined by (31.5) into (31.4) and the corresponding equivalent of (10.33) we obtain

$$\left.\begin{aligned}
&v^{(0)} = 0 = v^{(1)} \\
&u^{(0)}(\alpha,\beta) = u_0 = \text{constant}, \quad Y^{(0)}(\alpha) = Y_0 = \text{constant} = \eta_0/h \\
&\Pi_\beta^{(0)} = -1, \quad \Pi_\beta^{(1)} = 0, \quad u_\beta^{(1)} = v_\alpha^{(1)} = 0, \quad u_\alpha^{(1)} = -v_\beta^{(2)}, \\
&u_0 u_\alpha^{(1)} + \Pi_\alpha^{(1)} = 0, \quad v^{(2)}(Y_0) = u_0 Y_\alpha^{(1)}, \\
&v^{(2)}(-H) = 0, \quad \Pi^{(1)}(Y_0) = -Y^{(1)}\Pi_\beta^{(0)} = Y^{(1)}(\alpha)
\end{aligned}\right\} \qquad (31.6)$$

These expressions may be integrated to obtain

$$u^{(1)}(\alpha,\beta) = f(\alpha) = u^{(1)}(\alpha)$$

$$v^{(2)}(\alpha,\beta) = [v^{(2)}(\alpha,\beta) - v^{(2)}(\alpha, -H)] =$$

$$= -\int_{-H}^{\beta} f_\alpha \, d\beta = -(\beta + H) f_\alpha \qquad (31.7)$$

$$\Pi^{(1)}(\alpha,\beta) = -\int u_o f_\alpha \, d\alpha = -(u_o f + C) = \Pi^{(1)}(\alpha) = Y^{(1)}(\alpha)$$

$$Y_\alpha^{(1)} = \Pi_\alpha^{(1)} = -u_o f_\alpha = \frac{v_2(Y_o)}{u_o} = -\left(\frac{Y_o + H}{u_o}\right) f_\alpha$$

The identities in the last equation show that the solution for constant u_o is restricted to the unique value defined by

$$u(x,y) = u_o\sqrt{gh} = \sqrt{gh(Y_o + H)} = \sqrt{g(\eta_o + h_\infty)} = \text{constant} \qquad (31.8)$$

which corresponds to the infinitesimal-wave propagation velocity (28.3) and shows that the steady state solution will be in the neighborhood of the critical speed defined by a Froude number of unity. However, $u^{(1)} = f(\alpha)$ now provides a finite amplitude steady state solution that does not form a discontinuity, consequently the behavior of the second order shallow-water theory is mathematically completely different from the first order (28.2) shallow-water theory or the gas dynamics equations. The pressure variation is still hydrostatic, since $\Pi^{(1)}$ does not depend upon β, and only $v^{(2)}$ has a direct dependence upon β ($\equiv y$).

Now in order to continue the solution and determine $f(\alpha)$ we must introduce some ε^3 terms. By following the same procedure as used in collecting the ε^2 terms for (10.33) we obtain for the

particular case of steady flow over a flat horizontal bottom the following additional terms that are required for completing the second order solution:

$$u_\beta^{(2)} = \nu_\alpha^{(2)}, \quad u_\alpha^{(2)} = -\nu_\beta^{(3)}$$

$$u_o u_\alpha^{(2)} + u^{(1)} u_\alpha^{(1)} + \Pi_\alpha^{(2)} = 0, \quad u_o \nu_\alpha^{(2)} + \Pi_\beta^{(2)} = 0 \tag{31.9}$$

$$\nu^{(3)}(Y_o) = u_o Y_\alpha^{(2)} + u^{(1)} Y_\alpha^{(1)} - \nu_\beta^{(2)} Y^{(1)}, \quad \nu^{(3)}(-H) = 0$$

$$\Pi^{(2)}(Y_o) = -Y^{(2)} \Pi_\beta^{(o)} = Y^{(2)}$$

These expressions were first given by Keller [1948] and they may be directly integrated to give the following:

$$u^{(2)} = \int \nu_\alpha^{(2)} d\beta = -f_{\alpha\alpha} \int (\beta + H) d\beta = \left[-(1/2)(\beta^2 + 2H\beta) f_{\alpha\alpha} + R(\alpha)\right] = u^{(2)}(\alpha, \beta) \tag{31.10}$$

$$\Pi^{(2)}(\alpha, \beta) = Y^{(2)}(\alpha) - \left[\frac{Y_o^2 - \beta^2}{2} + H(Y_o - \beta)\right] u_o f_{\alpha\alpha}$$

$$\nu^{(3)}(\alpha, \beta) = \left[\nu^{(3)}(\alpha, \beta) - \nu^{(3)}(\alpha, -H)\right] = \int_{-H}^{\beta} -u_\alpha^{(2)} d\beta =$$

$$= \left[\frac{\beta^3 + H^3}{6} + \frac{H(\beta^2 - H^2)}{2}\right] f_{\alpha\alpha\alpha} - (\beta + H) R_\alpha$$

$$\nu^{(3)}(Y_o) = u_o Y_\alpha^{(2)} - u_o f f_\alpha - (u_o f + C) f_\alpha =$$

$$= 1/6 \,(Y_o^3 + 3H Y_o^2 - 2H^3) f_{\alpha\alpha\alpha} - (Y_o + H) R_\alpha$$

The last equation for $\nu^{(3)}$ gives the following expression for the ε^2 term in the surface profile

$$u_o Y_{(\alpha)}^{(2)} = \left[\begin{array}{c} u_o f^2 + Cf + (1/6)(Y_o^3 + 3H Y_o^2 - 2H^3) f_{\alpha\alpha} \\ - (Y_o + H) R + \text{Constant} \end{array}\right] \tag{31.11}$$

while a similar expression may be obtained directly from $\Pi^{(2)}(Y_o)$ by

equating its relation in (31.9) and (31.10) so as to obtain

$$u_o Y^{(2)}(\alpha) = u_o \Pi^{(2)}(Y_o) = - u_o [u_o u^{(2)} + 1/2\, u^{(1)^2}]_{\beta = Y_o} \qquad (31.12)$$

$$\left[\frac{u_o^2}{2} (Y_o^2 + 2H Y_o) f_{\alpha\alpha} - u_o^2 R(\alpha) - \frac{u_o}{2} f^2 + \text{constant} \right]$$

Since (31.11) and (31.12) must be identical, therefore we may equate them and find that $f(\alpha)$ must satisfy the ordinary differential equation

$$f_{\alpha\alpha} - \left(\frac{9}{2u_o^5}\right)(f)^2 - \left(\frac{3C}{u_o^6}\right) f + C_o = 0 \qquad (31.13)$$

after having introduced (31.8) to eliminate Y_o. Equation (31.13) may be integrated to

$$(1/3)u_o^6 (f_\alpha)^2 - u_o (f)^3 - C(f)^2 + (2/3)u_o^6 C_o (f) = \text{constant}. \qquad (31.14)$$

Upon noting from (31.7) that $f(\alpha) = u^{(1)}(\alpha)$ and

$$\frac{u_o}{C} f = - \left[1 + \frac{Y^{(1)}(\alpha)}{C} \right]$$

it is evident that (31.13) and (31.14) are the same equations as obtained by Boussinesq [1871, 1872], Rayleigh [1876], Korteweg and de Vries [1895], Lavrent'ev [1943], and Keller [1948]. The physical significance of each term in (31.14) was first pointed out by Benjamin and Lighthill [1954], who derived (31.14) in an entirely different manner, starting with the same series expansion of the stream function as introduced by Rayleigh [1876]. Benjamin and Lighthill [1954] use the continuity equation (30.49), the specific energy equation (30.50), and the specific momentum equation (30.51) to derive the equivalent of (31.14), and then they give a very useful discussion of the mathematical and physical behavior of its solutions.

The appropriate solution of (31.13) for the boundary conditions shown in Figure 37 is given by the square of the Jacobian elliptic function "cn" having the modulus $0 < k \leq 1$ and the real period

$$4K(k) = 4\int_0^{\pi/2} \frac{d\theta}{\sqrt{1 - k^2\sin^2\theta}} > 2\pi$$

Substituting

$$f(\alpha) = -B\ cn^2(A\alpha, k) \tag{31.15}$$

into (31.13) we find that (31.15) is a solution if, and <u>only</u> if, $0 < k \leq 1$ and

$$B = 4/3\ u_o^5 A^2 k^2 = \frac{C}{u_o}\left(\frac{k^2}{2k^2-1}\right) = \frac{C_o}{2A^2(1-k^2)} \tag{31.16}$$

Substituting (31.15) into (31.7) and (31.5) we obtain

$$\eta(x) = \eta_o + \omega^2 h^3 B u_o \left[cn^2(A\omega x, k) - \left(\frac{2k^2-1}{k^2}\right)\right] + 0(\varepsilon^2)$$

The boundary conditions in Figure 37c then yield

$$\eta(o) = \eta_o + \omega^2 h^3 B u_o \left(\frac{1-k^2}{k^2}\right) = a$$

$$\eta\left(\frac{K}{A\omega}\right) = \eta_o - \omega^2 h^3 B u_o \left(\frac{2k^2-1}{k^2}\right) = 0$$

$$a = (\omega^2 h^3 B u_o),\ \eta_o = a\left(\frac{2k^2-1}{k^2}\right)$$

$$\eta(x) = a\ cn^2\ (A\omega x, k) \tag{31.17}$$

Then upon introducing (31.8) and (31.16) into (31.17) we obtain

$$A\omega x = \frac{x}{h_\infty}\sqrt{\frac{3}{4k^2}\frac{(a/h_\infty)}{(1+\eta/h_\infty)^3}} = \frac{x}{h_\infty}\sqrt{\frac{3}{4k^2}\frac{(a/h_\infty)}{\left[1+\left(\frac{a}{h_\infty}\right)\left(\frac{2k^2-1}{k^2}\right)\right]^3}} =$$

$$= \frac{x}{h_\infty}\sqrt{\frac{3}{4k^2}\left(\frac{a}{h_\infty}\right)}\left\{1 - (3/2)\left(\frac{a}{h_\infty}\right)\left(\frac{2k^2-1}{k^2}\right) + \ldots\right\} =$$

$$= \frac{x}{h_\infty}\sqrt{\frac{3}{4k^2}\left(\frac{a}{h_\infty}\right)} + 0\left[\left(\frac{a}{h_\infty}\right)\left(\frac{2k^2-1}{k^2}\right)\right]^{3/2} \tag{31.18}$$

as the exact second order shallow-water theory solution for the first approximation to the cnoidal waves of Korteweg and de Vries [1895]. The remaining terms in (31.6) and (31.7) may similarly be solved to give

$$\frac{p(x,y)}{\rho g h_\infty} = \frac{\eta(x) - y}{h_\infty} + 0\left[\left(\frac{a}{h_\infty}\right)\left(\frac{2k^2-1}{k^2}\right)\right]^2$$

$$\frac{u(x)}{\sqrt{gh_\infty}} = 1 + \left(1 - \frac{1}{2k^2}\frac{a}{h_\infty}\right) - \frac{\eta(x)}{h_\infty} + 0\left[\left(\frac{a}{h_\infty}\right)\left(\frac{2k^2-1}{k^2}\right)\right]^2 \qquad (31.19)$$

$$\frac{v(x,y)}{\sqrt{gh_\infty}} = -\left(1 + \frac{y}{h_\infty}\right)\sqrt{\frac{3}{k^2}\left(\frac{a}{h_\infty}\right)^3}\ \mathrm{cn}\ \mathrm{sn}\ \mathrm{dn} + 0\left[\left(\frac{a}{h_\infty}\right)\left(\frac{2k^2-1}{k^2}\right)\right]^{5/2} =$$

$$= + \left(1 + \frac{y}{h_\infty}\right)\frac{d\eta(x)}{dx} + 0\left[\left(\frac{a}{h_\infty}\right)\left(\frac{2k^2-1}{k^2}\right)\right]^{5/2}$$

where cn, sn, dn are the Jacobian elliptic functions having the argument $(A\omega x, k)$, with $(A\omega x)$ defined by (31.18). It must be noted that $0 < k \leq 1$ so k can never become identically zero for two reasons. First, because for $k = 0$

$$\mathrm{cn}^2(A\omega x, 0) = \cos^2(A\omega x)$$

is not a solution of (31.13) or (31.14), and second, because the expansions given in (31.18) and (31.19) are only valid for $a \to 0$ as $k \to 0$.

The limiting case of $k = 1$ corresponds to an essentially infinite wave length since $K(1) \to \infty$, and the cnoidal wave solutions reduce to

$$\frac{\eta(x)}{h_\infty} = \left(\frac{a}{h_\infty}\right)\mathrm{sech}^2\left(\frac{x}{h_\infty}\sqrt{\frac{3}{4}\left(\frac{a}{h_\infty}\right)}\right) + 0\left(\frac{a}{h_\infty}\right)^2$$

$$\frac{p(x,y)}{\rho g h_\infty} = \frac{\eta(x) - y}{h_\infty} + 0\left(\frac{a}{h_\infty}\right)^2 \qquad (31.20)$$

$$\frac{u(x,y)}{\sqrt{gh_\infty}} = 1 + (1/2)\left(\frac{a}{h_\infty}\right) - \frac{\eta(x)}{h_\infty} + 0\left(\frac{a}{h_\infty}\right)^2$$

$$\frac{v(x,y)}{\sqrt{gh_\infty}} = \left(1 + \frac{y}{h_\infty}\right)\frac{d\eta(x)}{dx} + 0\left(\frac{a}{h_\infty}\right)^{5/2}$$

which provides the exact first approximation to the solitary wave.

All of these solutions, for the cnoidal wave and the solitary wave, are in exact agreement with the expressions first given by Korteweg and de Vries [1859], pages 430-431, if one neglects the terms of $0(a/h_\infty)^2$. It will now be proved that the terms of $0(a/h_\infty)^2$ must be neglected in these first approximations becuase the second approximations introduce additional terms having this order of magnitude.

We can continue to the next order of approximation by collecting the remaining terms corresponding to ε^3, and adding some of the ε^4 terms that are necessary in order to complete the solution

$$\Pi^{(3)}(Y_o) = Y^{(3)} - Y^{(1)}\,\Pi_\beta^{(2)}(Y_o)$$

$$u_\beta^{(3)} = v_\alpha^{(3)}, \quad u_\alpha^{(3)} = -v_\beta^{(4)} \tag{31.21}$$

$$u_o u_\alpha^{(3)} + u^{(1)} u_\alpha^{(2)} + u^{(2)} u_\alpha^{(1)} + \Pi_\alpha^{(3)} + v^{(2)} u_\beta^{(2)} = 0$$

$$u_o v_\alpha^{(3)} + u^{(1)} v_\alpha^{(2)} + \Pi_\beta^{(3)} + v^{(2)} v_\beta^{(2)} = 0$$

$$v^{(4)}(Y_o) = [u_o Y_\alpha^{(3)} + u^{(1)} Y_\alpha^{(2)} + u^{(2)} Y_\alpha^{(1)} - v_\beta^{(2)} Y^{(2)} - v_\beta^{(3)} Y^{(1)}$$

$$v^{(4)}(-H) = 0$$

Now we can combine the expression for $v^{(3)}$ in (31.10) with that in (31.21) to write

$$u^{(3)}(\alpha,\beta) = \int v_\alpha^{(3)}\,d\beta = \left[\frac{1}{24}(\beta^4 + 4H\beta^3 - 8H^3\beta)\,f_{\alpha IV}\right.$$

$$\left. - \tfrac{1}{2}(\beta^2 + 2H\beta)R_{\alpha\alpha} + S(\alpha)\right] \tag{31.22}$$

Then the expression for $v^{(4)}$ in (31.21) yields

$$v^{(4)}(\alpha,\beta) = -\int_{-H}^{\beta} u_{\alpha}^{(3)}(\alpha,\beta)dz = -\left[(\beta+H)\,S_{\alpha}\right. \tag{31.23}$$
$$\left. + \frac{1}{120}(\beta^5 + 5H\beta^4 - 20H^3\beta^2 + 16H^5) f_{\alpha\overline{V}} - \frac{1}{6}(\beta^3 + 3H\beta^2 - 2H^3)R_{\alpha\alpha\alpha}\right]$$

The boundary condition defined by the expression for $v^{(4)}$ in (31.21) thereby gives one relation for $Y^{(3)}$ that may be written as

$$u_o Y_{\alpha}^{(3)}(\alpha) = v^{(4)}(Y_o) - [u^{(1)} Y_{\alpha}^{(2)} - v_{\beta}^{(2)} Y^{(2)}] - [u^{(2)} Y_{\alpha}^{(1)} - v_{\beta}^{(3)} Y^{(1)}] =$$
$$= v^4(Y_o) - [u^{(1)} Y^{(2)}]_{\alpha} - [u^{(2)} Y^{(1)}]_{\alpha} \tag{31.24}$$

which may be directly integrated, upon substituting (31.23) for $v^{(4)}$, as

$$u_o Y_{\alpha}^{(3)} = \left[\int v^{(4)}(Y_o)\, d\alpha - u^{(1)}(Y_o) Y^{(2)} - u^{(2)}(Y_o) Y^{(1)}\right] =$$
$$= \text{constant} - \left\{\frac{1}{120}(Y_o^5 + 5HY_o^4 - 20H^3 Y_o^2 + 16H^5) f_{\alpha\overline{IV}} + \right.$$
$$- \frac{1}{6}(Y_o^3 + 3HY_o^2 - 2H^3)R_{\alpha\alpha} + (Y_o + H)S(\alpha) + \frac{f}{u_o}\left[\frac{u_o^2}{2}(Y_o^2 + 2HY_o) f_{\alpha\alpha} - u_o^2 R - \frac{u_o}{2} f^2\right] +$$
$$\left. + [(1/2)(Y_o^2 + 2HY_o) f_{\alpha\alpha} - R(\alpha)]\,[u_o f + C]\right\} \tag{31.25}$$

Another relation for $Y^{(3)}$ may also be obtained from the other boundary condition defined by the expression for $\Pi^{(3)}$ in (31.21), namely

$$Y^{(3)}(\alpha) = \Pi^{(3)}(Y_o) + Y^{(1)}\,\Pi_{\beta}^{(2)}(Y_o) \tag{31.26}$$

where $\Pi^{(3)}$ itself may be obtained by integrating the expressions for $\Pi_{\alpha}^{(3)}$ and $\Pi_{\beta}^{(3)}$ in (31.21) to obtain

$$\Pi^{(3)}(\alpha,\beta) = -u_o u^{(3)} - u^{(1)} u^{(2)} - 1/2[v^{(2)}]^2 + \text{constant} \tag{31.27}$$

Then substituting $\Pi^{(3)}$ from (31.27), $\Pi_{\beta}^{(2)}$ from (31.10), $u^{(1)} = f$, $u^{(2)}$ from (31.10), $u^{(3)}$ from (31.22), $y^{(1)} = -(u_o f + C)$ and $Y^{(2)}$ from (31.12) into (31.26) we obtain another relation for $Y^{(3)}$, namely,

$$u_o Y^{(3)}_{(\alpha)} = -\left\{ \frac{u_o^2}{24}\left(Y_o^4 + 4H Y_o^3 - 8H^3 Y_o\right) f_{\alpha\alpha\alpha\alpha} - \frac{u_o^2}{2}\left(Y_o^2 + 2H Y_o\right) R_{\alpha\alpha} \right.$$

$$+ u_o^2 S - \frac{u_o}{2}\left(Y_o^2 + 2H Y_o\right) f f_{\alpha} + u_o f R + \frac{u_o^5}{2}\left(f_{\alpha}\right)^2$$

$$\left. + \left(u_o f + C\right) u_o^4 f_{\alpha\alpha} + \text{constant} \right\} \qquad (31.28)$$

These two expressions for $Y^{(3)}$, (31.25) and (31.28), must be identically equal, therefore since u_o is defined by (31.8), we find that the unknown function R must satisfy the ordinary differential equation

$$\left[\frac{u_o^5}{3} R_{\alpha\alpha} - \left(\frac{c}{u_o} + 3f\right) R + \text{constant} \right] =$$

$$= \left[\frac{u_o^5}{30}\left(u_o^4 - 5H^2\right) f_{\alpha\alpha\alpha\alpha} - 1/2\left(u_o^4 - 3H^2\right) f f_{\alpha\alpha} \right.$$

$$\left. + \frac{c}{2u_o}\left(u_o^4 + H^2\right) f_{\alpha\alpha} + \frac{u_o^4}{2}\left(f_{\alpha}\right)^2 + \frac{1}{2u_o}\left(f\right)^3 \right] \qquad (31.29)$$

the other unknown function $S(\alpha)$ having been eliminated since $u_o^2 = \left(Y_o + H\right)$.

When $f(\alpha)$ is given by (31.15), then the solution of (31.29) is

$$R(\alpha) = \frac{C^2}{u_o^3}\left\{ \left(\frac{k^2}{2k^2-1}\right)^2 \left(1 - \frac{9}{4}\frac{H^2}{u_o^4}\right) cn^4(A\alpha, k) + \right. \qquad (31.30)$$

$$\left. \left(\frac{k^2}{2k^2-1}\right)\left(1 + \frac{3}{2}\frac{H^2}{u_o^4}\right) cn^2(A\alpha, k) - \frac{3}{10}\frac{k^2(1-k^2)}{(2k^2-1)^2}\left(1 - \frac{5}{2}\frac{H^2}{u_o^4}\right) - \frac{3}{5} \right\}$$

and (31.11) or (31.12) give the ε^2 term of the wave profile as

$$Y^{(2)}_{(\alpha)} = \left(\frac{C}{u_o}\right)^2 \left\{ \frac{3}{4}\left(\frac{k^2}{2k^2-1}\right)^2 cn^4(A\alpha, k) \right.$$

$$\left. - \frac{5}{2}\left(\frac{k^2}{2k^2-1}\right) cn^2(A\alpha, k) + \frac{12 - 57k^2 + 57k^4}{20(2k^2-1)^2} \right. \qquad (31.31)$$

Consequently the second approximation to the cnoidal wave profile is given from the preceding and (31.5) as

$$\eta(x) = \eta_o + \omega^2 h^3 y^{(1)} + \omega^4 h^5 y^{(2)} + 0(\varepsilon^3) =$$

$$= \left\{ \eta_o - \eta_1 \left[1 - \left(\frac{k^2}{2k^2 - 1} \right) cn^2(A\omega x, k) \right] + \right.$$

$$+ \frac{\eta_1^2}{\eta_o + h_\infty} \left[\frac{3}{4} \left(\frac{k^2}{2k^2 - 1} \right)^2 cn^4(A\omega x, k) - \frac{5}{2} \left(\frac{k^2}{2k^2 - 1} \right) cn^2(A\omega x, k) + \right.$$

$$\left. \left. + \frac{12 - 57k^2 + 57k^4}{20(2k^2 - 1)^2} \right] \right\} \qquad (31.32)$$

where

$$\eta_1 = C \omega^2 h^3 = (A\omega)^2 \frac{4}{3} (2k^2 - 1)(hu_o^2)^3 =$$

$$= (A\omega)^2 \frac{4}{3} (2k^2 - 1)(\eta_o + h_\infty)^3$$

Then the boundary conditions shown in Figure 37c yield the relations:

$$\eta(o) = a = \eta_o - \eta_1 \left(\frac{k^2 - 1}{2k^2 - 1} \right) + \frac{\eta_1^2}{\eta_o + h_\infty} \left[\frac{12 - 7k^2 - 28k^4}{20(2k^2 - 1)^2} \right]$$

$$\eta\left(\frac{K}{A\omega} \right) = 0 = \eta_o - \eta_1 + \frac{\eta_1^2}{\eta_o + h_\infty} \left[\frac{12 - 57k^2 + 57k^4}{20(2k^2 - 1)^2} \right] \qquad (31.33)$$

which may be solved to give the second approximation

$$\frac{\eta_o}{h_\infty} = \left(\frac{2k^2 - 1}{k^2} \right) \left(\frac{a}{h_\infty} \right) + \left(\frac{a}{h_\infty} \right)^2 \left(\frac{38 - 128k^2 + 113k^4}{20k^4} \right) + 0 \left(\frac{a}{h_\infty} \right)^3$$

$$\frac{\eta_1}{h_\infty} = \left(\frac{2k^2 - 1}{k^2} \right) \left(\frac{a}{h_\infty} \right) \left[1 + \left(\frac{a}{h_\infty} \right) \left(\frac{85k^2 - 50}{20k^2} \right) \right] + 0 \left(\frac{a}{h_\infty} \right)^3$$

$$\frac{\eta(x)}{h_\infty} = \left\{ \left(\frac{a}{h_\infty} \right) cn^2(A\omega x, k) - \frac{3}{4} \left(\frac{a}{h_\infty} \right)^2 cn^2(A\omega x, k)[1 - cn^2(A\omega x, k)] + \right.$$

$$\left. + 0 \left(\frac{a}{h_\infty} \right)^3 \right\} \qquad (31.34)$$

where now

$$(A\omega x) = \frac{x}{h_\infty}\sqrt{\frac{3}{4k^2}\left(\frac{\varepsilon}{h_\infty}\right)}\left(1+\frac{\eta_0}{h_\infty}\right)^{-3/2}\left[1+\left(\frac{a}{h_\infty}\right)\left(\frac{85k^2-50}{40k^2}\right)\right] =$$

$$= \frac{x}{h_\infty}\sqrt{\frac{3}{4k^2}\left(\frac{\varepsilon}{h_\infty}\right)}\left[1-\left(\frac{a}{h_\infty}\right)\left(\frac{7k^2-2}{8k^2}\right)\right]+0\left[\left(\frac{a}{h_\infty}\right)\left(\frac{2k^2-1}{k^2}\right)\right]^{5/2} \qquad (31.35)$$

The remaining ε^3 terms from (31.10) may then be combined with the ε terms from (31.7), by means of (31.5), to give

$$\frac{p(x,y)}{\rho gh_\infty} = \left\{\frac{\eta(x)-y}{h_\infty}-\left(\frac{a}{h_\infty}\right)^2\frac{3}{4k^2}\left(2\frac{y}{h_\infty}+\frac{y^2}{h_\infty^2}\right)\left[1-k^2+\right.\right.$$

$$\left.\left.+2(2k^2-1)\,cn^2(A\omega x,k)-3k^2cn^4(A\omega x,k)\right]+0\left[\left(\frac{a}{h_\infty}\right)\left(\frac{2k^2-1}{k^2}\right)\right]^3\right\}$$

$$\frac{u(x,y)}{\sqrt{gh_\infty}} = \left\{1+\left(1-\frac{1}{2k^2}\right)\left(\frac{a}{h_\infty}\right)-\left(\frac{21k^4-6k^2-9}{40k^4}\right)\left(\frac{a}{h_\infty}\right)^2+\right.$$

$$-\left(\frac{a}{h_\infty}\right)\left[1-\left(\frac{a}{h_\infty}\right)\left(\frac{7k^2-2}{4k^2}\right)-\left(\frac{a}{h_\infty}\right)\frac{3}{2}\left(2-\frac{1}{k^2}\right)\left(2\frac{y}{h_\infty}+\frac{y^2}{h_\infty^2}\right)\right]cn^2(A\omega x,k)$$

$$-\left(\frac{a}{h_\infty}\right)^2\left[\frac{5}{4}+\frac{9}{4}\left(2\frac{y}{h_\infty}+\frac{y^2}{h_\infty^2}\right)\right]cn^4(A\omega x,k)$$

$$\left.+\left(\frac{\varepsilon}{h_\infty}\right)^2\frac{3}{4}\left(\frac{1}{k^2}-1\right)\left(2\frac{y}{h_\infty}+\frac{y^2}{h_\infty^2}\right)+0\left[\left(\frac{a}{h_\infty}\right)\left(\frac{2k^2-1}{k^2}\right)\right]^3\right\}$$

$$\frac{v(x,y)}{\sqrt{gh_\infty}} = -\left\{\sqrt{\frac{3}{k^2}\left(\frac{a}{h_\infty}\right)^3}\left(1+\frac{y}{h_\infty}\right)cn\;sn\;dn\;(A\omega x,k)\right\}\cdot$$

$$\cdot\left\{1-\left(\frac{a}{h_\infty}\right)\left(\frac{5k^2+2}{8k^2}\right)-\left(\frac{a}{h_\infty}\right)\left(1-\frac{1}{2k^2}\right)\left(2\frac{y}{h_\infty}+\frac{y^2}{h_\infty^2}\right)\right.$$

$$\left.-\frac{1}{2}\left(\frac{a}{h_\infty}\right)\left(1-6\frac{y}{h_\infty}-3\frac{y^2}{h_\infty^2}\right)cn^2(A\omega x,k)\right\}+0\left[\left(\frac{a}{h_\infty}\right)\left(\frac{2k^2-1}{k^2}\right)\right]^{7/2}$$

(31.36)

For the solitary wave we have $k = 1$ and essentially infinite wave length so (31.36) reduces to

$$\frac{\eta(x)}{h_\infty} = \frac{a}{h_\infty}\,\mathrm{sech}^2(A\omega x) - (3/4)\left(\frac{a}{h_\infty}\right)^2 \mathrm{sech}^2(A\omega x)[1-\mathrm{sech}^2(A\omega x)] +$$

$$+ 0\left(\frac{a}{h_\infty}\right)^3$$

$$(A\omega x) = \frac{x}{h_\infty}\sqrt{\frac{3}{4}\left(\frac{a}{h_\infty}\right)}\left\{1 - \frac{5}{8}\left(\frac{a}{h_\infty}\right)\right\} + 0\left(\frac{a}{h_\infty}\right)^{5/2}$$

$$\frac{p}{\rho g h_\infty} = \frac{\eta(x) - y}{h_\infty} - \left(\frac{a}{h_\infty}\right)^2 \frac{3}{4}\left(2\frac{y}{h_\infty} + \frac{y^2}{h_\infty^2}\right)\left[2\mathrm{sech}^2(A\omega x) - 3\mathrm{sech}^4(A\omega x)\right]$$

$$+ 0\left(\frac{a}{h_\infty}\right)^3$$

$$\frac{u(x,y)}{\sqrt{gh_\infty}} = \left\{\begin{array}{l} 1 + \frac{1}{2}\left(\frac{a}{h_\infty}\right) - \frac{3}{20}\left(\frac{a}{h_\infty}\right)^2 - \frac{\eta(x)}{h} + 0\left(\frac{a}{h_\infty}\right)^3 \\ \quad + \frac{1}{2}\left(\frac{a}{h_\infty}\right)^2\left[1 + 6\left(\frac{y}{h_\infty}\right) + 3\left(\frac{y}{h_\infty}\right)^2\right]\mathrm{sech}^2(A\omega x) + \\ \quad - \frac{1}{2}\left(\frac{a}{h_\infty}\right)^2\left[1 + 9\left(\frac{y}{h_\infty}\right) + \frac{9}{2}\left(\frac{y}{h_\infty}\right)^2\right]\mathrm{sech}^4(A\omega x) \end{array}\right. \qquad (31.37)$$

$$\frac{v(x,y)}{\sqrt{gh_\infty}} = -\left\{\sqrt{3}\left(\frac{a}{h_\infty}\right)^{3/2}\left(1 + \frac{y}{h_\infty}\right)\mathrm{sech}^2(A\omega x)\tanh(A\omega x)\right\}\cdot$$

$$\cdot\left\{1 - \frac{7}{8}\left(\frac{a}{h_\infty}\right) - \left(\frac{a}{h_\infty}\right)\left(\frac{y}{h_\infty} + \frac{1}{2}\frac{y^2}{h_\infty^2}\right) - \frac{1}{2}\left(\frac{a}{h_\infty}\right)\left(1 - 6\frac{y}{h_\infty} - 3\frac{y^2}{h_\infty^2}\right)\mathrm{sech}^2(A\omega x)\right\}$$

$$+ 0\left(\frac{a}{h_\infty}\right)^{7/2}$$

The celerity or propagation velocity (c) of a solitary wave is defined by (31.37) as the constant uniform motion attained as $x \to \infty$,

$$\frac{c}{\sqrt{gh_\infty}} = \frac{u(\infty)}{\sqrt{gh_\infty}} = \left\{1 + (1/2)\left(\frac{a}{h_\infty}\right) - (3/20)\left(\frac{a}{h_\infty}\right)^2 + 0\left(\frac{a}{h_\infty}\right)^3\right\} \qquad (31.38)$$

In Figure 48 equation (31.38) is shown to be in better agreement with recent experimental data than is the commonly used Boussinesq [1871] - Rayleigh [1876] propagation velocity given by

$$\frac{c}{\sqrt{gh_\infty}} \approx \sqrt{1 + \left(\frac{a}{h_\infty}\right)} \approx \left\{1 + \frac{1}{2}\left(\frac{a}{h_\infty}\right) - \frac{1}{8}\left(\frac{a}{h_\infty}\right)^2 + \cdots\cdots\right\}$$

The past success of the Boussinesq-Rayleigh equation, as opposed to the progagation velocities derived by McCowan [1891] or Weinstein [1926], as indicated in Figure 48, is easily explained when one notices the close numerical agreement of the coefficients of the Boussinesq-Rayleigh equation with the exact second approximation given by (31.38).

A comparision of the second approximations with the first approximations to the cnoidal waves proves conclusively that only the proper order of (a/h_∞) must be retained for each order of approximation. For example, a comparison of (31.18) with (31.35) shows that a completely erroneous second approximation would be obtained by trying to extend the first approximation to include an additional (a/h_∞) term. The reason for this is evident upon comparing the first and second approximations for η_o in (31.17) and (31.34). Each successive approximation directly affects all the coefficients of the corresponding (a/h_∞) terms. Figure 49 shows the effect of the second approximation on a solitary wave.

Of course it must be remembered that the expansion method of Friedrichs [1948], that was used to obtain all the preceding results, is applicable only to shallow water, or long wave length wave propagations. However, this is precisely the nature of the solitary wave, especially if the amplitude (a/h_∞) is relatively small, since its effective wave length is essentially infinite. The wave length $(\lambda = 2K)$ is infinite by the mathematical definition given by $K(1) \to \infty$ when $k = 1$, however, any physical description would lead to a specific finite effective "wave length" since $LIM_{x \to \pm\infty}(x) = 0$ for a solitary wave of any finite amplitude. Also Friedrichs and Hyers [1954] proved that this expansion method does yield an existence proof for the solitary wave, and thereby demonstrates that it will

at least provide asymptotic descriptions of the exact solution for the solitary wave problem. The convergence of the expansion indicated by (31.37) for the solitary wave seem reasonable in view of their excellent agreement with experimental data. The corresponding existence proof for cnoidal waves (in the neighborhood of the critical speed defined by a Froude number of unity) was given by Littman [1957]. Again this justified the Friedrichs expansion method, at least as an asymptotic type of series development. An additional discussion of these existence proofs is given in section 35.

31 β - The Limiting Height and Velocity of Propagation of Cnoidal and Solitary Waves.

It is interesting to note that the pressure is still hydrostatic for $y \geq 0$, but is no longer hydrostatic as the bottom ($y = -h_\infty$) is appraoched with the second approximation. Similarly the variation of the horizontal velocity component with depth below the surface becomes important in the second approximation only upon approaching the flat horizontal bottom. However, the vertical velocity component is now seen to be the principal variation that violates the basic assumptions of first order shallow water theory. The first approximation given in (31.19) gives a monotonic variation in $v(y)$ that is obviously necessary from physical consideration in order to satisfy the continuity equation. However, this monotonic variation in $v(y)$ is of the higher order of $(a/h_\infty)^{3/2}$ so it can be neglected in the first order equations (28.2) as long as the resulting local variations in η are sufficiently small.

The second approximation to the vertical velocity component, as given in (31.36), now shows that the variation of $v(y)$ will no longer be monotonic as (a/h_∞) increases. This leads one to suspect that there is a limiting value to (a/h_∞) for cnoidal and solitary waves. For example, (31.36) shows that in the neighborhood of the wave crest where $x \to 0$ so that

$$cn^2(A\omega x) \to [1 - (A\omega x)^2] = \left[1 - \frac{3}{4k^2}\left(\frac{a}{h_\infty}\right)\left(\frac{x}{h_\infty}\right)^2 + 0\left(\frac{a}{h_\infty}\right)^2\right]$$

then $v(y)$ actually has a reversal in its direction if (a/h_∞) exceeds the value given by

$$\left(\frac{a}{h_\infty}\right)_{MAX} = \left(\frac{8k^2}{9k^2 + 2}\right) \tag{31.39}$$

for any value of $y \geq 0$.

This limiting value can be substantiated, at least in the limit as $k \to 1$, by noting that (31.33) has a real solution for η_1 only if

$$\left(\frac{2k^2 - 1}{k^2}\right)\left(\frac{a}{h_\infty}\right) < \left(\frac{\eta_o}{h_\infty}\right) \leq \frac{5\,(2k^2 - 1)^2}{7 - 37k^2(1 - k^2)}$$

leading to a limiting value of

$$\left(\frac{a}{h_\infty}\right)_{MAX} < \frac{5k^2(2k^2 - 1)}{7 - 37k^2(1-k^2)} \tag{31.40}$$

The most interesting application of these results are to the solitary wave defined by $k = 1$, in which case we find from (31.38), (31.39) and (31.40) that the limiting heights and the corresponding total velocity at infinity are given by

$$\left(\frac{a}{h_\infty}\right)_{MAX} = \frac{8}{11} = 0.7273 > \frac{5}{7} = 0.7143$$

$$\left[\frac{u(\infty)}{\sqrt{gh_\infty}}\right]_{MAX} = 1.284 > 1.281 \qquad (31.41)$$

Either of these limiting heights would be satisfactory for a solitary wave since recent experimental investigations by Ippen and Kulin [1955], Daily and Stephan [1952], and Perroud [1957] have shown that under properly controlled conditions most solitary waves have $(a/h_\infty) < 0.7$, the maximum recorded value being 0.72. Not only are the limiting values given by (31.39) or (31.40) in excellent agreement with recent experimental data, but they are consistent with the order of approximation involved. The (8/11) value is derived from the vertical velocity variation given to the order of $(a/h_\infty)^{5/2}$ by (31.36), while the (5/7) value corresponds to the terms governed by ε^2 or $(a/h_\infty)^2$ in (31.32).

Many attempts have been made to determine the limiting height of a solitary wave. However, nearly all of the theoretical calculations have been based on Stokes [1880, page 227] relation which assumes that for the limiting heights of any wave the wave crest must form a sharp peak or double point having an enclosed angle of 120° in order to reduce the relative local velocity to zero at the crest itself, e.g., see section 33 or Lamb [1932], page 418. This 120° enclosed angle at the wave crest was assumed by McCowan [1894], Stokes [1905], Gwyther [1900], Davies [1952], Packham [1952], Goody and Davies [1957] and Yamada [1957]. Several of these values are compared with experimental data, and the theoretical values given by (31.38) and (31.41), in Figure 48. It is seen that none of these

limiting heights for solitary waves are in as good an agreement with the experimental data as is (31.41). A reasonable explanation of the failure of the 120° sharp crest wave to provide a satisfactory limiting height for a solitary wave may be obtained by noting that Korteweg and de Vries [1895] proved that any finite amplitude profile that did not correspond to (31.17) or (31.20) would not be steady with respect to time. Consequently, (31.37) defines the only possible steady state solitary wave, and when $(a/h_\infty) > (8/11)$ the vertical velocity variation reverses its direction near the crest. This probably leads to an unsteady wave crest that breaks unsymmetrically.

Equation (31.38) shows that the solitary wave only occurs in supercritical flow since the Froude number corresponding to the propagation velocity is always greater than unity. Its velocity of propagation is always less than that of the corresponding hydraulic jump as may be seen by comparing (30.55) with (31.38), after expanding it in powers of $(a/d_1) = (a/h_\infty)$,

$$F_1 = \frac{u_1}{\sqrt{gh_\infty}} = 1 + \frac{3}{4}\left(\frac{a}{h_\infty}\right) - \frac{1}{32}\left(\frac{a}{h_\infty}\right)^2 + 0\left(\frac{a}{h_\infty}\right)^3 \qquad (30.55')$$

However, the cnoidal wave can occur in subcritical as well as in supercritical flow, and as shown by Benjamin and Lighthill [1954], the undulating flow in the subcritical region behind a hydraulic jump produced at all Froude numbers less than $\sqrt{3}$ may well be represented by these cnoidal waves. The fact that cnoidal waves can form in subcritical flow is easily shown, even in the first approximation, by writing the horizontal velocity component from (31.19) as

$$\frac{u(o)}{\sqrt{gh_\infty}} = \left[1 - \frac{1}{2k^2} \left(\frac{a}{h_\infty} \right) \right] < 1 \text{ for all } k \leqq 1$$

$$\frac{u\left(\frac{K}{A\omega}\right)}{\sqrt{gh_\infty}} = \left[1 + \left(1 - \frac{1}{2k^2}\right) \left(\frac{a}{h_\infty} \right) \right] < 1 \text{ for } k^2 < 1/2 \qquad (31.42)$$

Therefore (31.19) shows that any definition of the wave propagation velocity would be subcritical when $k^2 < 1/2$. Stokes [1847] has given two logical definitions of the celerity or propagation velocity of permanent periodic wave forms, and each one would define a critical celerity corresponding to a different value of k, varying as $1/2 \leqq k^2 < 1$, the solitary wave (k = 1) being always supercritical for a finite amplitude. However, the existence proof for cnoidal waves by Littman [1957] is only valid for average velocities (defined as the velocity of the vertical plane that would have zero average flux across it) that are near critical. An interesting physical and mathematical explanation of these flow restrictions is given by Benjamin and Lighthill [1954]. The main consideration, as shown in Figure 55 and section 35, is that the finite amplitude periodic waves corresponding to $k^2 < 0.9$ may be better described by using infinitesimal wave theory. This becomes necessary because the wave length of the cnoidal waves decreases rapidly with k^2 when k is near one. Figure 55 indicates that not only must the wave length be large compared to the water depth, in order to satisfy the shallow water expansion method, but also the amplitude of the cnoidal wave must become extremely small for values of $k^2 < 0.9$, or for subcritical flow.

Korteweg and de Vries [1895] have also shown how negative cnoidal or solitary waves can be formed when the water is very shallow and surface tension (T) is considered. Their correct first approximation may be written as

$$\frac{\eta(x)}{h_\infty} = \pm \left(\frac{a}{h_\infty}\right) \operatorname{cn}^2(A\omega x,\ k)$$

$$(A\omega x) = \frac{x}{h_\infty} \sqrt{\frac{3}{4k^2} \frac{(a/h_\infty)}{\left|1 - \frac{3T}{\rho g h_\infty^2}\right|}} \qquad (31.43)$$

where the negative algebraic value is assigned to the surface profile whenever

$$h_\infty < \sqrt{\frac{3T}{\rho g}} \approx \frac{1}{2} \text{ cm. for water} \qquad (31.44)$$

These negative waves have a very small amplitude and a very large wave length, but can create a surprising particle motion. It is interesting to notice that the depth of h_∞ = 1/2 cm, which, if it could be maintained, would eliminate both solitary and cnoidal waves, is the same depth found from (31.1') and (31.2) to give nearly the same value of $\sqrt{gh_\infty}$ for both the propagation velocity and the group velocity of infinitesimal waves (also see section 15). Consequently the depth of 1/2 cm seems to be the optimum for ordinary water (T = 72.8 dynes/cm.) whenever one uses small models to simulate results appropriate to the first order shallow water theory of (28.2), since this particular depth minimizes the effect of group velocity and variation with wave length for the infinitesimal waves, and minimizes the second order effect due to the existence of finite amplitude cnoidal or solitary waves. However, the variation of η must remain sufficiently small since a finite increase in η above h_∞ = 1/2 cm. could still produce cnoidal or solitary waves. Also, the short wave length or capillary ripples that will form must be neglected in these model tests.

TABLE I

f (deg.)	$1+\frac{\eta}{h_o}$	F_*	F	K	f (deg.)	$1+\frac{\eta}{h_o}$	F_*	F	K
0	2/3	1.000	1.000	∞	26	0.234	1.516	2.56	-0.160
1	0.624	1.062	1.098	2.68	27	.223	1.527	2.64	-.177
2	.598	1.101	1.160	2.07	28	.212	1.538	2.73	-.196
3	.576	1.129	1.214	1.40	29	.201	1.549	2.82	-.216
4	.555	1.156	1.267	1.014	30	.190	1.559	2.92	-.234
5	.535	1.182	1.319	.758	31	.180	1.569	3.02	-.252
6	.516	1.207	1.371	.590	32	.170	1.579	3.13	-.271
7	.498	1.229	1.422	.476	33	.160	1.588	3.24	-.291
8	.481	1.249	1.470	.394	34	.151	1.597	3.36	-.313
9	.464	1.269	1.520	.318	35	.141	1.605	3.49	-.336
10	.448	1.288	1.570	.263	36	.132	1.613	3.63	-.36
11	.432	1.306	1.622	.215	37	.123	1.621	3.78	-.38
12	.417	1.323	1.674	.170	38	.115	1.629	3.93	-.40
13	.402	1.340	1.727	.133	39	.107	1.637	4.01	-.43
14	.387	1.356	1.781	.103	40	.099	1.644	4.26	-.46
15	.373	1.372	1.835	.072	41	.092	1.651	4.44	-.49
16	.359	1.387	1.89	.046	42	.085	1.657	4.63	-.52
17	.345	1.402	1.95	.020	43	.078	1.663	4.85	-.54
18	.331	1.416	2.01	-.004	44	.072	1.669	5.08	-.58
19	.318	1.430	2.07	-.028	45	.066	1.675	5.33	-.62
20	.305	1.444	2.13	-.050	46	.060	1.681	5.62	-.66
21	.292	1.457	2.20	-.071	47	.054	1.686	5.95	-.70
22	.280	1.470	2.27	-.089	48	.048	1.691	6.30	-.75
23	.268	1.482	2.34	-.108	49	.043	1.696	6.68	-.81
24	.256	1.494	2.41	-.126	50	.038	1.700	7.11	-.86
25	.245	1.505	2.48	-.143	65° 53'	0	$\sqrt{3}$	∞	$-\infty$

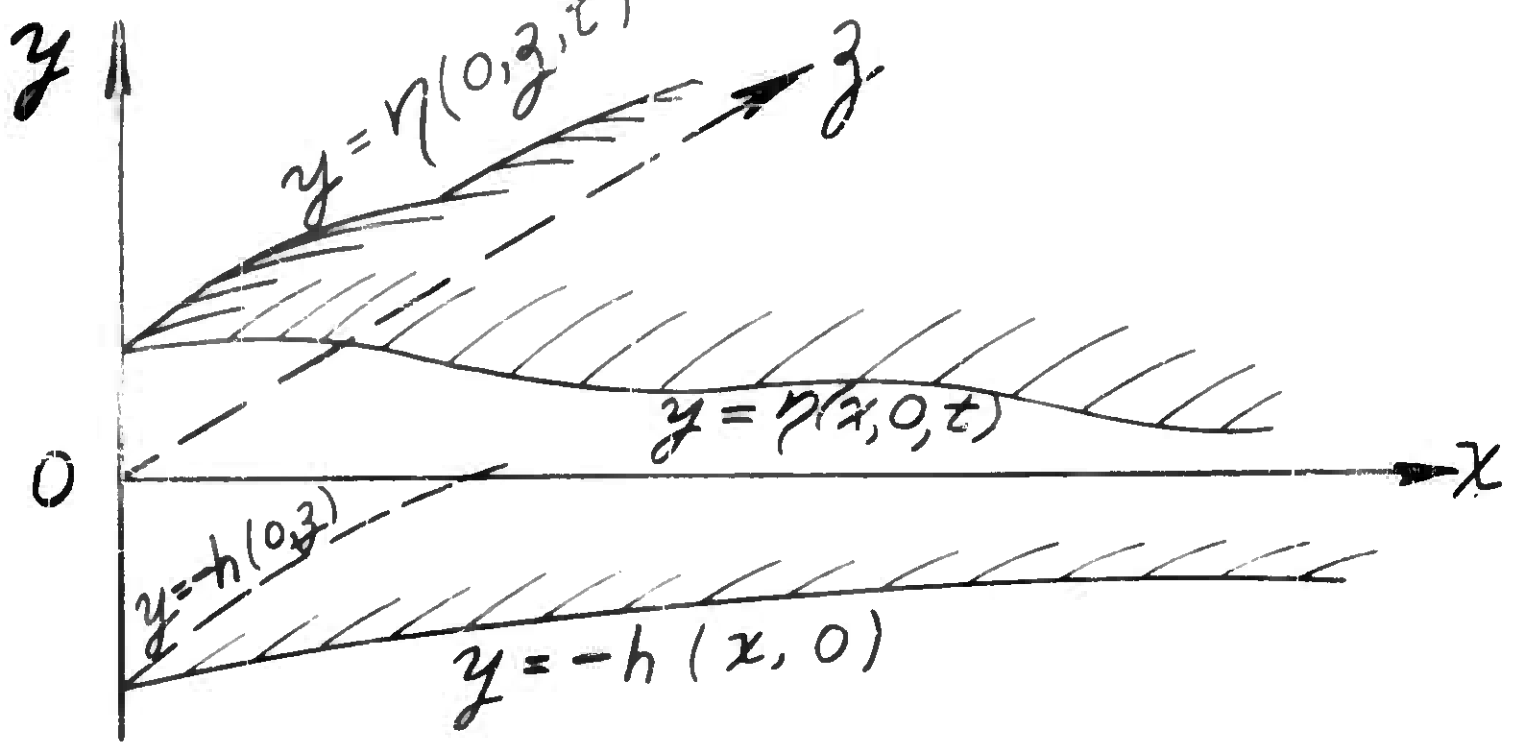

FIG. 37(a)

NON-STEADY WAVES OVER A SLOPING BOTTOM, $h(x,z)$

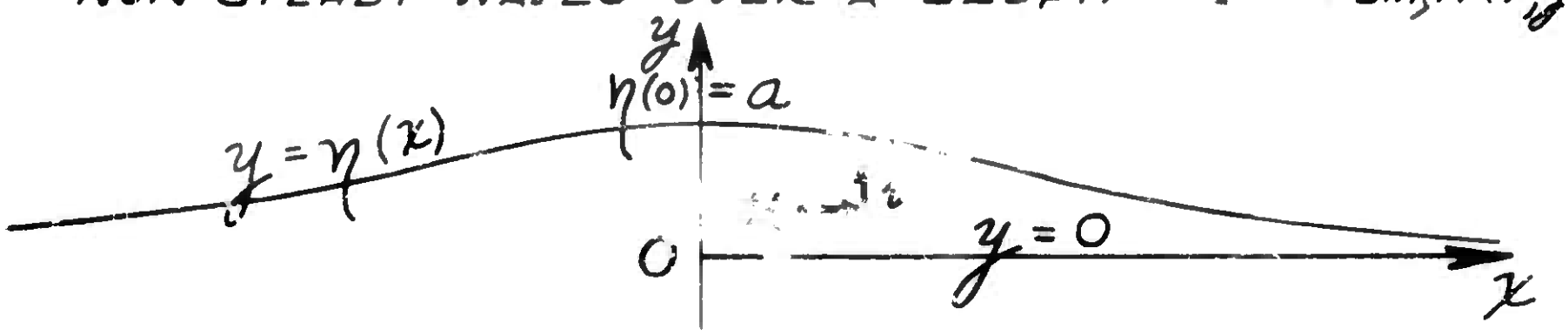

FIG. 37(b)

SOLITARY WAVE OVER A FLAT HORIZONTAL BOTTOM

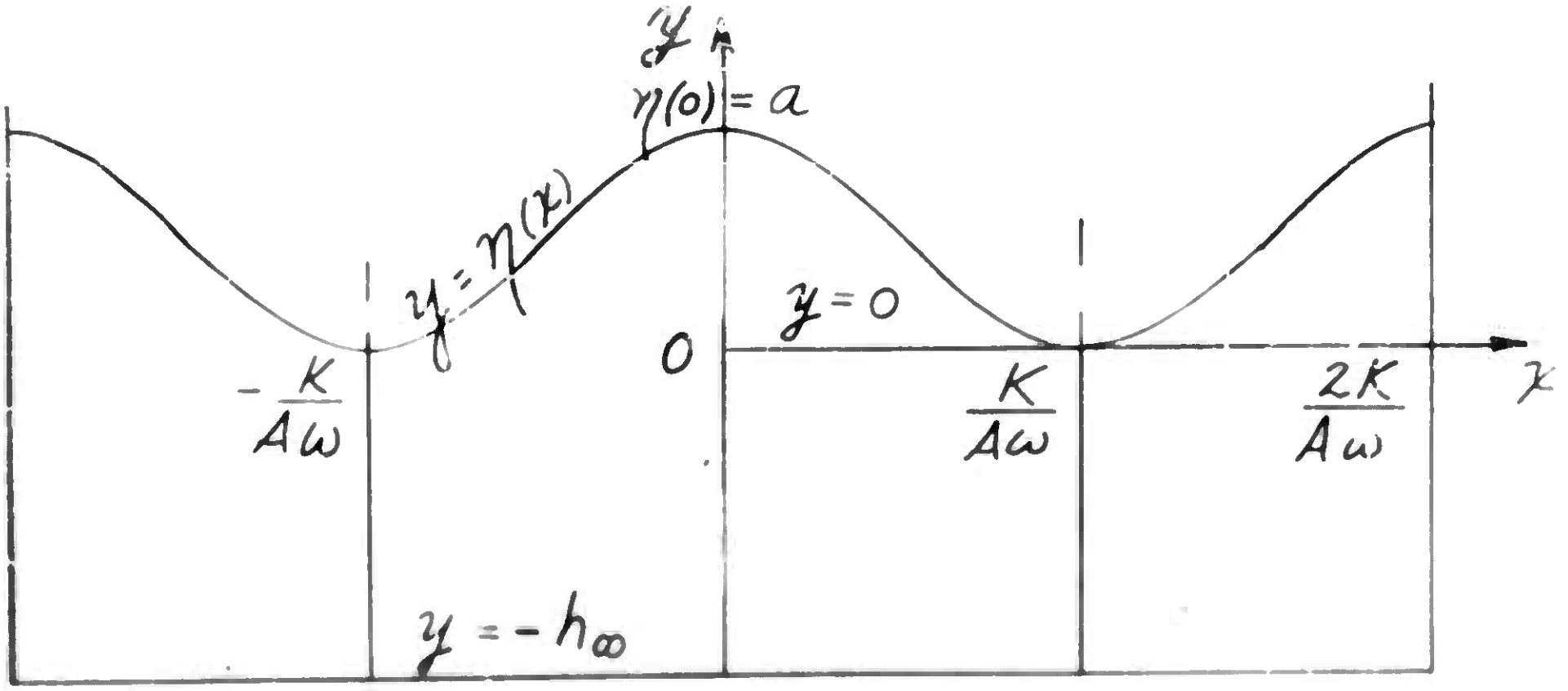

FIG. 37(c)

CNOIDAL WAVE $\eta(x) = a\,cn^2(A\omega x, k)$

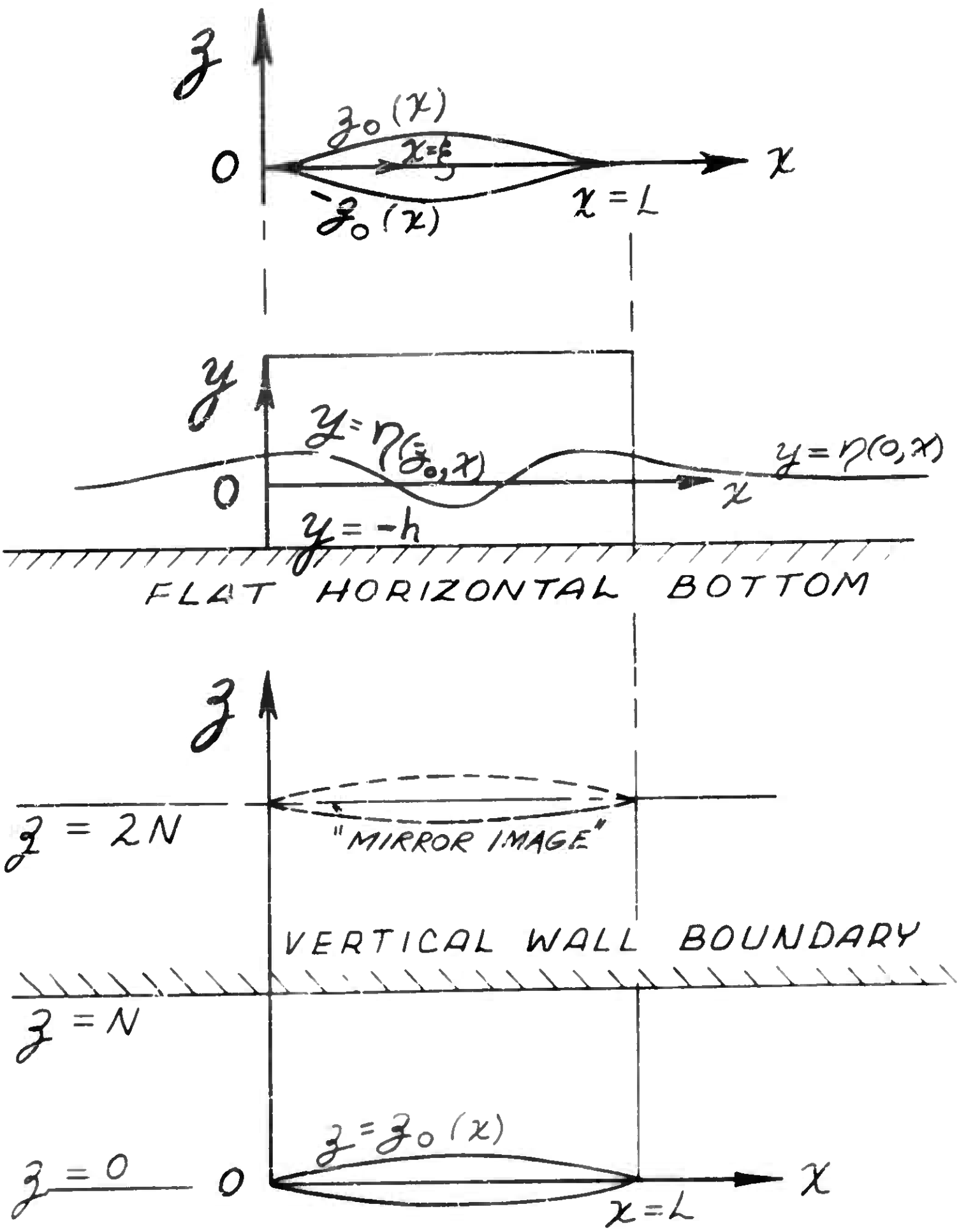

FIG. 38- SHALLOW-WATER FLOW ABOUT A TWO-DIMENSIONAL SYMMETRICAL CYLINDER PERPENDICULAR TO THE FLAT HORIZONTAL BOTTOM

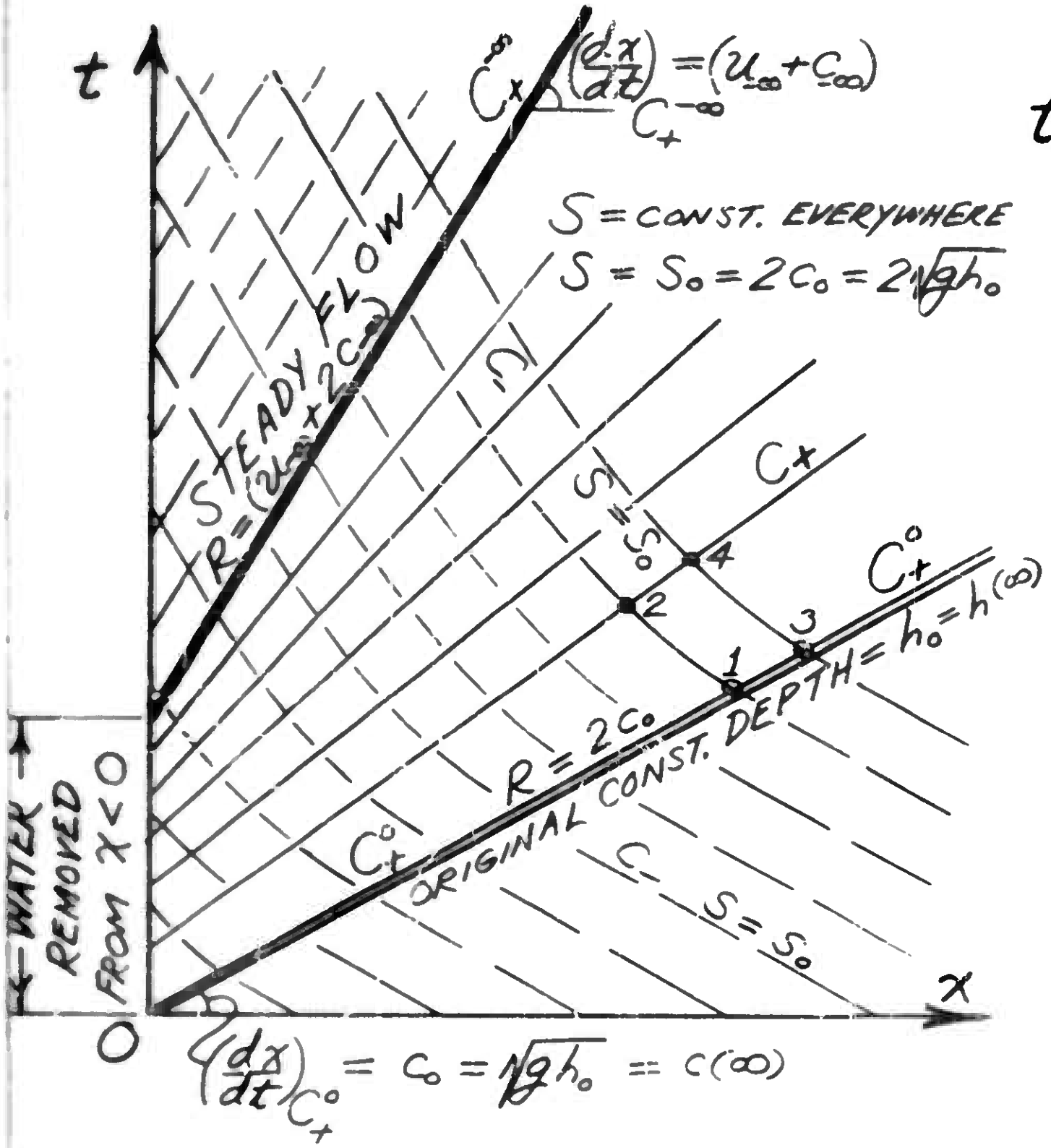

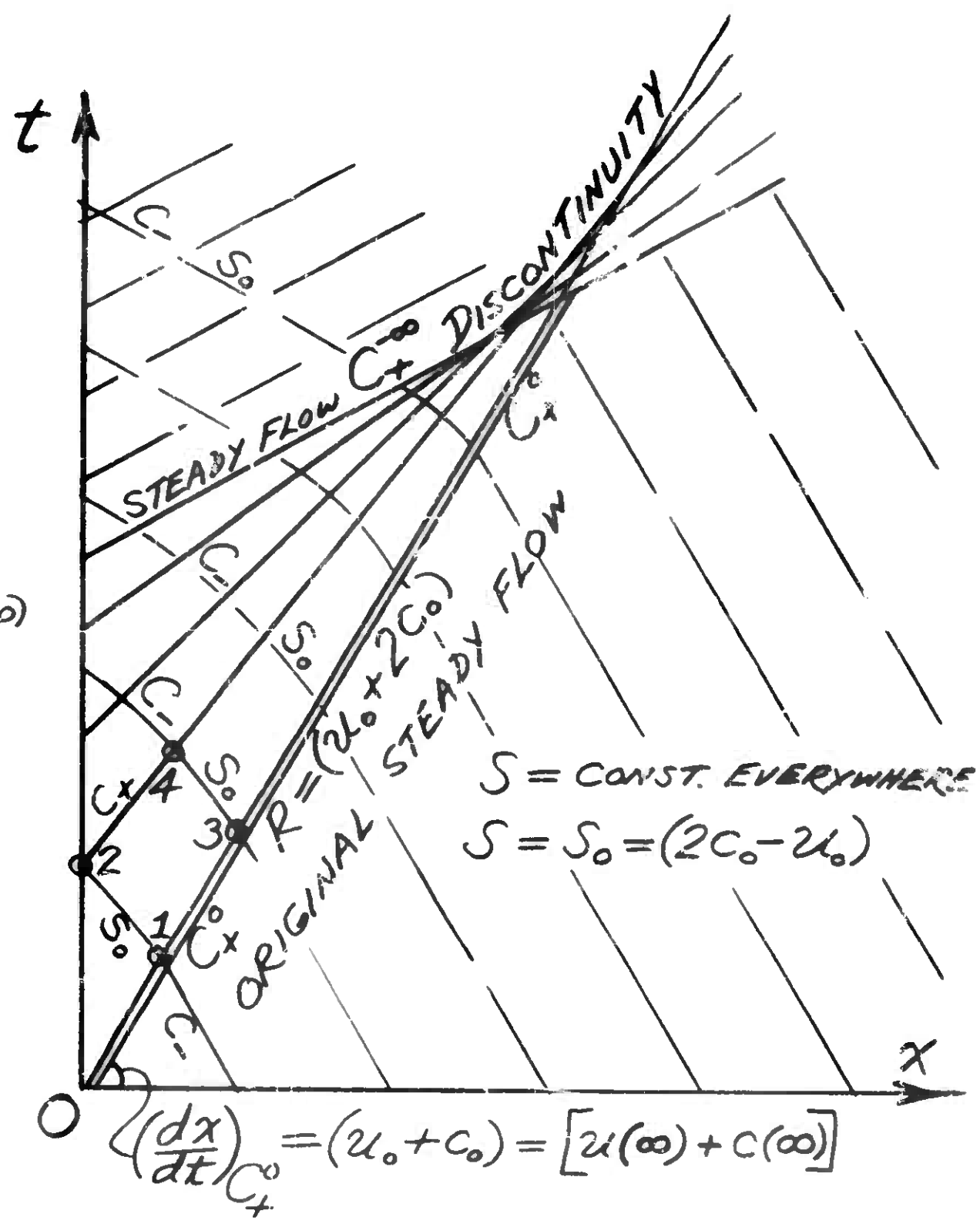

FIG. 39 - SIMPLE FORWARD-FACING WAVES, $S = \text{CONST.}$

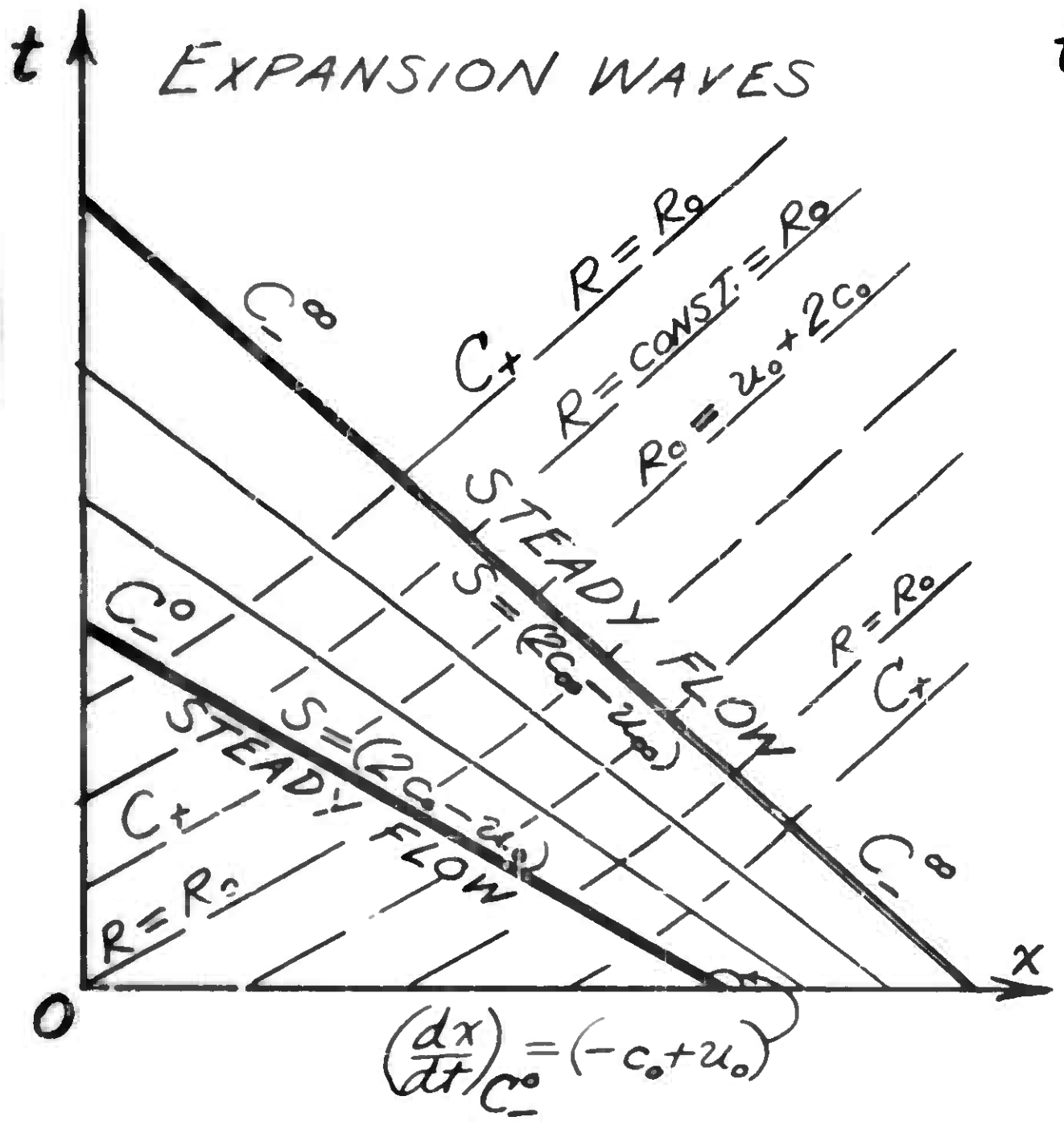

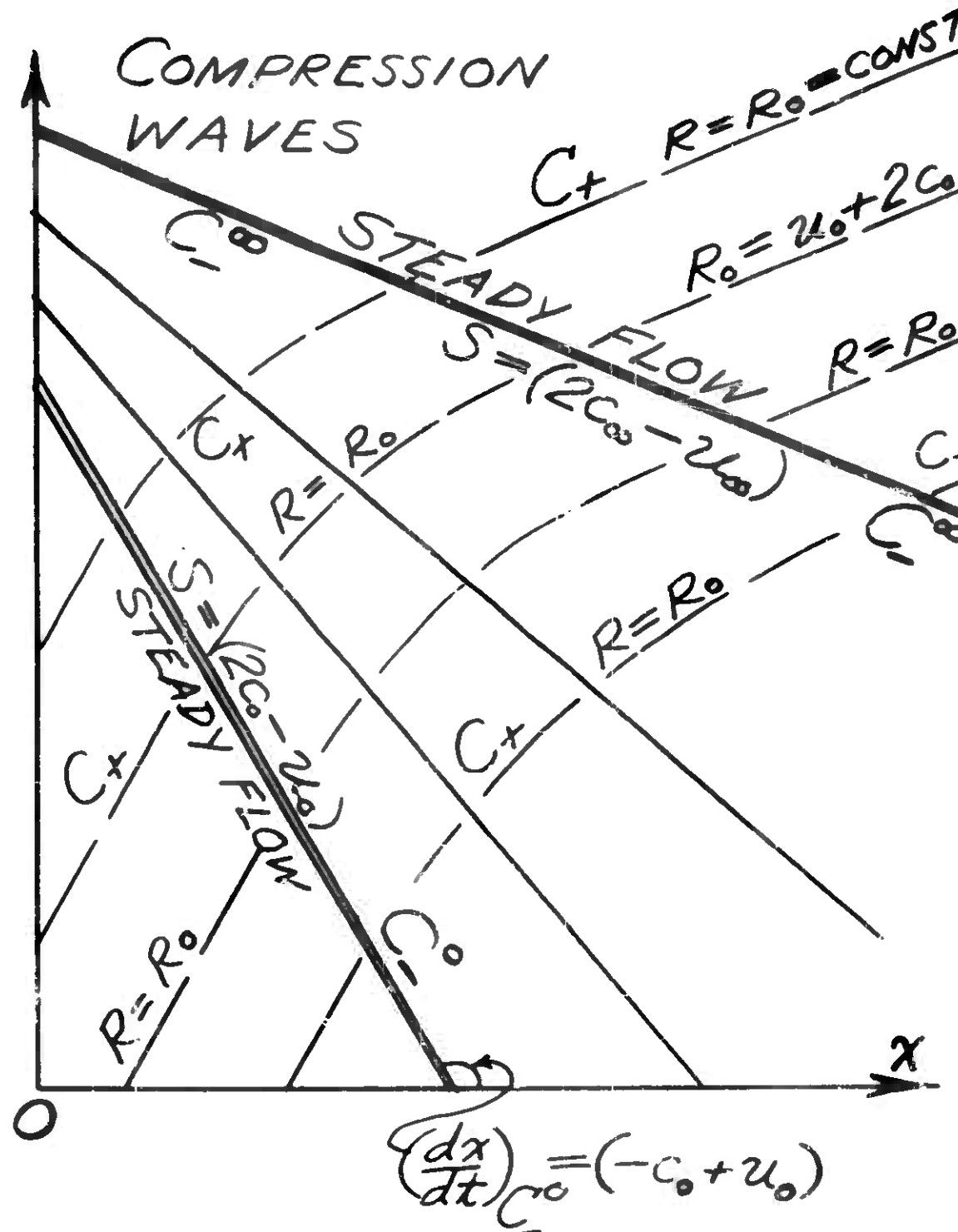

FIG. 40 - SIMPLE BACKWARD-FACING WAVES, $R=$ CONST.

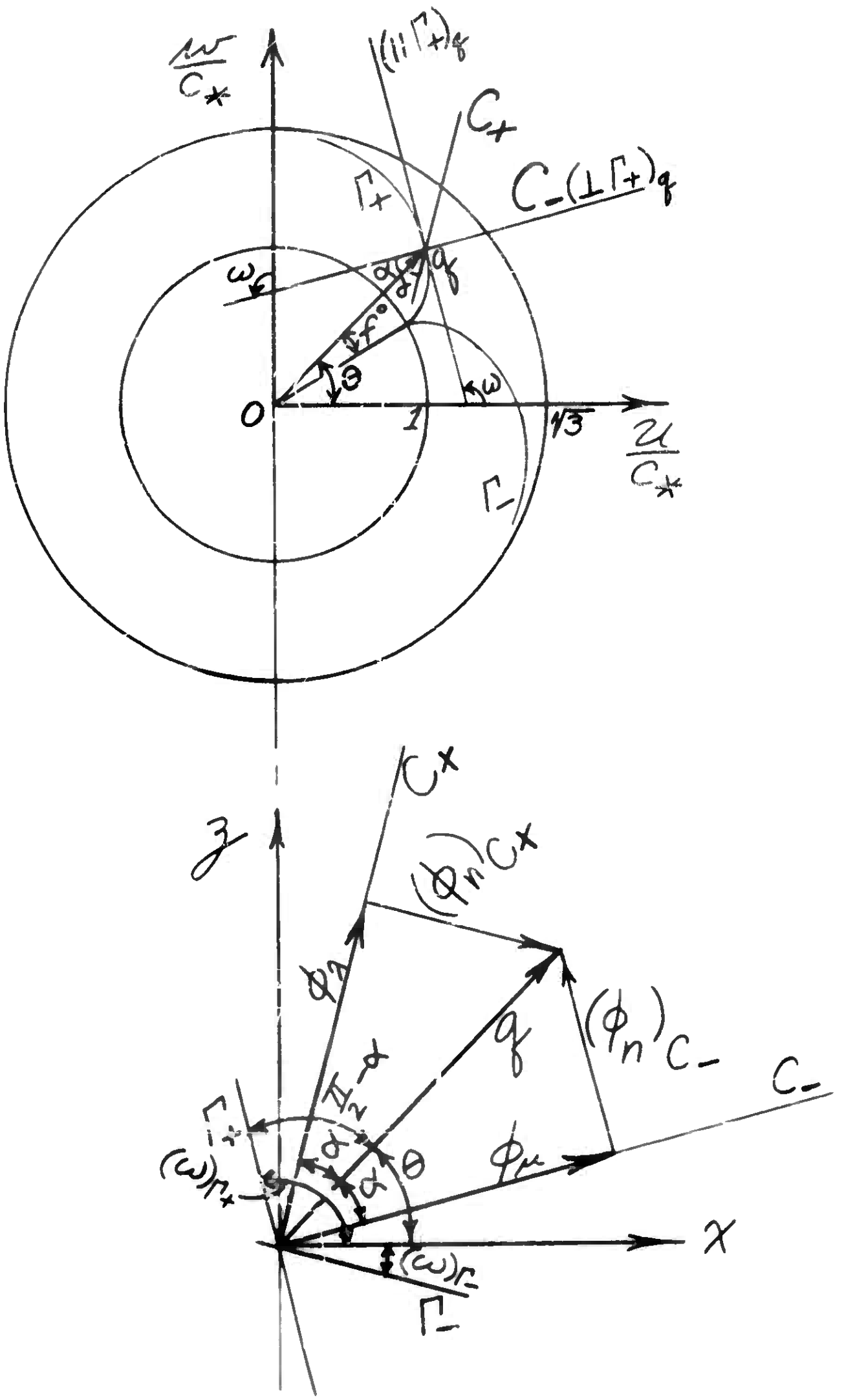

FIG. 41 – CHARACTERISTIC DIRECTIONS IN THE HODOGRAPH (u, w) PLANE AND THE PHYSICAL (x, z) PLANE.

$$F^2 = 2\left(\frac{h_0}{h} - 1\right) = \left(\frac{2F_*^2}{3 - F_*^2}\right) = 2\left[\left(\frac{C_0}{C}\right)^2 - 1\right]$$

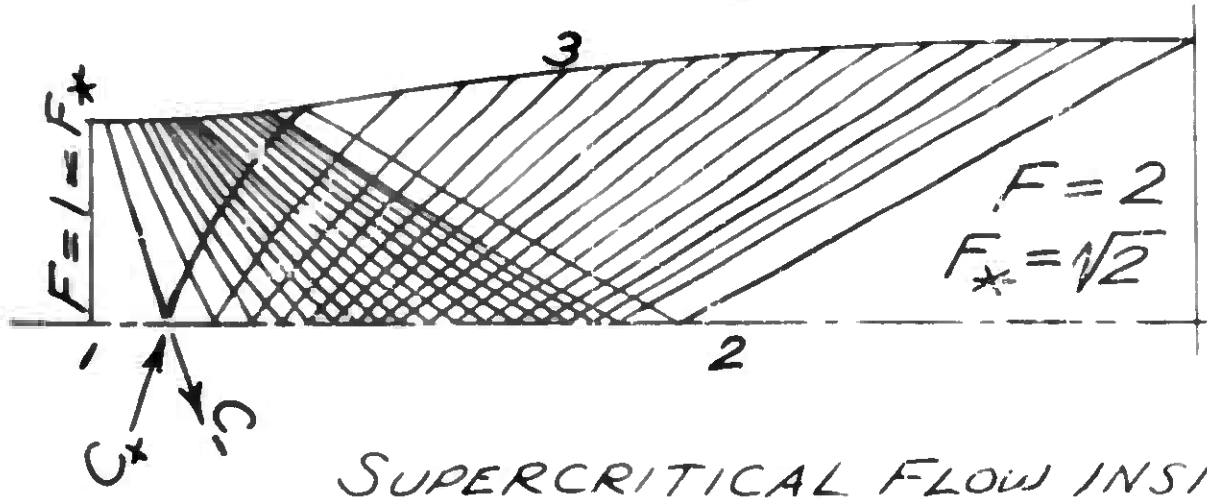

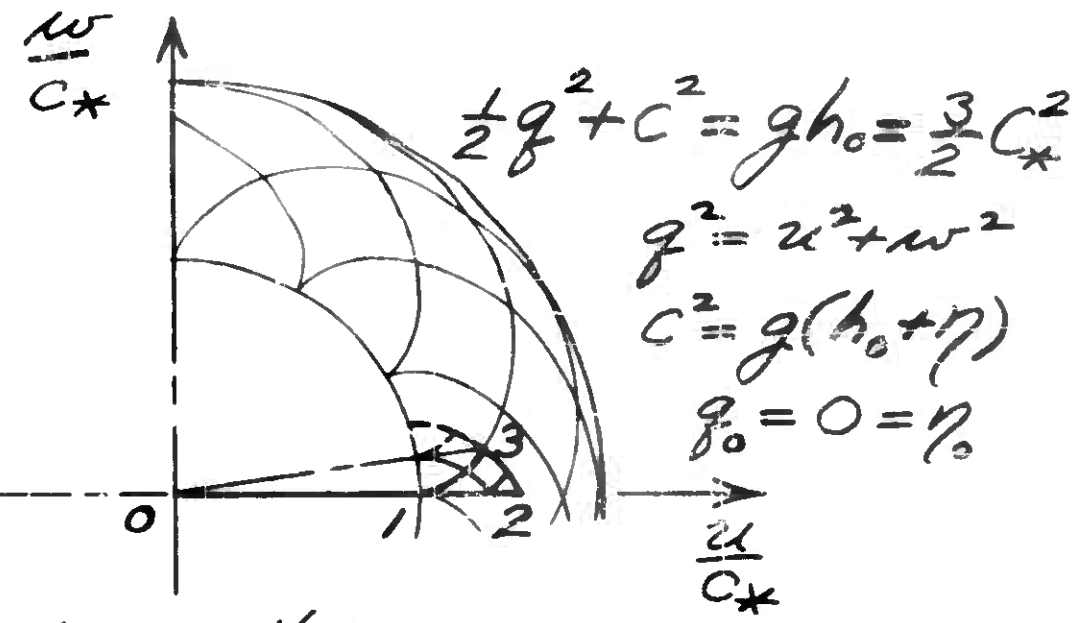

SUPERCRITICAL FLOW INSIDE $\frac{1}{2}$-LAVAL NOZZLE.

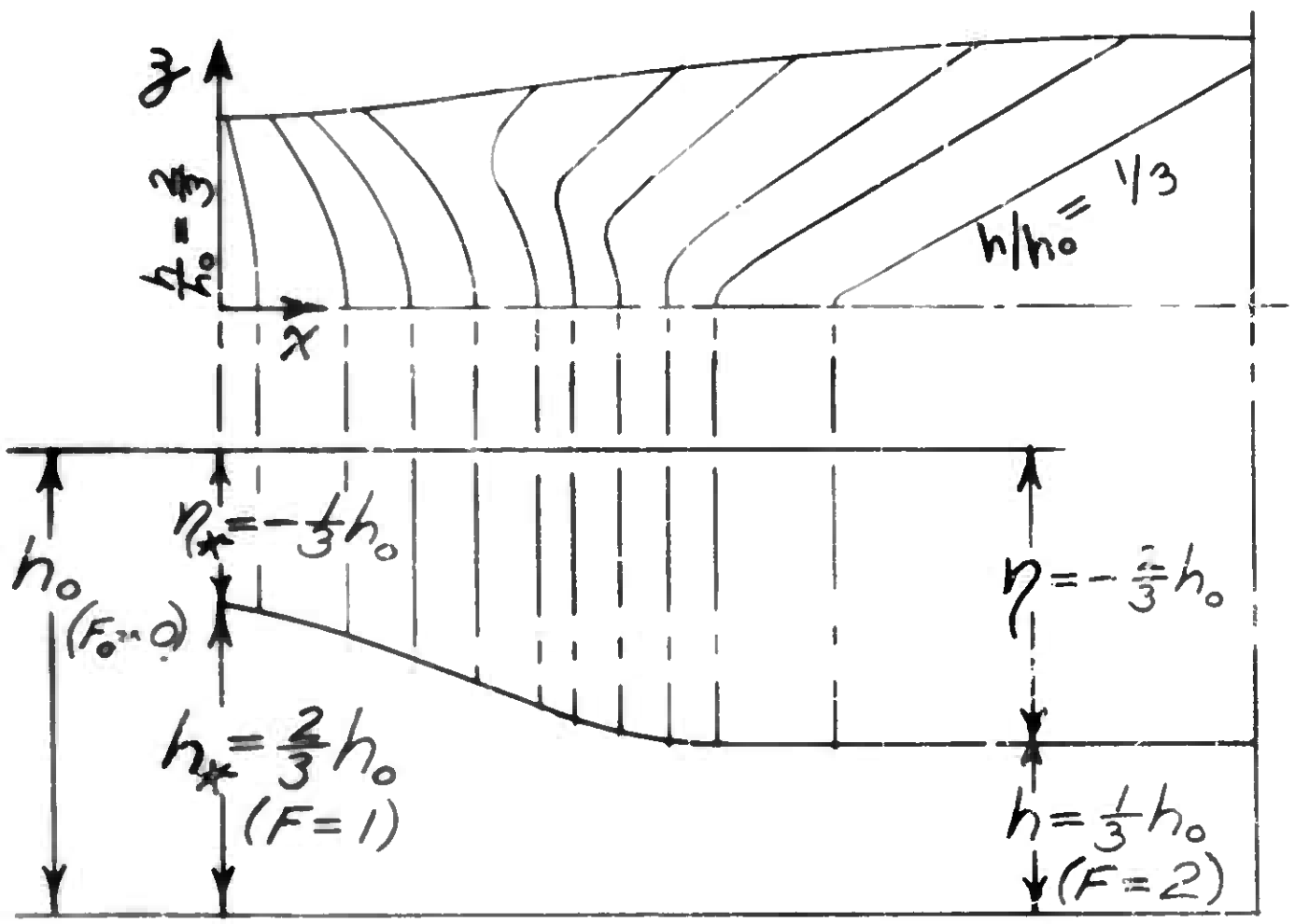

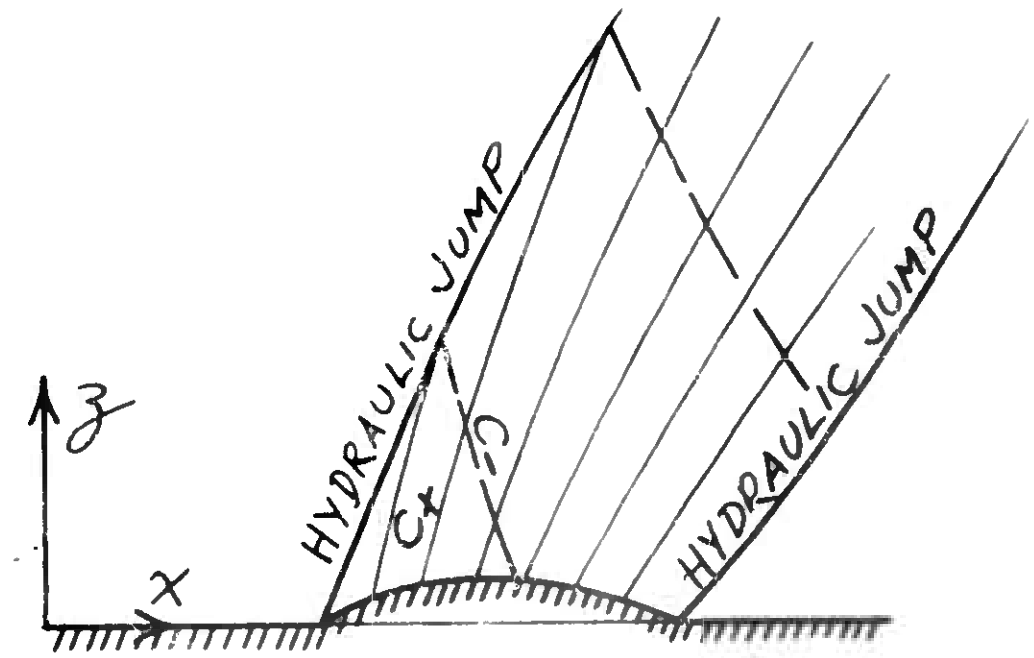

SUPERCRITICAL FLOW OUTSIDE TWO-DIMENSIONAL BUMP.

FIG. 42 — REFLECTION OF EXPANSION WAVES AND NOZZLE DESIGN.

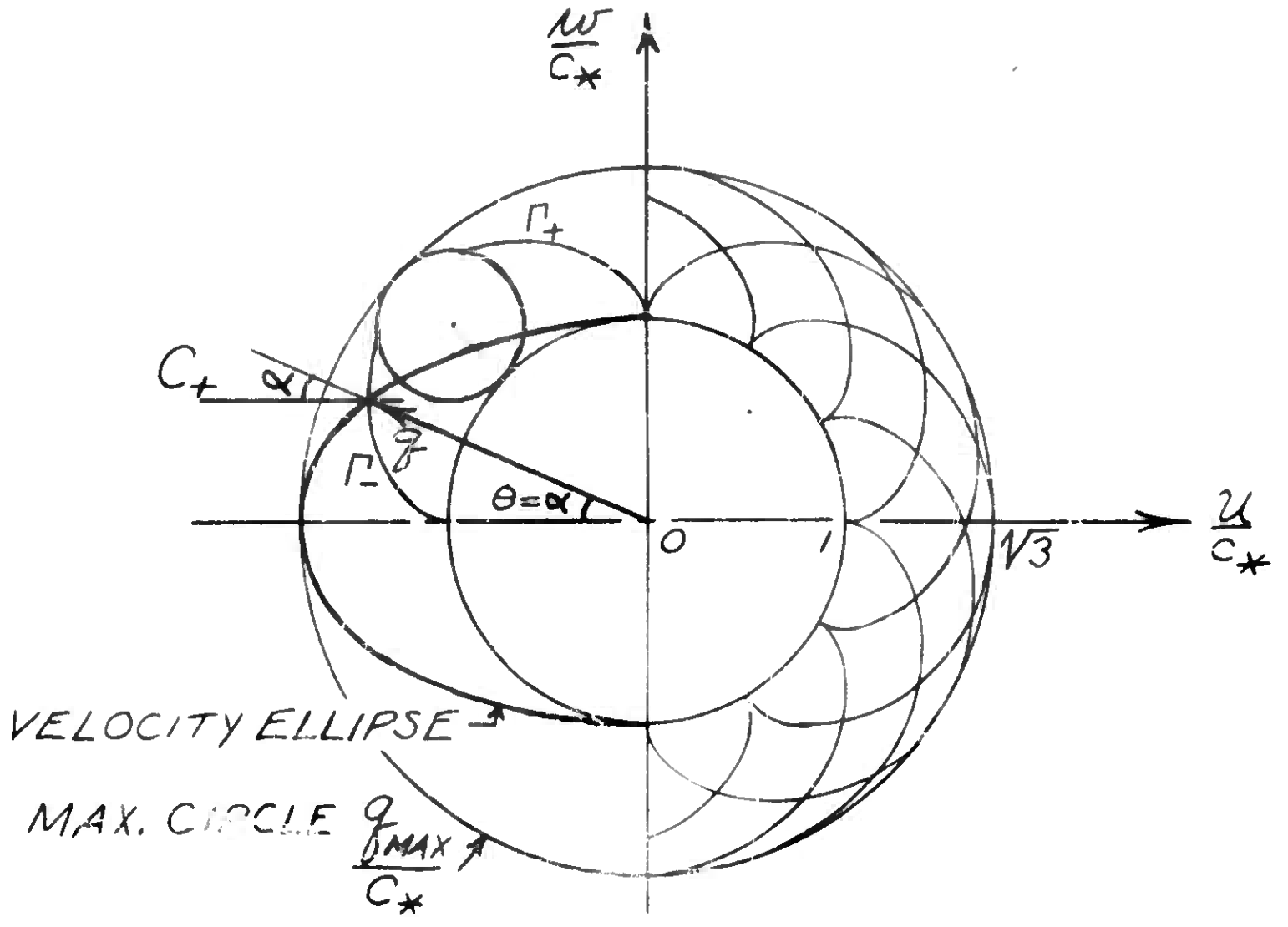

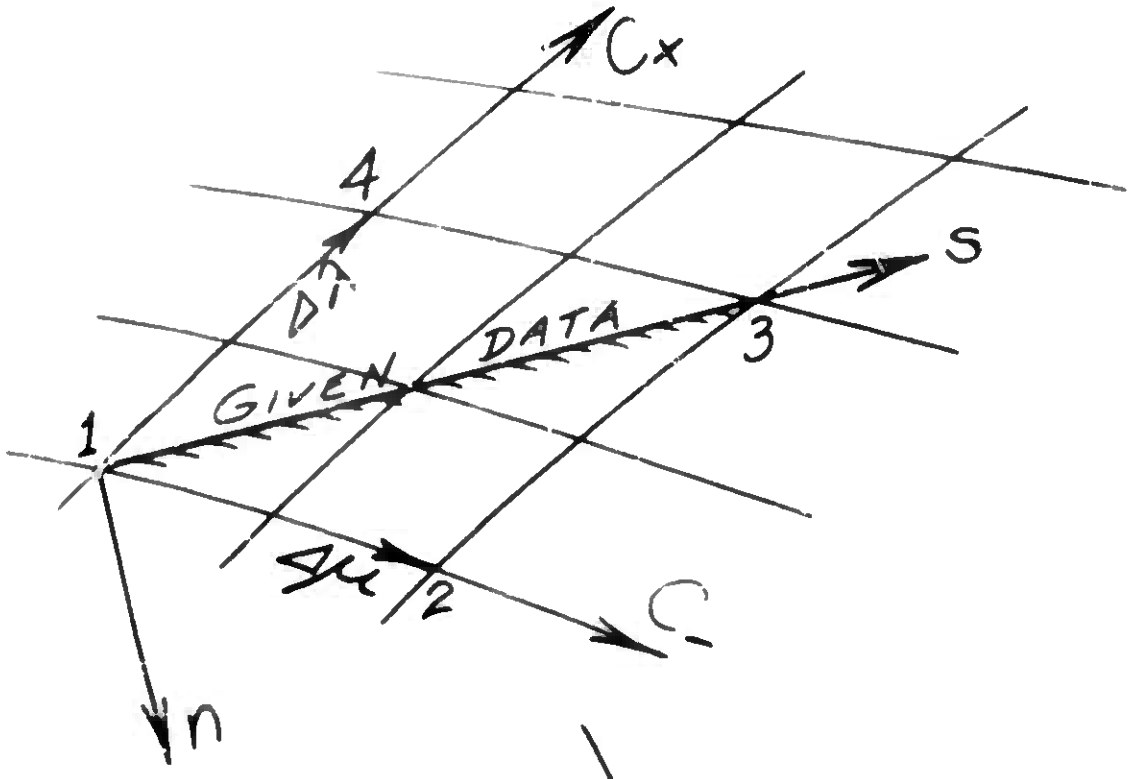

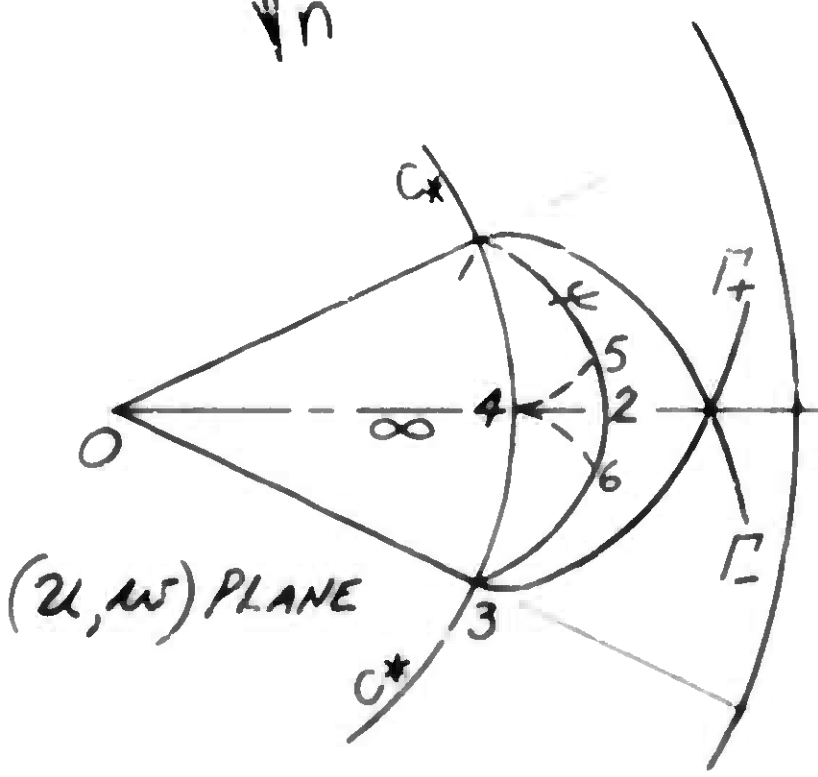

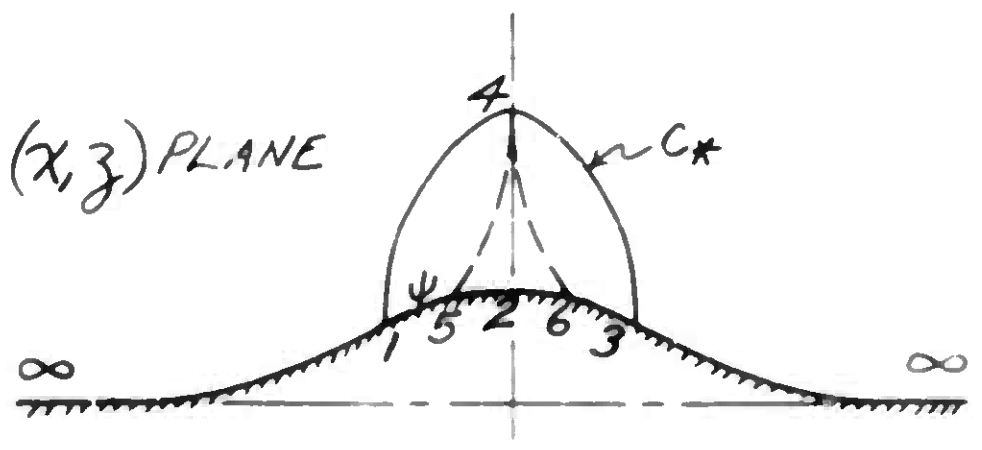

FIG. 43 – HODOGRAPH (u, w) PLANE CHARACTERISTIC EPICYCLOIDS.

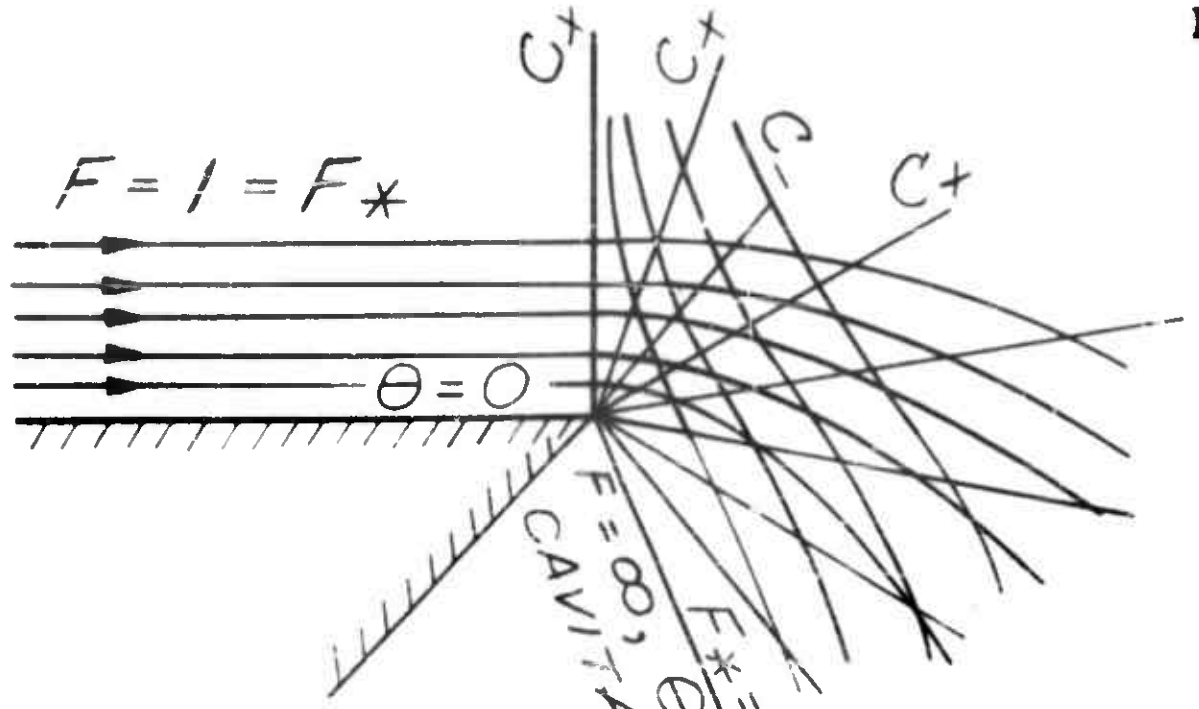

COMPLETE CENTERED
SIMPLE EXPANSION WAVE.

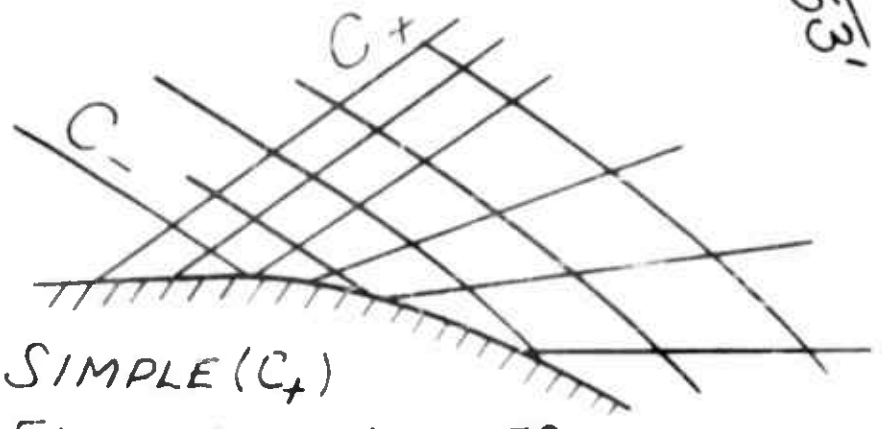

SIMPLE (C_+)
EXPANSION WAVES

SIMPLE (C_+) COMPRESSION WAVES
FORMING A DISCONTINUOUS (H. J.)
INCREASE IN WATER DEPTH.

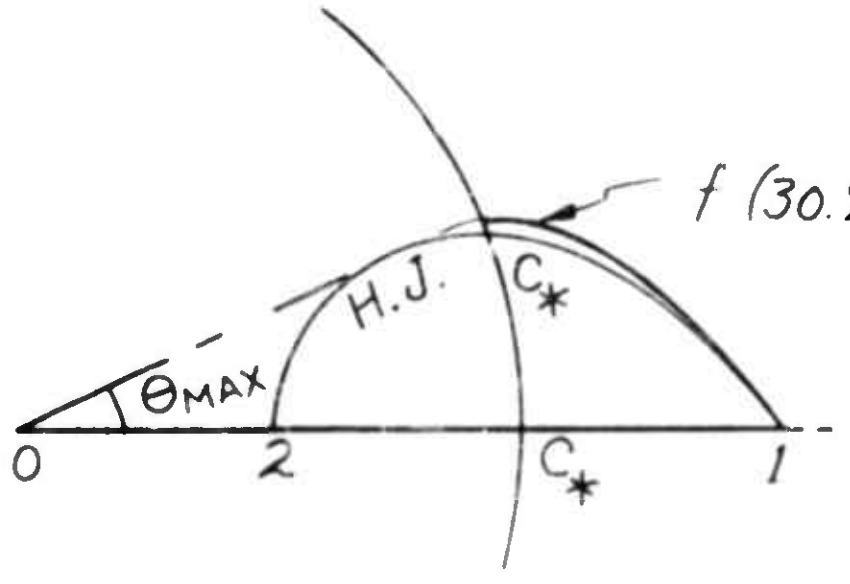

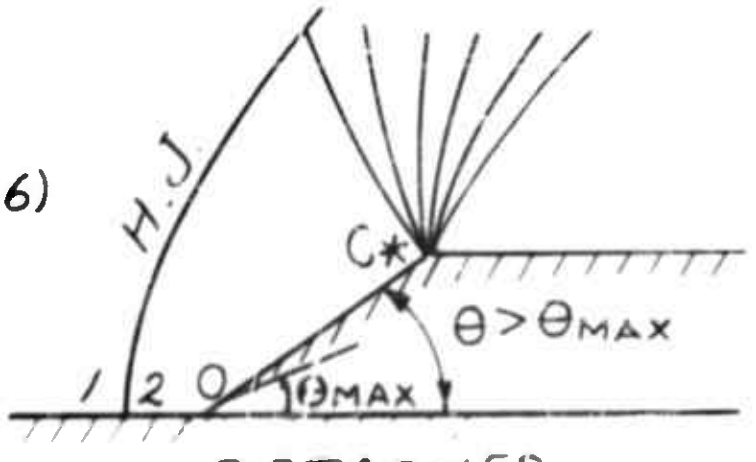

DETACHED
HYDRAULIC JUMP

FIG 44 - SIMDLE WAVES AND THE FORMATION OF HYDRAULIC JUMPS

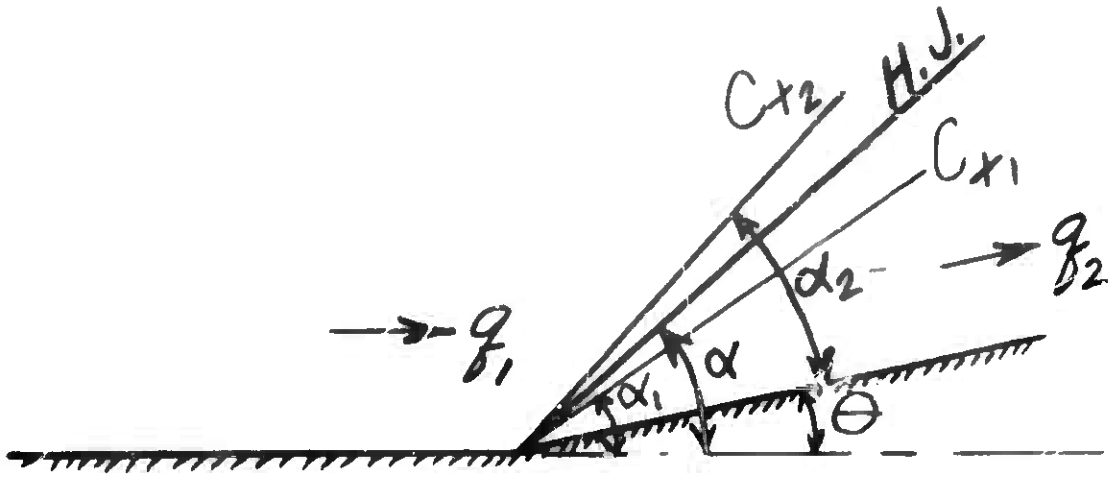

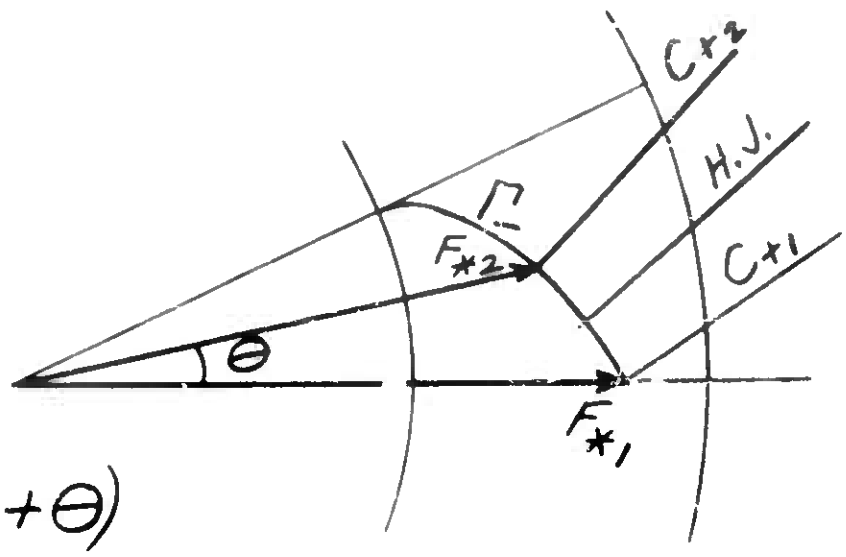

OBLIQUE HYDRAULIC JUMP, $\alpha \approx \frac{1}{2}(\alpha_1 + \alpha_2 + \theta)$

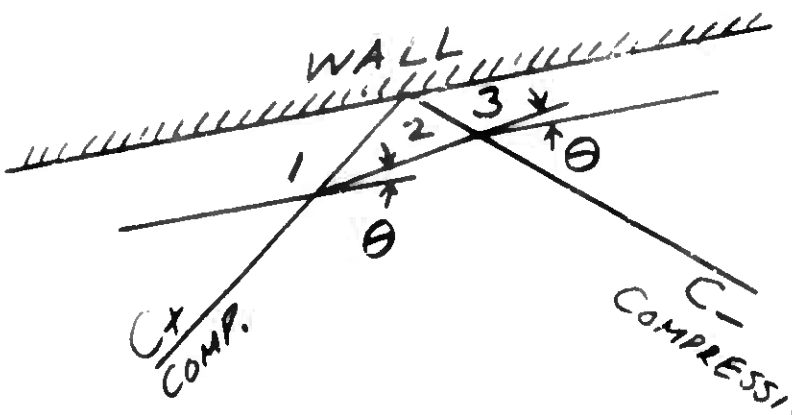

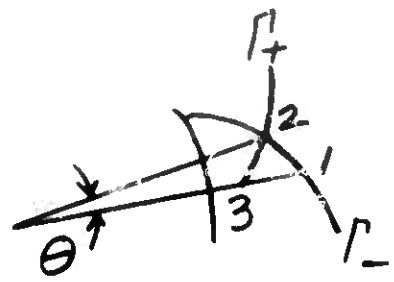

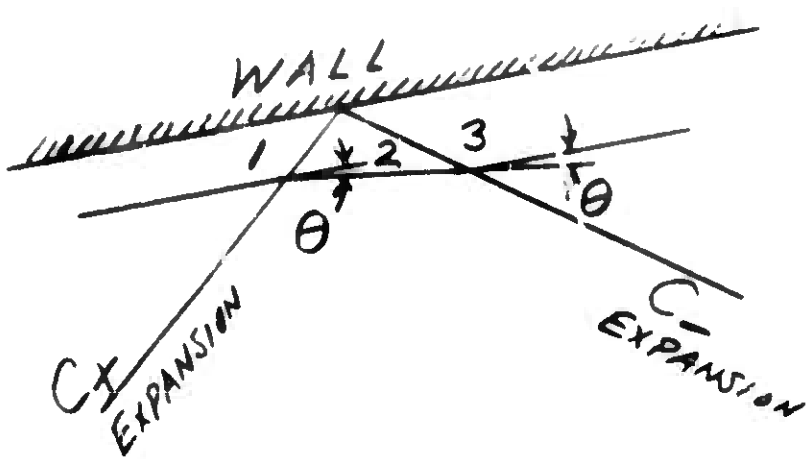

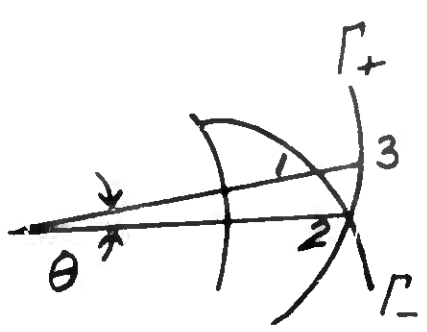

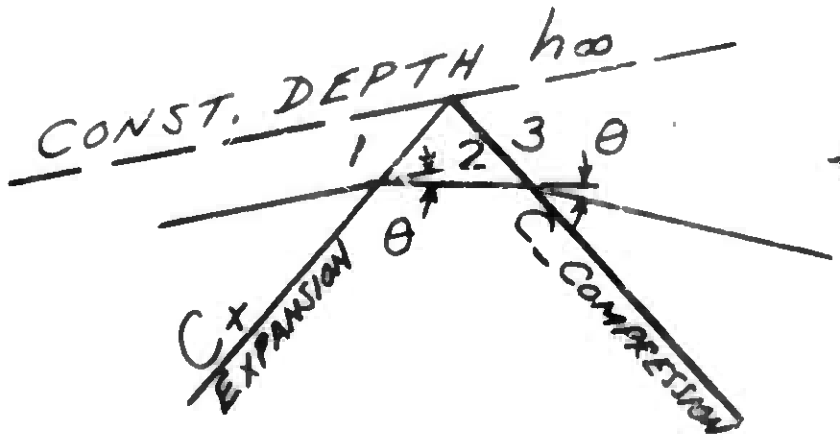

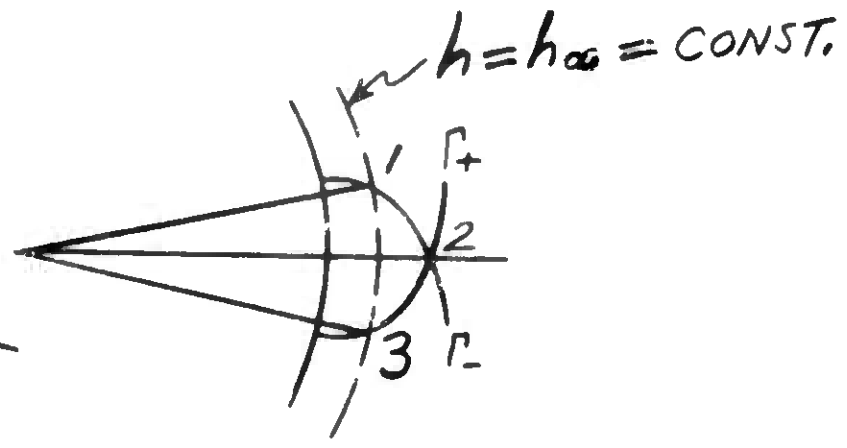

FIG. 45 – REFLECTION OF COMPRESSION & EXPANSION WAVES.

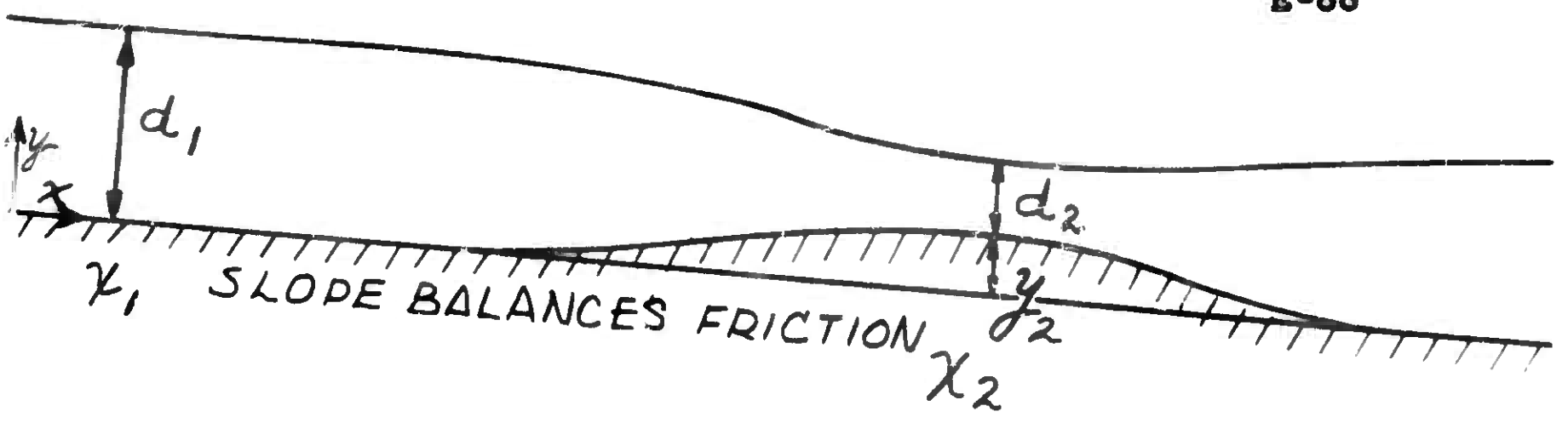

FIG. 46(a) - ONE DIMENSIONAL FLOW OVER A SLOPING BOTTOM, $\left|\frac{dy}{dx}\right| \ll 1$ SO CENTRIFUGAL FORCE NEGLIGIBLE.

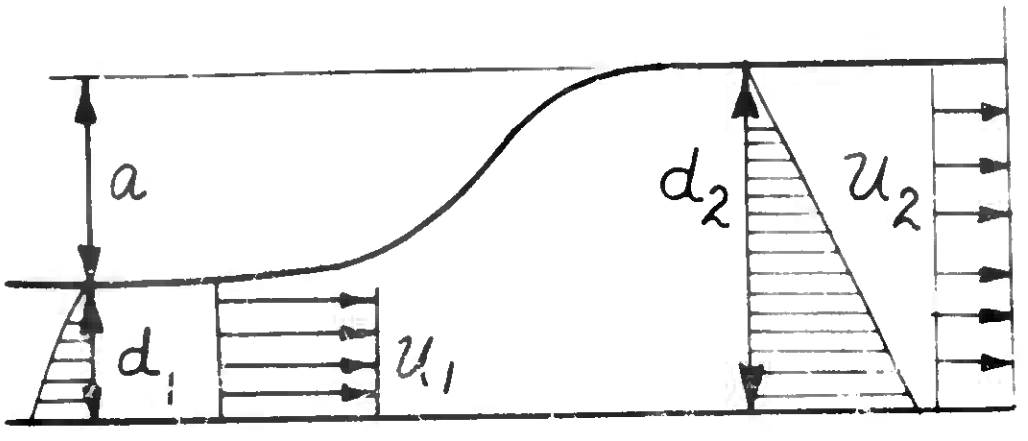

x_1 SLOPE = 0 x_2

$F_1 = (u_1/\sqrt{g d_1}) > \sqrt{3}$

FIG 46(b) - NORMAL HYDRAULIC JUMP

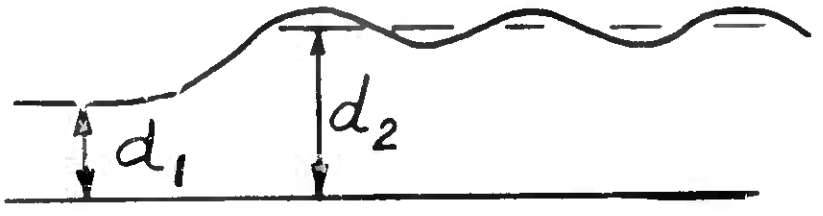

$F_1 < \sqrt{3}$

FIG. 46(c) - UNDULATING H.J.

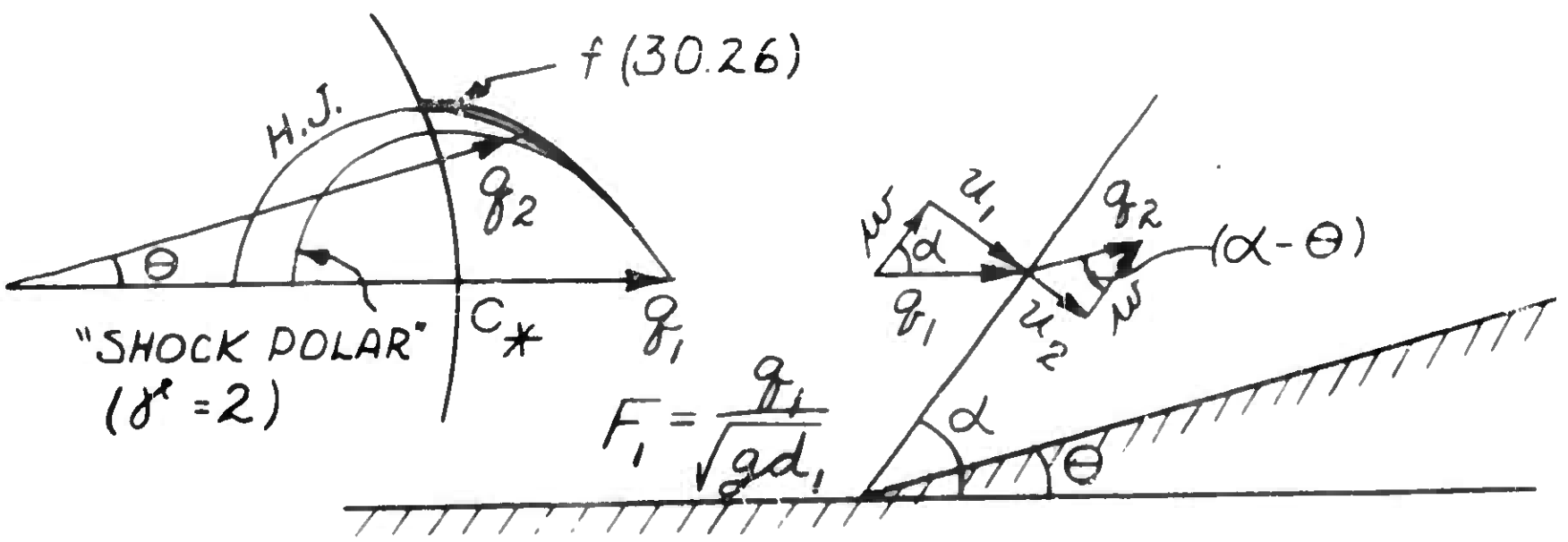

FIG. 46(d) - OBLIQUE HYDRAULIC JUMP WITH $w = w_1 = w_2$

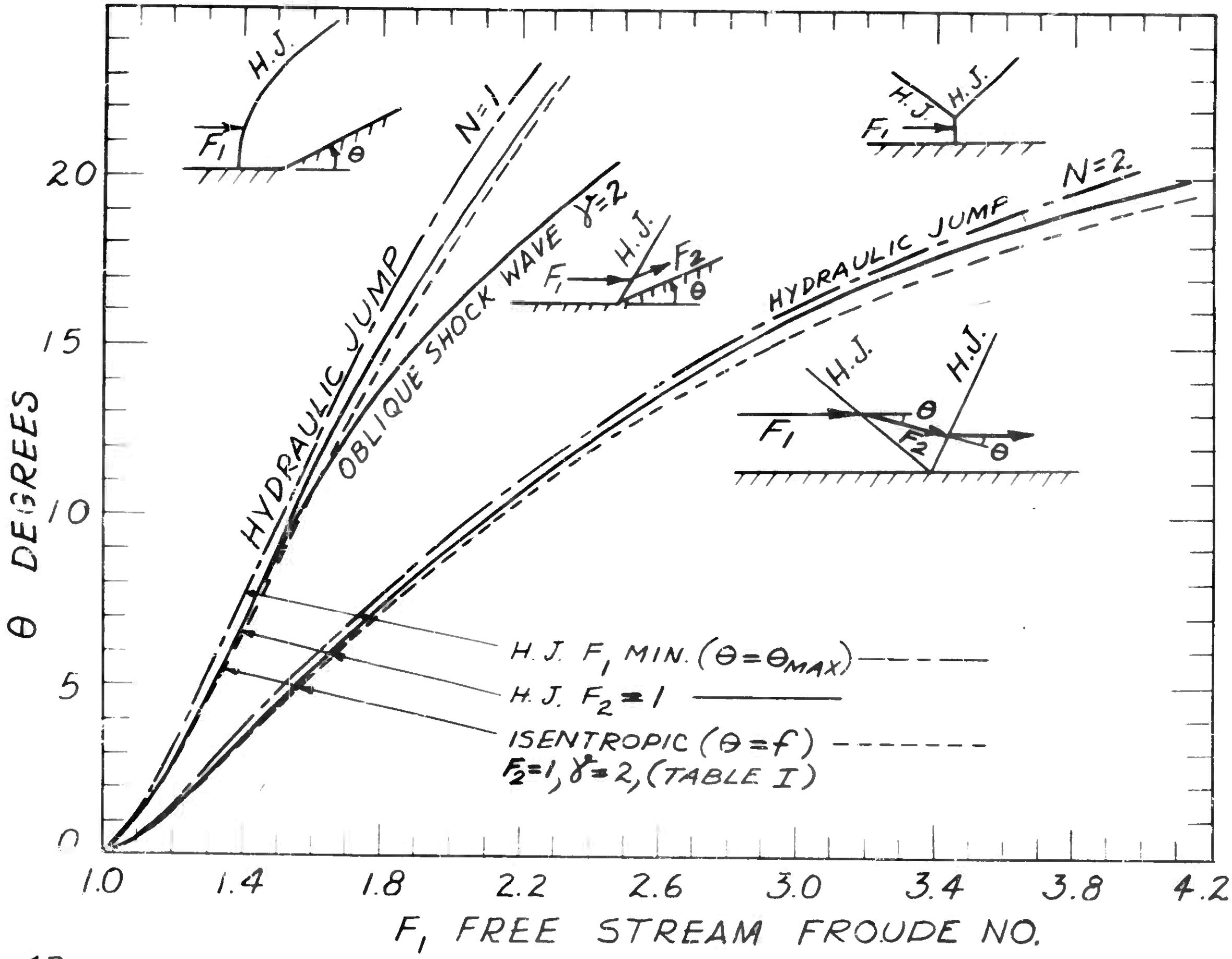

FIG. 4.7 – MAXIMUM FLOW DEFLECTION(N=1), & REFLECTION(N=2).

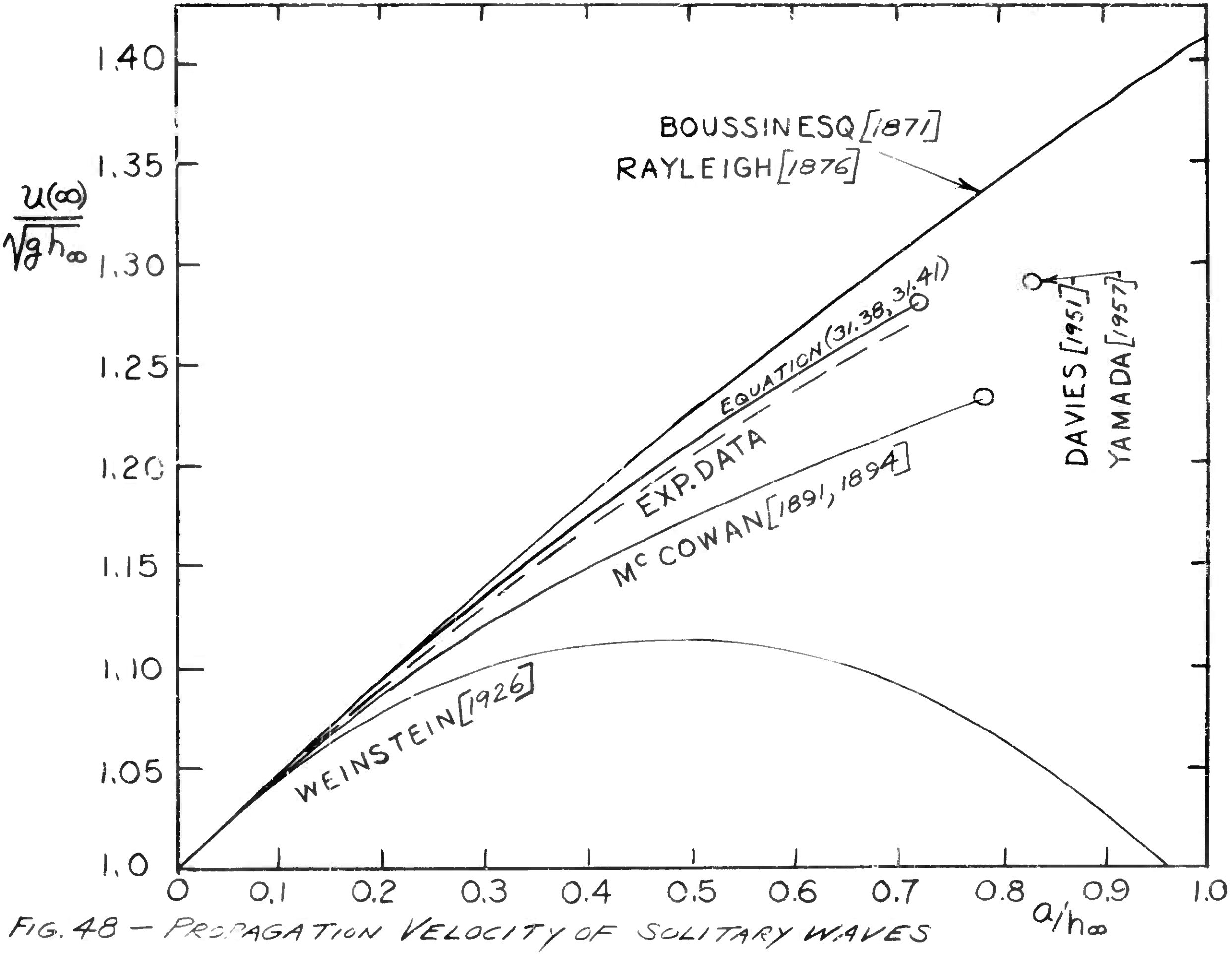

FIG. 48 – PROPAGATION VELOCITY OF SOLITARY WAVES

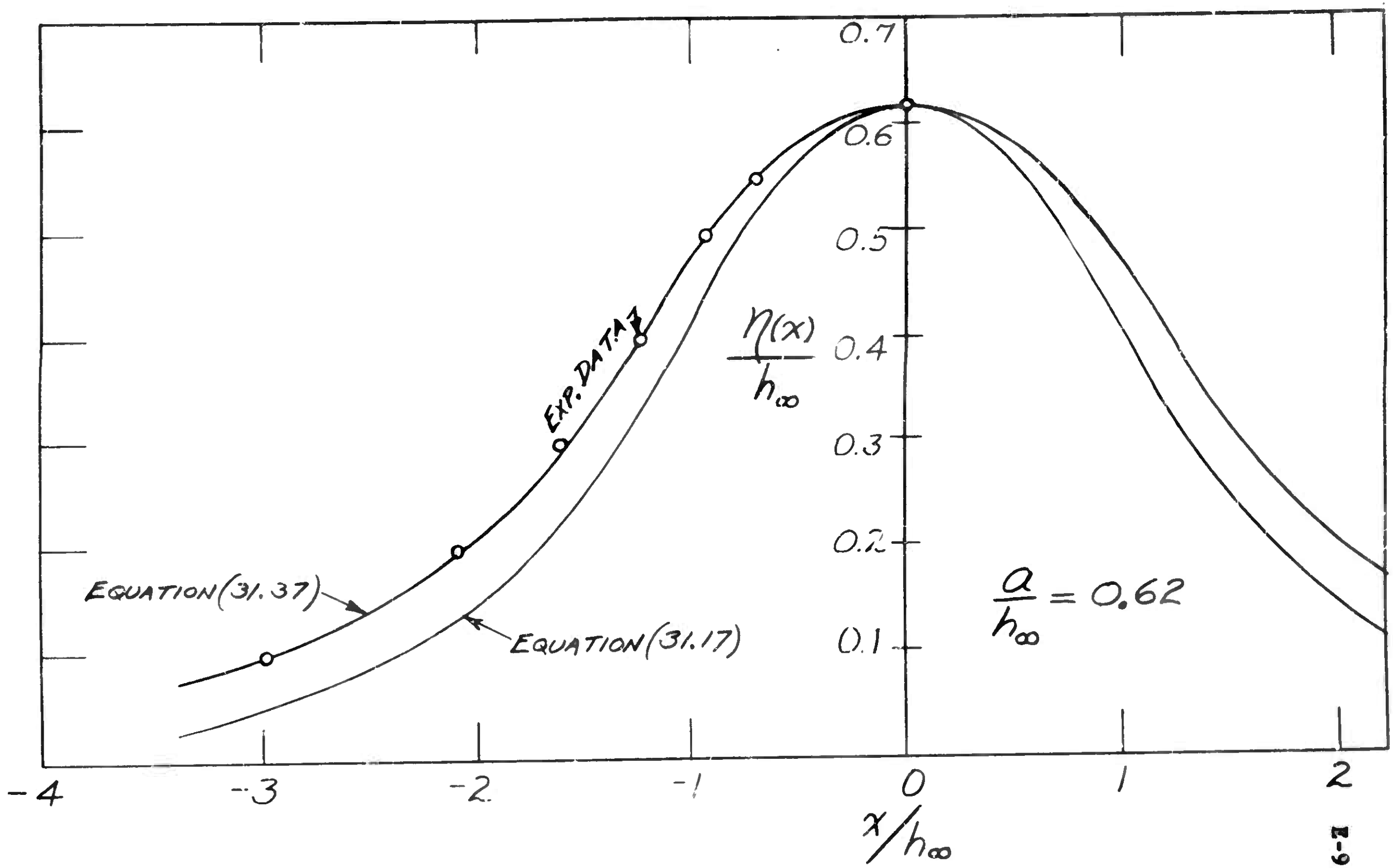

FIG. 49 — COMPARISON OF FIRST (31.17) AND SECOND (31.37) APPROXIMATION TO THE SOLITARY WAVE PROFILE, $\eta(x)$.